SIGNALS FOR THE ELECTROWEAK SYMMETRY BREAKING ASSOCIATED WITH THE TOP QUARK

By

Timothy Maurice Paul Tait

A DISSERTATION

Submitted to
Michigan State University
in partial fulfillment of the requirements
for the degree of

DOCTOR OF PHILOSOPHY

Department of Physics and Astronomy

1999

ABSTRACT

SIGNALS FOR THE ELECTROWEAK SYMMETRY BREAKING ASSOCIATED WITH THE TOP QUARK

By

Timothy Maurice Paul Tait

The mechanism of the electroweak symmetry-breaking (EWSB) is studied in the context of the heavy top quark, whose large mass may provide a clue as to the mechanism which generates the mass of the $W^{\pm}$ and Z bosons. As a result, it seems quite likely that the top quark may be special in the sense that it is involved in dynamics not experienced by the light fermions. Examples of this include models such as the top-condensate model in which a bound state of top quarks condenses, generating both the top mass and the gauge boson masses, and supersymmetric models in which the large top Yukawa coupling naturally explains the EWSB by radiatively driving the squared mass of a scalar particle (which is positive at a large energy scale) negative at low energies. Specific collider signatures of the third family result from such scenarios, and can be used to test the hypothesis that the top plays a role in the EWSB. In particular, single top production, as a measure of the top's weak interactions, provides an excellent probe of nonstandard top quark properties. The physics of single top production at hadron colliders is carefully studied, with a particular eye towards what can be learned from single top, including the signs of new physics that may show up in the single top rate.

This dissertation is dedicated to those who have contributed indirectly to its existence by providing much-needed support and encouragement. Among many others, this includes my grand-parents, Maurice and Jean Jones, and Mimi, who taught me to see the beauty inherent in the world; and my Parents, Susan and Peter Tait, and Rex and Maureen Daysh, who taught me how to live in it. Finally, this work is for Simona; you are the light of my life. Each day you are in my life makes it brighter, and in the end it is this that makes it worth living.

ACKNOWLEDGEMENTS

It is a pleasure to acknowledge those people who have helped me grow into the physicist I am today. Foremost is my thesis advisor, C.–P. Yuan, who has shared with me many of his ideas on which to pursue research, and encouraged me to learn interesting and invaluable ideas, techniques, and skills. Ed Berger at Argonne National Lab has also provided invaluable guidance in research, encouragement to pursue technically challenging calculations, and has supported me financially when the means to do so did not exist at Michigan State University. I have further benefitted from the exposure to high energy physicists which have given me very important information, advice, and a context in which to fit my own work. At Michigan State University this includes Carl Schmidt, Wu-Ki Tung, Wayne Repko, Dan Stump, Jon Pumplin, Maris Abolins, Raymond Brock, and Joey Huston. At Argonne, it includes Cosmas Zachos, Alan White, Geoff Bodwin, Don Sinclair, and Eve Kovacs. All have had a large impact on my research. I am also grateful to my committee members Vladimir Zelevinsky and William Hartmann for useful guidance.

I am further grateful to Michael Klasen, Stephen Mrenna, Francisco Larios, Lorenzo Diaz-Cruz, Ehab Malkawi, Hong-Jian He, and Csaba Balazs, my collaborators, for fun and interesting work, and to my colleagues in physics, Simona Murgia, Phil Tsai, Andy Lloyd, Hal Widlansky, Doug Carlson, Mike Wiest, Xiaoning Wang, Hung-Liang Lai, David Bowser-Chao, Kate Frame, Jim Amundson, Glenn Ladinsky, Chris Glosser, Pavel Nadolsky, Rocio Vilar, Gervasio Gomez, Miguel Mostafa, Juan Valls, Andrea Petrelli, Lionel Gordon, Jean-Françios Lagäe, Carmine Pagliarone, Zack Sullivan, Brian Harris, and Gordon Chalmers for many hours of interesting discussions.

Contents

List of Tables

List of Figures

Chapter 1

Introduction : The Standard Model

The Standard Model of Particle Physics [1, 2] (SM) contains, in principle, a complete description of all of the phenomena currently observed in high energy physics experiments, including the strong and electroweak interactions. However, as will be explained below, the model contains a number of theoretical puzzles which indicate that it is not the "ultimate" theory, but instead should be replaced by some more fundamental theory at higher energy scales. In fact, the striking success of the SM at explaining the currently available data places strong constraints on the nature of any theory that hopes to extend or supplant it at higher energies. As this work is an examination of several such models, we will begin with a presentation of the SM, examining its strengths and short-comings, in order to better understand these theories which hope to replace it. We shall see that the one of the great mysteries of the SM is the mechanism for the electroweak symmetry breaking (EWSB) that provides masses for both the weak bosons and the fermions. Because of their large masses, the fermions of the third family, and the top quark in particular, provide a natural place to explore hypotheses concerning the EWSB. In the succeeding chapters we examine specific ways in which experiments at supercolliders can study the possibility of a

connection between the EWSB and heavy top through single top production, production of scalars in association with bottom quarks, and supersymmetric particle production.

The SM is a quantum field theory of fermionic matter particles interacting with bosonic vector particles. The interactions are fixed by requiring the theory to be locally gauge invariant under transformations in the group $\mathrm{SU}(3)_C \times \mathrm{SU}(2)_L \times \mathrm{U}(1)_Y$. It is quite remarkable that this condition is enough to uniquely fix the structure of the renormalizable interactions between fermions and vector particles.

1.1 Yang-Mills Gauge Theory

We begin with a brief presentation of the construction of a Lagrangian invariant under local gauge transformations, as these ideas form the basic building blocks of the SM. In the Yang-Mills gauge theory [3] invariant under Lie group $\mathcal{G}$ with N group generators T^a $(a = 1..N)$, we can express the generators as Hermitian matrices with commutators,

$$[T^a, T^b] = i\, f^{abc}\, T^c, \tag{1.1}$$

where the f^{abc} are the structure constants of $\mathcal{G}$. An element of the local gauge transformation acting on a set of Dirac fermions may be expressed as

$$\Psi(x) \rightarrow e^{i\alpha^a(x)T^a}\, \Psi(x), \tag{1.2}$$

where the real function $\alpha^a(x)$ is the local transformation parameter. Clearly the usual free field Lagrangian density for a set of Dirac spinors is not invariant under this transformation, because the transformation of $\partial_\mu \Psi(x)$ will generate a term in which the derivative acts on $\alpha^a(x)$. This is remedied by introducing a covariant

derivative,

$$D_\mu = \partial_\mu + i\, g\, T^a\, A^a_\mu(x), \tag{1.3}$$

which insures that $D_\mu \Psi$ transforms like Ψ under the gauge group provided that the real vector field $A^a_\mu(x)$ transforms according to,

$$T^a\, A^a_\mu(x) \to e^{i\alpha^a(x)T^a} \left\{ T^b\, A^b_\mu(x) - \frac{i}{g}\partial_\mu \right\} \left(e^{i\alpha^c(x)T^c} \right)^\dagger . \tag{1.4}$$

This allows us to write down the gauge-invariant kinetic terms for the Dirac fermion,

$$\mathcal{L}_{\rm FK} = i\, \overline{\Psi}\, \gamma^\mu\, D_\mu\, \Psi - m\, \overline{\Psi}\, \Psi, \tag{1.5}$$

where for brevity we no longer explicitly write the fields as functions of space-time. The presence of the covariant derivative, dictated by the gauge invariance, has thus forced us to include an interaction between the fermion fields Ψ and the vector fields A^a. It should be noted that a four-component Dirac spinor may be written in terms of a left-handed and a right-handed two-component Weyl spinor [4]. One can formulate a theory of massless fermions in two-component form, which proceeds much as it is described above, but with no mass term in $\mathcal{L}_{\rm FK}$.

In order for the vector field to be dynamical it must also have kinetic terms in the Lagrangian. It is easy to verify that,

$$\mathcal{L}_{\rm GK} = -\frac{1}{4} F^{a\mu\nu}\, F^a{}_{\mu\nu} \tag{1.6}$$

with,

$$F^a{}_{\mu\nu} = \partial_\mu A^a_\nu - \partial_\nu A^a_\mu - g\, f^{abc}\, A^b_\mu\, A^c_\nu \tag{1.7}$$

will serve[1], and itself respects gauge invariance, with g the same coupling that appears in the covariant derivative for the fermion. In the case in which $\mathcal{G}$ is a non-Abelian

[1] A term of the form $\frac{\theta}{2} F^{a\mu\nu} \tilde{F}^a_{\mu\nu}$ with $\tilde{F}^a_{\mu\nu} = 1/2 \epsilon_{\mu\nu\alpha\beta} F^{a\alpha\beta}$ is also gauge invariant, and could be included in $\mathcal{L}_{\rm GK}$. For an Abelian group $\mathcal{G}$ this term corresponds to a total derivative, and thus does not contribute to the dynamics. In the case of a non-Abelian group this term is related to the CP properties of the theory. For simplicity we will not consider such a term here.

group (and thus the structure constants do not vanish), this term will contain cubic and quadratic interactions of the gauge field, in addition to the kinetic terms. It is important to note that $\mathcal{L}_{\mathrm{GK}}$ does not contain a mass term for the vector field. In fact, such a term is forbidden by gauge invariance, and thus the vector fields are necessarily massless as a result of the gauge symmetry. This theory may now be quantized by employing, i.e., the Faddeev-Popov formalism [5] to quantize only the physical degrees of freedom.

In addition to fixing the form of the renormalizable interactions, the gauge symmetry plays a further role in the construction of a model in that it corresponds to conserved currents as predicted by Noether's theorem[2] [6], and implies relations among the Green's functions known as Ward-Takahashi identities [7]. The Ward identities, and thus the gauge symmetry itself, play an important role in the proof of the decoupling of the ghost states from physical amplitudes [8], and in proving the unitarity and renormalizability [7, 8, 9] of the Yang-Mills theory. The gauge symmetry is therefor seen as an essential ingredient for a theory of vector particles.

1.2 The Standard Model

1.2.1 Spin 1 Gauge Boson Fields

Having briefly reviewed the general Yang-Mills theory of a set of fermions interacting with gauge bosons as is dictated by local invariance under a symmetry group $\mathcal{G}$, we now specify to the SM, with symmetry group $\mathcal{G} = \mathrm{SU}(3)_C \times \mathrm{SU}(2)_L \times \mathrm{U}(1)_Y$. The $\mathrm{SU}(3)_C$ gauge symmetry corresponds to the strong interaction of quantum chromodynamics (QCD). Its eight gauge bosons G^a_μ are known as gluons. The $\mathrm{SU}(2)_L \times \mathrm{U}(1)_Y$

[2]Noether's theorem guarantees that a continuous symmetry corresponds to a conserved current at the classical level. Some symmetries, known as anomalous symmetries, are broken by quantum effects. The requirement that a desired classical symmetry survives quantization can provide non-trivial constraints on the theory.

sector contains the combined electromagnetic and weak interactions, generally referred to as the electroweak symmetry. The three $\mathrm{SU}(2)_L$ bosons are denoted W^i_μ and couple to the weak iso-spin, whereas the $\mathrm{U}(1)_Y$ gauge boson, B_μ couples to hypercharge. Since the gauge bosons of one of the symmetry subgroups in $\mathcal{G}$ do not transform under the other gauge symmetries in the product of groups, the gauge kinetic term may be simply written as a sum of the individual gauge kinetic terms,

$$\mathcal{L}_{GK} = -\frac{1}{4}B_{\mu\nu}B^{\mu\nu} - \frac{1}{4}W^i_{\mu\nu}W^{i\mu\nu} - \frac{1}{4}G^a_{\mu\nu}G^{a\mu\nu}, \tag{1.8}$$

where,

$$\begin{aligned} B_{\mu\nu} &= \partial_\mu B_\nu - \partial_\nu B_\mu, \\ W^i{}_{\mu\nu} &= \partial_\mu W^i_\nu - \partial_\nu W^i_\mu - g_2\,\epsilon^{ijk}\,W^j_\mu\,W^k_\nu, \\ G^a{}_{\mu\nu} &= \partial_\mu G^a_\nu - \partial_\nu G^a_\mu - g_3\,f^{abc}\,G^b_\mu\,G^c_\nu, \end{aligned} \tag{1.9}$$

with g_i the gauge couplings, and ϵ^{ijk} and f^{abc} the structure constants for SU(2) and SU(3), respectively.

As will be explained in detail below, the electroweak symmetry is spontaneously broken, resulting in mixing between the B_μ and W^3_μ fields, and non-zero masses for three of the gauge bosons ($W^\pm$ and Z^0). The photon (A) remains massless, due to a residual $\mathrm{U}(1)_{\mathrm{EM}}$ gauge symmetry that remains unbroken. The physical (mass-eigenstate) gauge bosons and their masses are shown in Table 1.1.

1.2.2 Spin $\frac{1}{2}$ Matter Fields

The SM contains three families (also called generations) of spin $\frac{1}{2}$ matter fields, in the fundamental representation of the gauge groups. Each family is a "copy" of the other families with respect to gauge quantum numbers, but have diverse masses. Each generation contains a charged and a neutral lepton, which interact electroweakly, and

Table 1.1: Vector Boson Masses

Particle	Symbol	Mass (GeV)	
Photon	A	0	Electromagnetic Force
W Boson	$W^{\pm}$	80.33	Charged Weak Force
Z Boson	Z^0	91.187	Neutral Weak Force
Gluon	G^a	0	Strong Force

an up-type and a down-type quark, which interact both electroweakly and with the gluons. A list[3] of the fermions, including their masses, is presented in Table 1.2.

In Table 1.3 can be found the transformation properties of the fermions of the first family under the gauge groups. Since the second and third families are copies of the first family as far as the quantum number assignment is concerned, only the first family is presented. The left- and right-chiral fermions have different quantum numbers, with the left-chiral fields arranged in doublets,

$$L_L = \begin{pmatrix} \nu_e \\ e \end{pmatrix}_L, \quad Q_L = \begin{pmatrix} u \\ d \end{pmatrix}_L, \tag{1.10}$$

and the right-chiral fermions are in singlets,

$$e_R, \quad u_R, \quad d_R. \tag{1.11}$$

The gauge invariance under $\mathrm{SU}(2)_L$ thus forbids the presence of a mass term for the fermions. As we will see below, in the SM, fermion masses are generated by the same spontaneous symmetry-breaking Higgs mechanism that provides mass for the weak

[3]It is worth mentioning that the association of a particular doublet of leptons with a particular doublet of quarks in order to form a generation is arbitrary in the SM, because there are no local interactions between quarks and leptons. The SM makes this identification in a natural way by identifying the doublet containing the heaviest charged lepton with the doublet containing the heaviest quarks (and so on), but one could in principle associate any quark doublet with any lepton doublet and call that a family.

Table 1.2: Lepton and Quark Masses

Particle	Symbol	Mass (GeV)	
Electron neutrino	ν_e	0	
Electron	e	0.00051	First
Up quark	u	0.002 to 0.008	Generation
Down quark	d	0.005 to 0.015	
Muon neutrino	ν_μ	0	
Muon	μ	0.106	Second
Charm quark	c	1.0 to 1.6	Generation
Strange quark	s	0.1 to 0.3	
Tau neutrino	ν_τ	0	
Tau	τ	1.78	Third
Top quark	t	175	Generation
Bottom quark	b	4.1 to 4.5	

bosons. There is no right-handed neutrino in the SM, and thus the neutrino is a massless Dirac field. With respect to the color gauge group of quantum chromodynamics the quark fields are arranged in triplets,

$$q = \begin{pmatrix} q_r \\ q_g \\ q_b \end{pmatrix}, \tag{1.12}$$

where we have used the common convention of referring to the $\mathrm{SU}(3)_C$ indices as red (r), green (g), and blue (b).

The gauge invariant kinetic Lagrangian for a particular fermion, Ψ, is given in Equation 1.5 with the covariant derivative given by,

$$D_\mu = \partial_\mu + i\, g_1 \frac{Y}{2} B_\mu + i\, g_2\, \tau^j\, W_\mu^j + i\, g_3\, \lambda^a\, G_\mu^a, \tag{1.13}$$

with Y the hypercharge of the fermion, and τ^j and λ^a the generators of SU(2) and

Table 1.3: Quantum Numbers of the Fermions

Chirality	Q	T_L^3	Y	C
ν_{eL}	0	1/2	-1	0
e_L	-1	-1/2	-1	0
u_L	2/3	1/2	1/3	r, g, b
d_L	-1/3	-1/2	1/3	r, g, b
e_R	-1	0	-2	0
u_R	2/3	0	4/3	r, g, b
d_R	-1/3	0	-2/3	r, g, b

SU(3) in the representation appropriate for Ψ. The hypercharge has been normalized such that the electric charge of the fermion is given by $Q = T_L^3 + \frac{Y}{2}$.

1.2.3 Masses and the Higgs Mechanism

As we have seen, the gauge symmetries of the SM forbid explicit masses for vector bosons (as is true for any gauge theory) and fermions (as is true in the case of the SM, in which left- and right-chiral fermions transform differently). In order to describe the world seen in particle physics experiments, these objects must acquire masses. This may be resolved by introducing a spontaneous breaking of the electroweak symmetry, through the Higgs Mechanism [10]. The spontaneous symmetry-breaking (SSB) occurs when the Lagrangian is invariant under the gauge transformations, but the vacuum state does not respect the symmetry. In the SM this is accomplished by introducing a weak iso-spin doublet of complex scalar fields, the Higgs doublet. This

doublet carries hypercharge +1, and thus can be expressed as,

$$\Phi = \frac{1}{\sqrt{2}}\begin{pmatrix} \phi_1 + i\,\phi_2 \\ \eta + i\,\phi_3 \end{pmatrix} = \left(e^{i\,\theta^i(x)\tau^i}\right)^\dagger \begin{pmatrix} 0 \\ \sigma(x) \end{pmatrix}. \tag{1.14}$$

where the second form (which displays the space-time dependence of the four fields θ^i and σ explicitly for clarity) illustrates an interesting property of the Higgs doublet, which can be seen by noting that under a $\mathrm{SU}(2)_L \times \mathrm{U}(1)_Y$ gauge transformation, the doublet transforms as,

$$\Phi \rightarrow e^{i\,\frac{\beta(x)}{2}}\, e^{i\,\alpha^i(x)\tau^i}\, \Phi, \tag{1.15}$$

and thus comparing Equations 1.14 and 1.15 indicates that provided the expectation value of σ is non-zero (which indicates that SSB has occurred), one may choose a particular gauge in which three of the four real degrees of freedom of the Higgs doublet vanish. Since on the one hand it is possible to "gauge away" these fields, while on the other physical quantities are independent of the choice of gauge, this indicates that these degrees of freedom are unphysical. As we shall see below, under SSB these unphysical scalars reappear as the longitudinal polarizations of the weak bosons.

The scalar field can be given gauge invariant terms in the Lagrangian,

$$\mathcal{L}_\Phi = (D_\mu \Phi)^\dagger\,(D^\mu \Phi) - \mu^2 \Phi^\dagger\,\Phi - \lambda\left(\Phi^\dagger\,\Phi\right)^2, \tag{1.16}$$

with,

$$D_\mu = \partial_\mu + i\,g_1\,\frac{1}{2}B_\mu + i\,g_2\,\tau^j W_\mu^j, \tag{1.17}$$

where the first (kinetic) term in Equation 1.16 is required by gauge invariance, and the remaining terms correspond to a mass-like term and a self-interaction of the Φ field. These latter two terms together are generally referred to as the Higgs potential.

One can also construct gauge invariant Yukawa couplings between the doublet and the fermions,

$$\begin{aligned}\mathcal{L}_{Yukawa} &= \sum_{n=1}^{3}\sum_{m=1}^{3}\Big(\, y_e^{nm}\,\overline{e}_R^n\,\Phi^\dagger\,L_L^m \;+\; y_e^{nm*}\,\overline{L}_L^m\,\Phi\,e_R^n\,\Big) \\ &+\Big(\, y_d^{nm}\,\overline{d}_R^n\,\Phi^\dagger\,Q_L^m \;+\; y_d^{nm*}\,\overline{Q}_L^m\,\Phi\,d_R^n\,\Big) \\ &+\Big(\, y_u^{nm}\,\overline{u}_R^n\,\tilde{\Phi}^\dagger\,Q_L^m \;+\; y_u^{nm*}\,\overline{Q}_L^m\,\tilde{\Phi}\,u_R^n\,\Big),\end{aligned} \tag{1.18}$$

with,

$$\tilde{\Phi} = i\,\tau^2\,\Phi^*, \tag{1.19}$$

and the sum over n and m is over the three families of fermions.

Spontaneous symmetry-breaking is exhibited by assuming[4] $\mu^2 < 0$. Under these conditions the minimum of the Higgs potential shifts (in field space) from $\Phi = 0$ to,

$$\Phi^\dagger\Phi \;=\; \phi_1^2 + \phi_2^2 + \phi_3^2 + \eta^2 = \frac{-\mu^2}{\lambda} = v^2. \tag{1.20}$$

The field thus acquires a non-zero vacuum expectation value (VEV). Expressing this condition in terms of the real scalars $\phi^{1..3}$ and η, we see that the minimization condition allows for any of these (or a combination of them) to carry the VEV. Choosing $<\eta>= v$, we expand about v,

$$\Phi = \begin{pmatrix} \phi^+ \\ \frac{v+h+i\,\phi_3}{\sqrt{2}} \end{pmatrix}, \tag{1.21}$$

with $\phi^+ = (\phi^1 + i\,\phi^2)/\sqrt{2}$ and $\eta = v + h$. Inserting this into Equation 1.16, we see after some algebra (which can be simplified by working in the unitary gauge, $\phi^{1..3} = 0$) that tree-level mass terms for the h field and gauge bosons are present,

[4] It is important to note that λ must be positive in Equation 1.16 in order for the theory to possess a stable vacuum.

$$\mathcal{L}_{\rm MB} \;=\; -\left(\frac{2\,\lambda\,v^2}{2}\right)\,h^2 \;+\; \left(\frac{g_2\,v}{2}\right)^2 W^{+\mu}\,W^-_\mu \qquad (1.22)$$

$$+\left(\frac{v}{2}\right)^2 \left(g_2 W^3_\mu - g_1 B_\mu\right)\left(g_2 W^{3\mu} - g_1 B^\mu\right),$$

along with many other interaction terms. The fields $W^\pm_\mu$ are defined as $W^\pm_\mu = (W^1_\mu \mp i\,W^2_\mu)/\sqrt{2}$ to be electric charge eigenstates. Physically, the appearance of mass terms for the gauge bosons after SSB can be explained by the gauge bosons absorbing ("eating") the unphysical would-be Goldstone bosons, $\phi^{1..3}$, which serve as the longitudinal degrees of freedom that distinguish massive from massless vector fields. This is referred to as the electroweak symmetry-breaking and can be denoted $\mathrm{SU}(2)_L \times \mathrm{U}(1)_Y \to \mathrm{U}(1)_{\rm EM}$, because the U(1) to which the photon corresponds remains unbroken. An interesting heuristic picture for the Higgs mechanism is that the Higgs potential generates dynamics which "fills" the vacuum with Higgs field. The resulting masses for the vector bosons and fermions are then seen as a result of these particles interacting with this "medium" as they move through the vacuum.

As was mentioned previously, the SSB has mixed the B_μ and W^3_μ gauge bosons. The mass eigenstates thus consist of the massive Z boson and massless photon,

$$\begin{pmatrix} Z_\mu \\ A_\mu \end{pmatrix} = \begin{pmatrix} \cos\theta_W & -\sin\theta_W \\ \sin\theta_W & \cos\theta_W \end{pmatrix} \begin{pmatrix} W^3_\mu \\ B_\mu \end{pmatrix}, \qquad (1.23)$$

with the weak mixing angle θ_W given by,

$$\tan\theta_W = \frac{g_1}{g_2}. \qquad (1.24)$$

It is conventional to discuss the SM couplings in terms of the coupling of the photon to the electron, e, the weak mixing parameter, $\sin^2\theta_W$, and the masses of the Z and Higgs bosons, M_Z and M_h, as opposed to the original couplings, g_1, g_2, μ^2, and λ in which the theory was formulated. From the presentation above, it should be clear how to relate these two sets of parameters at tree-level. At higher orders in perturbation theory, the relations depend on the renormalization scheme.

It is worth noting that the $W^{\pm}$ and Z mass terms in Equation 1.22 arose from the covariant derivative part of Equation 1.16 (the term that was fixed by gauge invariance). This has two interesting consequences for the masses generated. The first is that once the gauge couplings g_1 and g_2 are specified, the $W^{\pm}$ and Z masses are determined by v and the representation of Φ (this property is general for the Higgs mechanism). The second property is specific to the particular quantum numbers assigned to the SM Higgs doublet; the quantity,

$$\rho = \frac{M_W}{M_Z \cos\theta_W}, \tag{1.25}$$

is equal to one at tree level in the SM, and thus provides a test of the SM realization of SSB compared to other models.

1.2.4 Fermion Masses and the CKM Matrix

We saw in the previous section how the SSB provides masses for the gauge bosons. In the SM, the same mechanism provides masses for the fermions through the Yukawa interactions in Equation 1.18. As the values of these couplings are not fixed by the gauge symmetry, they can be tuned to correspond to the particular fermion masses observed in nature. This is complicated by the fact that in general the interaction eigenstates need not be the same as the mass eigenstates because of the off-diagonal (in family-space) interactions between fermions and the Higgs doublet in Equation 1.18. In terms of the 3×3 interaction eigenstate mass matrices, M_u, M_d, and M_e, the fermion mass terms can be expressed,

$$\mathcal{L}_{\rm MF} = \bar{\mathbf{u}}_R \, M_u \, \mathbf{u}_L + \bar{\mathbf{d}}_R \, M_d \, \mathbf{d}_L + \bar{\mathbf{e}}_R \, M_e \, \mathbf{e}_L + H.c., \tag{1.26}$$

where $+H.c.$ indicates the Hermitean conjugate of the preceeding terms. The bold-faced fermion fields now indicate a vector containing the fields of a given type for all

three families,

$$\mathbf{u}_L = \begin{pmatrix} u_L \\ c_L \\ t_L \end{pmatrix}, \qquad \mathbf{d}_L = \begin{pmatrix} d_L \\ s_L \\ b_L \end{pmatrix}, \qquad \mathbf{e}_L = \begin{pmatrix} e_L \\ \mu_L \\ \tau_L \end{pmatrix}, \tag{1.27}$$

and similar notation for $\mathbf{u}_R$, $\mathbf{d}_R$, and $\mathbf{e}_R$. To make the connection between $\mathcal{L}_{\mathrm{MF}}$ and Equation 1.18 explicit, we present as an example the the mass matrix for up-type quarks after SSB,

$$M_u = \frac{v}{\sqrt{2}} \begin{pmatrix} y_u^{11} & y_u^{12} & y_u^{13} \\ y_u^{21} & y_u^{22} & y_u^{23} \\ y_u^{31} & y_u^{32} & y_u^{33} \end{pmatrix}. \tag{1.28}$$

To express the fermion masses in terms of mass eigenstates, one uses the fact that it is possible to rotate the left- and right-chiral fields among the three generations. A general unitary rotation of the fields may be denoted,

$$\begin{gathered} \mathbf{u}_R \to R_u\, \mathbf{u}_R, \qquad \mathbf{d}_R \to R_d\, \mathbf{d}_R, \qquad \mathbf{e}_R \to R_e\, \mathbf{e}_R, \\ \mathbf{u}_L \to L_u\, \mathbf{u}_L, \qquad \mathbf{d}_L \to L_d\, \mathbf{d}_L, \qquad \mathbf{e}_L \to L_e\, \mathbf{e}_L, \end{gathered} \tag{1.29}$$

and the condition for mass eigenstates may be expressed by requiring that these transformations diagonalize the interaction eigenstate mass matrices. Employing D_i (with $i = u, d, e$) to indicate the diagonalized matrix, this may be written,

$$D_u = R_u^\dagger\, M_u\, L_u, \qquad D_d = R_d^\dagger\, M_d\, L_d, \qquad D_e = R_e^\dagger\, M_e\, L_e. \tag{1.30}$$

The requirement that the nine free entries in D_u, D_d, and D_e correspond to the fermion masses observed in nature provides some information about the Yukawa interactions in Equation 1.18. The remaining information must come from studying the effect of the quark mixing on the quark interactions with other particles.

Having transformed to mass eigenstates, it is still necessary to examine the effect of these rotations on the interactions of the fermions with the vector and Higgs bosons.

From the fact that the mass terms came from the fermion interactions with the Higgs doublet, it is clear that the interactions of h with the fermions are diagonal in the mass eigenbasis. For the gauge bosons, it is simple to show that the left- and right-handed pieces of the A, G, and Z coupling to fermion f are proportional to $L_f^\dagger L_f = 1$ and $R_f^\dagger R_f = 1$, respectively. Thus, these interactions are the same in mass and interaction eigenbasis. On the other hand, the $W^\pm$ interactions with the quarks pick up a factor of $L_u^\dagger L_d$, which allows the $W^\pm$ interactions to couple up- and down-type quarks of different generations. The lepton sector has no equivalent effect, because in the SM the massless neutrinos have no mass diagonalization requirement, and thus may always be rotated such that the $W^\pm$ couplings are diagonal in the generations.

Thus, the only observable matrix related to the generational rotations is $V = L_u^\dagger L_d$, the Cabibbo-Kobayashi-Maskawa (CKM) matrix [11]. By convention, the matrix L_u is set to the unit matrix, and in that case $V = L_d$. Since in the SM only the combination is of physical relevance, this does not result in a loss of generality (though it should be kept in mind that for a more general model it may be important to recall that $V = L_u^\dagger L_d$ is the true relation). Thus we write,

$$\begin{pmatrix} d \\ s \\ b \end{pmatrix}_{\text{Weak}} = \begin{pmatrix} V_{ud} & V_{us} & V_{ub} \\ V_{cd} & V_{cs} & V_{cb} \\ V_{td} & V_{ts} & V_{tb} \end{pmatrix} \begin{pmatrix} d \\ s \\ b \end{pmatrix}_{\text{Mass}}, \tag{1.31}$$

with, in the "standard parameterization" advocated by the Particle Data Group [12],

$$V = \begin{pmatrix} c_{12}c_{13} & s_{12}c_{13} & s_{13}e^{-i\delta_{13}} \\ -s_{12}c_{23} - c_{12}s_{23}s_{13}e^{-i\delta_{13}} & c_{12}c_{23} - s_{12}s_{23}s_{13}e^{-i\delta_{13}} & s_{23}c_{13} \\ s_{12}s_{23} - c_{12}c_{23}s_{13}e^{-i\delta_{13}} & -c_{12}s_{23} - s_{12}c_{23}s_{13}e^{-i\delta_{13}} & c_{23}c_{13} \end{pmatrix}. \tag{1.32}$$

In this equation, $c_{ij} = \cos\theta_{ij}$ and $s_{ij} = \sin\theta_{ij}$, with i and j labeling the generations. δ_{13} is a complex phase that can induce CP violating effects. While a general 3×3 unitary matrix has three independent phases, this parameterization has used the

fact that we may redefine the quark fields to include a complex phase such that only δ_{13} remains. In a model containing physics beyond the SM, extended fermion interactions may allow for effects related to more of these mixing matrices than the single combination that is the CKM matrix. For example, a model that includes masses for the neutrinos, it may be appropriate to introduce a CKM-like matrix to include a $W^{\pm}$ coupling to leptons of various mixed generations.

Experimental measurements of the hadrons containing various types of quarks provide information about all of the CKM elements except V_{tb}. As we will see in Chapter 2, V_{tb} can be measured by studying single top production. In fact, in the SM there are only three generations of fermions and thus the requirement that the CKM matrix be unitary already provides strong limits that V_{tb} be close to one. Nonetheless, it is important to directly measure V_{tb}, since a deviation from the SM limit on V_{tb} would be a signal of physics beyond the Standard Model. In the very least, one could find an indication of a fourth generation of quarks that is strongly mixed with the third family, but almost unmixed with the first two families by measuring V_{tb} to be considerably smaller than unity.

1.3 Theoretical Puzzles of the Standard Model

1.3.1 General Considerations

In spite of its enormous success in explaining high energy physics phenomena, the SM still contains a number of theoretical flaws and puzzles that lead us to believe it should be replaced by a more fundamental theory at higher energy scales. As there are a large number of opinions and approaches to this question, the discussion below will necessarily be somewhat personalized and incomplete. In this section we will discuss some general puzzles of the SM, followed by more detailed discussion of issues

concerning the EWSB and the fermion mass hierarchy that will be explored in the rest of this work.

In fact it is quite obvious that the SM is "only an effective theory" because it does not include gravity. A truly fundamental theory should explain all four of the forces observed in nature. The SM contains a description of the electromagnetic, weak, and strong nuclear forces, but does not address how to include gravitational interactions within its framework. In fact, because of the negative mass dimension of the gravitational coupling constant ($1/M^2_{Planck}$), simple power counting of loop diagrams indicate that a field theory of gravity is not expected to be renormalizable. Thus, there is no way to consistently include quantum corrections to gravitational phenomena within a field theory of point-like objects such as the SM. Further, the evolution of the structure of the universe under gravitational interactions is sensitive to the cosmological constant, which is observed to be very small (or zero). Why this constant is so small compared to typical particle physics energy scales remains a mystery.

Even if one were to focus on only a more modest goal of a theory without gravity, the SM still contains many puzzling features. For example, it includes 18 free parameters, including the three gauge couplings e, $\sin^2\theta_W$, and g_3; the two Higgs potential couplings that may be expressed as M_Z and M_h; and 9 fermion masses and 4 CKM mixing parameters that contain the physical information about the Higgs Yukawa interactions with the fermions. As the Higgs boson has not been observed, its mass is the only undetermined quantity in the SM[5]. This large number of parameters can itself be seen as a drawback of the SM. It would seem more attractive if there

[5]Recall that in the SM V_{tb} is fixed by the unitarity of the CKM matrix. It is worth noting that precision measurements have become sensitive to radiative corrections involving the Higgs. Thus, indirect constraints on M_h already exist, as well as excluded regions of M_h that correspond to predictions for signals that have not been observed at colliders [13, 14].

were a deeper symmetry or structure that could explain the origin of these seemingly arbitrary quantities in terms of a smaller set of parameters.

A seemingly straight-forward means to accomplish this would be to invoke a larger gauge symmetry, with the quarks and leptons put together in its multiplets. The SM contains a separate symmetry for the strong interactions, and a mixture of two symmetries results in the weak and electromagnetic interactions. Each symmetry has its own coupling constant, and thus the theory still includes three separate forces. Following a reductionist mentality, it is an attractive idea that these three forces should be unified into one single force. This "grand unified" theory (GUT) could then be spontaneously broken (by SSB similar to the EWSB, for example) at a high energy scale (M_{GUT}), resulting in the three symmetry groups we see at low energies.

However, it is still not clear how this works (if it works at all). A grand unified theory should have one coupling constant at M_{GUT}, which indicates that the three couplings we see at low energies should converge at some high energy scale. By running the SM couplings, one finds that they approximately unify at $\sim 10^{15}$ GeV, but do not quite meet at a single energy scale. Of course, in carrying out this computation one must assume that there is no additional heavy matter between the weak scale and the GUT scale, and so one must be careful in drawing conclusions. Even if one were to resolve this issue, however, it would still raise the question why the grand unified symmetry is apparently broken to $\mathrm{SU}(3)_C \times \mathrm{SU}(2)_L \times \mathrm{U}(1)_Y$ at $M_{GUT} \sim 10^{15}$ GeV, whereas the electroweak symmetry is broken, $\mathrm{SU}(2)_L \times \mathrm{U}(1)_Y \to \mathrm{U}(1)_{\mathrm{EM}}$ at the weak scale $v \sim 246$ GeV. Such a large hierarchy seems unnatural.

1.3.2 The Electroweak Symmetry-Breaking

As we saw above, the SM uses a Higgs doublet to generate the EWSB. Thus, there is a physical Higgs boson h remaining after generation of the $W^{\pm}$ and Z masses. The

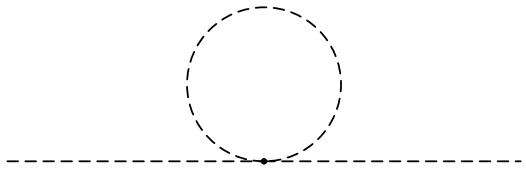

Figure 1.1: A Feynman diagram illustrating quantum corrections to the scalar mass coming from a self-interaction.

Higgs boson has yet to be discovered experimentally, and thus we still lack direct evidence that the method of SSB employed by the SM is correct. In fact, from the discussion above it should be clear that the Higgs sector of the SM contains most of the assumptions that went into the SM. For example, the interactions of gauge bosons with each other and the fermions is fixed in terms of the three gauge couplings g_1, g_2, and g_3. On the other hand, all fifteen of the remaining parameters in the SM are related to the Higgs interactions with the fermions and with itself [15].

The Higgs boson is also a source of fine-tuning in the SM. If one computes the quantum corrections to its mass coming from the self-interaction in the Higgs potential (from Feynman diagrams such as that shown in Figure 1.1), one finds that the corrections have the form,

$$\delta M_h^2 \sim \lambda \Lambda^2, \tag{1.33}$$

where Λ is a cut-off introduced to represent the high energy scale at which the SM ceases to be a good description of nature. We have already seen that such a scale is expected to occur at the Planck mass (though if there is new physics at lower energy scales then it could also be lower). This indicates that whatever the mass of the Higgs is at tree-level, quantum corrections tend to push it to the scale Λ. In order for the Higgs to have mass around the weak scale, one must require an amazing degree of cancellation between the bare Higgs mass and the quantum corrections to occur such that we subtract two quantities of order Λ (possibly as high as $M_{Planck} \sim 10^{19}$ GeV) and arrive at a difference on the order of the weak scale, v. It is in this sense that

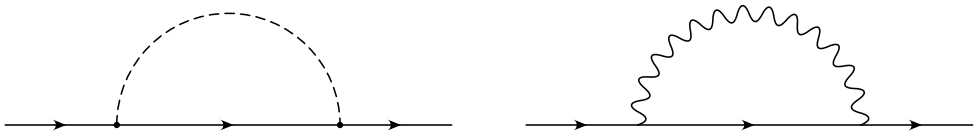

Figure 1.2: Feynman diagrams illustrating quantum corrections to the fermion mass coming from interactions with a scalar or a vector boson.

the Higgs mass requires fine-tuning. It seems quite unnatural that such a delicate cancellation should occur between these two a priori unrelated quantities.

It is not very satisfying to simply accept that the Higgs might be an extremely heavy particle. If that is the case, then one must ask the question why the EWSB contains these two very different energy scales, M_h, and M_Z. This itself seems quite unnatural. Further, if $M_h >$ about 1 TeV, the interaction between the longitudinal $W^{\pm}$ and Z bosons becomes non-perturbative [16], and the perturbative expansion of the SM will no longer suffice to accurately compute scattering amplitudes. In fact, precision measurements at LEP [13] and the Tevatron [14] indicate that for consistency with the SM, the data prefers a Higgs boson lighter than a few hundred GeV.

While on the subject of radiative corrections to particle masses, we note that the situation is very different for fermion masses, which have quantum corrections (from Feynman diagrams such as the ones shown in Figure 1.2),

$$\delta m_f \sim g^2 \, m_f \, \log\left(\frac{\Lambda}{m_f}\right), \tag{1.34}$$

where g is the coupling of the fermion to the boson in Figure 1.2. In this equation, we see two features. The first is that the correction to m_f is proportional to m_f itself[6]. The second occurs because the requirement that δm_f be proportional to m_f

[6]This can be easily understood from the fact that a theory of fermions with no masses contains a chiral symmetry that protects the fermion mass from acquiring quantum corrections. Introducing a fermion mass, m_f, breaks this symmetry, and since m_f is now the order parameter that indicates that the symmetry is broken, the quantum corrections are proportional to it.

means any function of lambda multiplying m_f must be dimensionless (and because of ultraviolet (UV) singularities in the loop integrals, divergent as $\Lambda \to \infty$). Thus the correction depends only on $\log \Lambda$ and it is clear that the corrections to m_f are naturally of the same order as m_f itself.

A further weakness of the SM coming from the Higgs sector is the problem of "triviality". This problem arises in any theory of a scalar field interacting with itself via a quartic interaction. From Equation 1.16 and the discussion following it, it is clear that such a term is vital in the SM to induce SSB. The problem can be studied by examining the running coupling for the quartic scalar interaction. From next-to-leading order (NLO) in perturbation theory, the running coupling may be expressed,

$$\lambda(\mu) = \frac{\lambda_0}{1 - \frac{3\,\lambda_0}{4\,\pi^2} \log(\frac{\mu}{\mu_0})}, \tag{1.35}$$

with $\lambda_0 = \lambda(\mu_0)$ the value of the coupling at some reference energy scale. This expression shows that for a given $\lambda(\mu_0)$, there is a large energy scale for which the denominator goes to zero, and thus the coupling blows up. If the SM is to remain perturbatively valid all the way to the Planck scale, this limits the size of $\lambda(\mu_0)$ at the weak scale. As we saw above, $\lambda(\mu_0)$ is related to M_h, and so this statement can be reformulated as saying that if the SM is to remain valid to the Planck scale, M_h must be smaller than about 1 TeV. The precise M_h for which the break-down occurs also depends on contributions from the heavy top quark, and is best studied non-perturbatively (i.e., on a lattice) because as the coupling becomes large, results based on the perturbative expansion are not expected to be very reliable. This issue is generally referred to as "triviality" because the only way to guarantee that the SM is valid to an arbitrarily high energy scale is to take $\lambda(\mu_0) \to 0$, which results in a trivial, non-interacting scalar theory.

Because of these apparent problems (triviality and fine-tuning) associated with

scalar fields, there are a number of proposed extensions of the SM that hope to address these weaknesses. There are two widely considered models that fall into this category. The first class of models, the supersymmetry (SUSY) models [17], invoke an additional symmetry relating bosons and fermions to stabilize the Higgs sector of the SM. Under SUSY, each field of the SM is given a partner with identical charges, but spin differing by $\frac{1}{2}$. Loops of fermions appear in the quantum corrections to the Higgs mass with a negative sign relative to the scalar contributions, and cancel the quadratic divergences, thus removing the fine-tuning problem. In the minimal supersymmetric standard model (MSSM) [18], the quartic Higgs interaction is related to the gauge interactions, with a different behavior under the renormalization group than the quartic interaction of the SM. This takes care of the triviality problem.

The second class of model can be generically referred to as dynamical symmetry breaking models. There are many models of this kind, with the common feature that the Higgs mechanism results not from a fundamental scalar field acquiring a VEV, but from a composite scalar operator condensing. This composite operator may be built from heavy fermion fields whose masses, as shown above, are not subject to large quantum corrections. Thus, the problems with a scalar field are side-stepped by requiring that the scalar is not fundamental. At high enough energies the low energy effective theory in terms of a scalar particle breaks down, and one is left with a theory without scalar particles, whose high energy behavior is thus improved. Examples of this type of theory include technicolor models [19], top-condensate models [20], and top-color models [21].

1.3.3 The Fermion Mass Hierarchy

Having discussed some of the issues involved in using the Higgs mechanism to generate masses for the gauge bosons, we now examine the fermions. A deep puzzle of the SM

is the question as to why there exist three generations, interacting identically with the gauge bosons, but very differently with the Higgs doublet, as can be seen by the wide range of masses listed in Table 1.2. Outstanding issues include the questions of why there are three families (and not some other number), why neutrinos are massless whereas the other fermions are massive, why the top quark is so much heavier than the other fermions, why the light fermions have masses so much smaller than v (and masses that are so diverse from one another), and why the CKM matrix is almost diagonal and has such a small CP violating phase.

A particular puzzle is the top quark. The top is the only quark to have a mass on the same order as v, and thus a Yukawa interaction close to 1. From that point of view, it seems that the top is the "natural" quark, while all of the other quarks are odd in that their Yukawa couplings are very very small. Another point of view is that the top quark is heavy because it is special in some way, perhaps having been given a special role in the mechanism of EWSB (as, for example, in the top-condensation models which provide the large top mass and the EWSB through the same mechanism). Following this line of thought, it is very natural to study the top quark very carefully. If the top is special in some way, then studies of top should reveal in what way the top is special, and what that means for the EWSB. In the very least, careful study of the top interaction with the Higgs would indicate whether or not the mechanism that generates the top mass is identical to that which generates the boson masses.

1.3.4 The Electroweak Chiral Lagrangian

As we have seen, the Higgs sector of the SM represents the single largest source of our ignorance concerning particle physics : the mechanism of the EWSB. Thus, it seems reasonable that one could expect new phenomena to appear at energies

not much greater than the weak scale, and thus within the range of supercollider experiments currently underway and planned for the future. In order to search for signals of new physics effectively, there are generally two sorts of deviations from the SM that one could consider a sign of new physics. The first is some sort of exotic particle beyond those predicted by the SM. The supersymmetric partners present in a supersymmetrized SM are one example of this type of new phenomenon, and composite scalar bound states of top quarks (or some other heavy fermion) that often arise in dynamical EWSB models are another. Searches for particles of this type are necessarily model-dependent, because one must specify how the "new particle" interacts with the known ones, thus determining how it is produced, what (if anything) it decays into, and even how it interacts with the material of a particle detector. The second class of new phenomenon involves modified properties of the known particles of the SM. This type of modification could be caused, for example, by quantum effects from particles too heavy to be directly produced at colliders. This kind of new phenomenon can be tested in a model-independent way by carefully measuring various masses and interactions of the known particles (and being careful to avoid "assuming the SM" in interpreting the results).

A powerful tool with which one can examine new phenomena is the electroweak chiral Lagrangian (EWCL) [22]. The philosophy behind the EWCL is that since we observe the masses of the $W^{\pm}$ and Z bosons, in some sense we have already seen the would-be Goldstone bosons [23]. Using these ingredients, one can construct the most general effective Lagrangian that realizes the $\mathrm{SU}(2)_L \times \mathrm{U}(1)_Y$ symmetry nonlinearly while preserving $\mathrm{SU}(3)_C \times \mathrm{U}(1)_{\mathrm{EM}}$. The result is an effective theory that is constructed to encapsulate what is known about the presence of the gauge symmetry, while allowing for more freedom in how the symmetry is spontaneously broken than the particular realization of the Higgs mechanism employed in the SM. Further, such a

construction allows one to search for new phenomena in a model-independent fashion. The results may then be applied to learn something about what sort of new physics is consistent with observed data, or to confirm or rule out a given model of physics beyond the Standard Model. Whenever possible, we will present results in the context of the EWCL, in order to be as model-independent as possible.

As the EWCL is to be regarded as an effective theory, one generally includes non-renormalizable interactions. Such interactions have coupling constants with dimensions of inverse mass, and are thus attributed to residual low energy effects from high energy physics (which presumably are renormalizable if one were to know the full high energy theory). Thus, by observing such effects one hopes to learn something about the scale at which these effects become important, and the details of the full theory could be studied. An example of such an operator is a flavor-changing neutral current (FCNC) operator which connects the top quark, the charm quark, and the gluon. In order to respect the $\mathrm{SU}(3)_C$ gauge symmetry, the lowest possible mass dimension of operator is dimension 5 and may be written [24],

$$\mathcal{L}_{gtc} = \frac{g_S}{\Lambda_{gtc}} G^a_{\mu\nu} \left(\kappa_1 \, \bar{t} \, \sigma^{\mu\nu} \, \lambda^a \, c \; + \; \kappa_2 \, \bar{t} \, \sigma^{\mu\nu} \, \gamma_5 \, \lambda^a \, c + H.c. \right), \tag{1.36}$$

where $\kappa_{1,2}$ parameterize the strength of the interaction in terms of $g_S = g_3$ and Λ_{gtc}, which contains the mass dimension of the coupling, may be thought of as the scale at which the effective theory breaks down. The matrix $\sigma^{\mu\nu}$ is related to the Dirac matrices by,

$$\sigma^{\mu\nu} = \frac{i}{2} \left[\gamma^\mu, \gamma^\nu \right] = \frac{i}{2} \left(\gamma^\mu \, \gamma^\nu - \gamma^\nu \, \gamma^\mu \right). \tag{1.37}$$

In constructing this operator, we have followed the usual EWCL procedure of defining the fermion fields such that they transform under $\mathrm{SU}(2)_L \times \mathrm{U}(1)_Y$ the same way they transform under $\mathrm{U}(1)_{\mathrm{EM}}$[7]. As we shall see in Chapter 2, this operator may have

[7] This may be accomplished by including an exponential of the Goldstone bosons in the definition of the fermion field. In the Unitary gauge, this corresponds with the usual definition.

important implications for single top production.

1.3.5 Final Remarks

In presenting the SM, and in exposing its weaknesses, we have obtained some sense of what a theory that hopes to improve our understanding of the electroweak symmetry-breaking needs to accomplish. Many theories propose a wide variety of ways to accomplish this, and finding ways to prove or disprove these theories is one of the current challenges for experimental high energy physics. The remainder of this dissertation is an exploration of several classes of models, with an eye towards the question of how we could discover whether or not these models represent a viable picture of reality. As we have argued, the top quark is a likely place to find new phenomena because of its huge mass. Thus, we begin by studying the process of single top production, which is expected to provide us with the first real understanding of the top's weak interactions. We will employ a mixture of model-independent tools (such as the EWCL) as well as predictions of specific models to show that Run II of the Fermilab Tevatron and the CERN Large Hadron Collider (LHC) represent a wealth of information about the top quark itself, and thus most likely about the EWSB as well.

Chapter 2

Single Top Production

As we saw in Chapter 1, the SM suffers from a number of weaknesses that are in one way or another related to the mechanism of the EWSB, both in the generation of the gauge boson masses and the fermion masses. The attractive idea that the top quark may play a special role in the EWSB was introduced. The definitive test of this hypothesis must come from studying the properties of the top quark. Careful measurement will reveal if it is indeed a SM top, or something different. Indeed, if signals of something beyond the SM exist in top quark observables, careful study of them will provide a means to determine what properties the more fundamental theory must possess in order to explain the observed deviation.

The question of how to discover physics beyond the SM related to the top quark reduces to the question of how the top's properties may be determined in a model-independent fashion, and without making strong assumptions that will bias the interpretation of the measurements. Experiments at the Tevatron[1] Run II and the LHC[2] will observe thousands of top quarks, and thus it is important to examine various ways to probe top quark properties. In this chapter we present a detailed exposition of the available means to obtain information about top, weighing the strengths and

[1]Run II of the Tevatron will involve $p\bar{p}$ collisions with an expected center-of-mass energy of $\sqrt{s} = 2$ TeV.

[2]We use LHC to denote a pp collider with center-of-mass energy $\sqrt{s} = 14$ TeV.

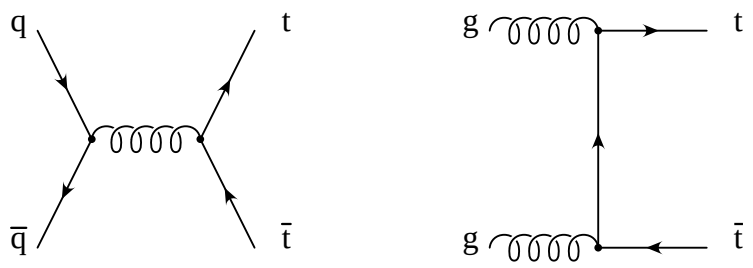

Figure 2.1: Representative Feynman diagrams showing QCD production of $t\,\bar{t}$ pairs: $q\,\bar{q}, g\,g \rightarrow t\,\bar{t}$.

weaknesses of each. In particular we will see that single top production at a hadron collider represents a vital means to study the weak interactions of the top quark, and thus test the possibility of a relationship between top and EWSB. In this entire chapter, we assume a top mass of $m_t = 175$ GeV, unless explicitly noted otherwise.

2.1 Top Quark Properties at a Hadron Collider

At hadron colliders, the dominant mechanism for producing top quarks is to produce pairs of t and $\bar{t}$ through the strong interaction [25], as is shown in Figure 2.1. As dictated by the QCD-improved parton-model [26], the cross section for hadrons scattering into $t\,\bar{t}$ pairs is computed by considering the partonic reactions $q\,\bar{q} \rightarrow t\,\bar{t}$ through a virtual gluon and through fusion of two gluons, $g\,g \rightarrow t\,\bar{t}$. These partonic cross sections are then convolved with universal parton distribution functions (PDF's) [27] which contain non-perturbative information about the likelihood of finding a particular parton inside a parent hadron carrying a given fraction of the parent hadron's momentum. It is well known that the gluon distribution function is much larger at very low momentum fraction than the corresponding valence quark distributions, but falls much more rapidly as the momentum fraction increases. For the production of massive top quarks, this has the consequence that at a collider with relatively low center of mass energy such as the Tevatron the dominant subprocess will be from $q\,\bar{q}$

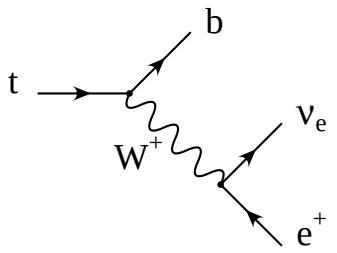

Figure 2.2: Feynman diagram showing the top decay into $W^+ b$, including the leptonic decay $W^+ \to e^+ \nu_e$.

fusion, whereas a collider with a much higher center of mass energy such as the LHC has a dominant contribution from $g\,g$ fusion. It is clear that the rate of $t\,\bar{t}$ production (coming from either subprocess) represents a measure of the top's coupling to the gluons.

The large rate of $t\,\bar{t}$ production (about 7.55 pb at the Tevatron Run II and 760 pb at the LHC [25, 28]) insures that it is an important means to study the top quark. As we have seen, it is an important measure of the top's strong interactions, and could also be sensitive to some kind of new physics resonance in $t\,\bar{t}$ production. It also allows one to measure the top quark mass, m_t, by reconstructing the top mass from the top decay products. From Run I of the Tevatron, a combined CDF and DØ measurement of $m_t = 174.3 \pm 5.1$ GeV based on direct observation of top has been made, and it is hoped that improved statistics at Run II of the Tevatron will allow a more precise measurement of ± 2 GeV [14].

Top quarks are identified by their decay products. In the SM, the top decays into a W^+ boson and a down-type quark (predominantly bottom because $V_{tb} \gg V_{ts}, V_{td}$) [29], through Feynman diagrams such as that shown in Figure 2.2. Its width can thus be computed in terms of the top mass, the gauge couplings, and the CKM elements V_{td}, V_{ts}, and V_{tb}. The SM prediction is found to be about 1.5 GeV, much larger than for any other quark. This large decay width indicates that the top decays very

quickly, before it has time to hadronize[3] [30]. This fact means that even aside from the strong motivation to study top as a means to understand the EWSB, there is also interest in top because it is the only quark that we are able to study "bare". Since the top decays into a W^+ and b with a branching ratio (BR) close to one, top decays are distinguished by the W^+ decay products. The hadronic decays ($W^+ \to q\,q'$) are dominant (with BR $\sim$ 6 / 9), however the leptonic decays ($W^+ \to \ell^+\,\nu_\ell$) generally provide a clean signature at a hadron collider.

Clearly studying top decays provides some information about the top's weak interactions. However, there is an important fact to keep in mind while considering top decays; a study of decays can measure BR's but since it does not actually measure the decay width itself, it is not directly proportional to the coupling, and thus cannot measure the magnitude of the W-t-b coupling. Thus, if the W-t-b vertex is modified, but no new decay modes appear, the BR for $t \to W^+\,b$ will remain close to 1, despite the fact that new physics is affecting the structure of the interaction. A further problem in using top decays to search for new physics is that exotic top decays may be unobservable or unrecognized as originating from top quarks, and therefore could be missed. Despite these weaknesses, as we shall see in Section 2.4, top decays are an excellent opportunity to explore the Dirac structure of the W-t-b interaction, testing the left-handed nature of the SM weak interactions of the top.

A powerful probe of the top's weak interactions is provided by single top production, in which a top (or anti-top) quark is produced singly through the weak interaction. There are three important modes of single top production in the SM: the s-channel W^* mode [31] in which a virtual off-shell W boson is produced which then decays into $t\,\bar{b}$; the t-channel W-gluon fusion mode [32] in which a W is exchanged

[3] A simple heuristic way to understand this is to notice that the top width (1.5 GeV) is very much larger than $\Lambda_{\rm QCD} \sim 200$ MeV, the scale at which non-perturbative effects in the strong force become important.

between a bottom quark and a light quark, resulting in a top and a jet; and the tW^- mode [33] in which a bottom quark radiates an on-shell W^- boson, resulting in a tW^- final state. The SM rates of these three processes at the Tevatron and LHC, as a function of the top mass, are presented in Figure 2.3.

Single top production represents a genuine opportunity to probe the magnitude of the W-t-b vertex because in this case the size of the cross section is directly proportional to the W-t-b coupling. In the SM, this allows one to measure V_{tb}. In a model of new physics involving the top, this could lead to a discovery of the new physics. In the following sections we will discuss the three modes of single top production in some detail, first in the context of the SM, and then in regards to their sensitivity to new physics effects. The issue of the top polarization will also be discussed, and it will be demonstrated that not only can the polarization of the top be observed, but it can provide interesting information about the structure of the interactions of the top.

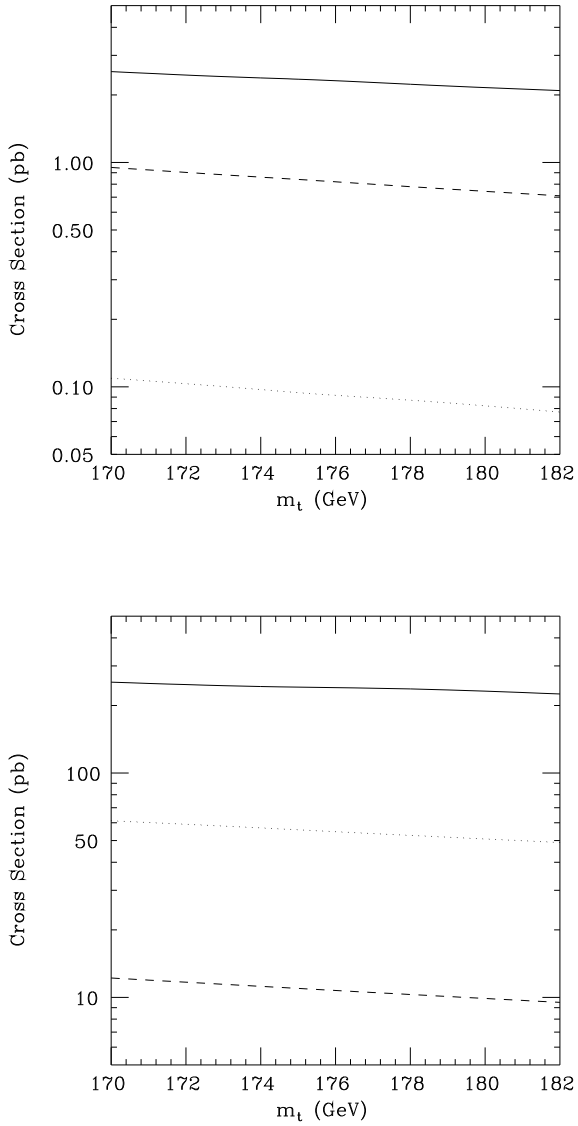

Figure 2.3: The SM rate of the three modes of single top production, as a function of m_t (summing the rates of t and $\bar{t}$ production), at the Tevatron (upper figure) and LHC (lower figure). The solid curve is the NLO t-channel rate, taken as the average of the results from CTEQ4M and MRRS(R1) PDF's. The dashed curve is the NLO s-channel rate, taken as the average of the results from CTEQ4M and MRRS(R1) PDF's. The dotted curve is the LO tW^- rate, including large log corrections, taken as the average of the CTEQ4L and MRRS(R1) results.

2.2 Single Top Production in the SM

The production mechanisms for the three modes of single top production are quite different, and it is worth spending some time discussing the particular physics aspects of each mode individually. In this discussion, we avoid detailed consideration of the particular kinematics and detection strategy for each mode, as this has been considered elsewhere [31, 32, 34]. Instead we concentrate on the inclusive rates and the effects of nonstandard physics on each process, as our goal is to understand how single top production serves as an important probe of new physics effects. We begin with the SM rates, and discuss the theoretical issues involved in SM single top production.

In fact, it will be shown that the three modes are separately susceptible to quite different types of new physics [35], and can potentially be observed independently from each other [34]. Thus, each mode is an independent source of information about the top quark. One sometimes finds in the literature [36, 37] analyses that treat all of the single top modes together as one signal. This practice of combining three signals with quite distinct kinematic signatures together is not good physics; it wastes the information contained in each mode separately. As we will see, the three modes provide complimentary information about the top, and thus are worth examining independently. Further, because the W-gluon fusion rate is generally much larger than the other two modes, these "combined analyses" are really optimized to see that mode, with a small fraction of the other modes that manages to fake the characteristics of a typical t-channel event included as well. Thus there is little practical difference between a combined analysis and one focused on the t-channel process. For these reasons, it is highly preferable to avoid thinking of single top as one process, when it is really three separate ones.

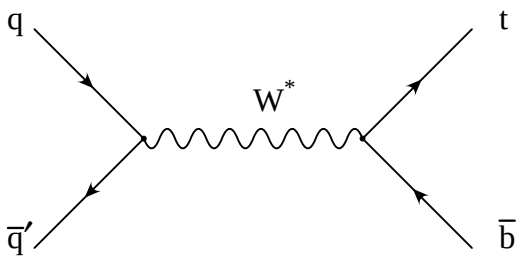

Figure 2.4: Feynman diagram for the s-channel mode of single top production: $q\,\bar{q}' \to W^* \to t\,\bar{b}$.

2.2.1 W^* Production

The W^* mode of single top production proceeds through an s-channel W boson, as shown in Figure 2.4. The final state consists of a top quark and a central jet containing a $\bar{b}$. Because the initial partons include both a quark and an anti-quark, this process is relatively large at a high energy $p\,\bar{p}$ collider such as the Tevatron, where valence anti-quarks are present in the $\bar{p}$. It has been computed at NLO in QCD corrections [38], and it has been found that the corrections coming from initial state radiation of soft and collinear gluons are rather strong and substantially increase the cross section. The resulting NLO cross section is $\sigma_s = 0.84$ pb at the Tevatron Run II and $\sigma_s = 11.0$ pb at the LHC. The rather small increase in the cross section in going from the Tevatron to LHC (compared to the other channels) can be understood from the fact that the LHC is a $p\,p$ collider, and thus has no valence anti-quarks. In Tables 2.1, 2.2 and 2.3, we present the NLO cross section, as a function of the top quark mass for the Tevatron Run II and LHC, for several choices of the scale[4] and the CTEQ4M [39] and MRRS(R1) [40] PDF's. The mean cross section is defined to be the average of the CTEQ4M and MRRS(R1) results evaluated at the canonical scale choice. These rates are for the production process, $q\,\bar{q}' \to t\,\bar{b}$ only, and do not include the branching ratios for any particular top decay. V_{tb} has been assumed to be one, and V_{ts} and V_{td}

[4]In principle the factorization scale and the renormalization scale may be chosen independently. In practice, we follow the usual procedure of choosing them to be equal to each other.

have been neglected, as they are so small that their effect on the cross section is much less than 1% of the s-channel rate.

The theoretical prediction for the cross section shows a rather small dependence on the renormalization and factorization scales of about $\pm 5\%$, when the scale is varied from the default value of $\mu_0^s = \sqrt{s}$ by a factor of 2, indicating that the uncomputed higher order QCD corrections are probably small. The distribution functions of quarks and anti-quarks in the proton are relatively well-determined by deeply inelastic scattering (DIS) data, and thus this important input to the theoretical prediction is rather well understood. The mass of the top quark is another important quantity that will affect the predicted cross section. The W^* mode is particularly sensitive to this quantity, because it not only determines the phase space of the produced particles, but also controls how far off-shell the virtual W^* boson must be.

Table 2.1: The NLO rates of $q\,\bar{q}' \to W^* \to t\,\bar{b}$ (in pb) at the Tevatron Run II. At the Tevatron, the rate of $\bar{t}$ production is equal to the t production rate.

	CTEQ4M			MRRS(R1)			
m_t (GeV)	$\mu = \mu_0^s/2$	$\mu = \mu_0^s$	$\mu = 2\mu_0^s$	$\mu = \mu_0^s/2$	$\mu = \mu_0^s$	$\mu = 2\mu_0^s$	$\sigma_s^{(mean)}$
170	0.53	0.49	0.46	0.495	0.46	0.425	0.475
171	0.52	0.485	0.445	0.485	0.45	0.415	0.465
172	0.51	0.475	0.435	0.475	0.435	0.405	0.455
173	0.495	0.46	0.425	0.46	0.425	0.395	0.44
174	0.48	0.445	0.415	0.45	0.415	0.385	0.43
175	0.465	0.43	0.405	0.44	0.405	0.375	0.42
176	0.45	0.415	0.395	0.425	0.395	0.365	0.41
177	0.445	0.405	0.385	0.415	0.385	0.36	0.405
178	0.435	0.40	0.375	0.405	0.375	0.35	0.39
179	0.43	0.395	0.365	0.395	0.365	0.34	0.38
180	0.42	0.39	0.355	0.385	0.355	0.335	0.37
181	0.41	0.38	0.345	0.375	0.35	0.325	0.36
182	0.395	0.365	0.34	0.37	0.34	0.315	0.355

Table 2.2: The NLO rates of $q\,\bar{q}' \to W^* \to t\,\bar{b}$ (in pb) at the LHC.

	CTEQ4M			MRRS(R1)			
m_t (GeV)	$\mu = \mu_0^s/2$	$\mu = \mu_0^s$	$\mu = 2\mu_0^s$	$\mu = \mu_0^s/2$	$\mu = \mu_0^s$	$\mu = 2\mu_0^s$	$\sigma_s^{(mean)}$
170	7.2	7.5	7.8	7.0	7.3	7.4	7.4
171	7.1	7.4	7.6	6.8	7.1	7.25	7.25
172	6.9	7.2	7.5	6.7	6.9	7.1	7.05
173	6.8	7.1	7.3	6.55	6.8	6.95	6.95
174	6.7	6.9	7.1	6.4	6.65	6.8	6.78
175	6.5	6.8	7.0	6.3	6.5	6.65	6.65
176	6.4	6.6	6.9	6.2	6.4	6.5	6.5
177	6.3	6.5	6.7	6.05	6.25	6.4	6.38
178	6.1	6.4	6.6	5.9	6.1	6.25	6.25
179	6.0	6.3	6.4	5.8	6.0	6.1	6.15
180	5.9	6.1	6.3	5.7	5.9	6.0	6.0
181	5.8	6.0	6.2	5.6	5.75	5.9	5.88
182	5.7	5.9	6.1	5.5	5.65	5.8	5.78

Table 2.3: The NLO rates of $q\,\bar{q}' \to W^* \to b\,\bar{t}$ (in pb) at the LHC.

	CTEQ4M			MRRS(R1)			
m_t (GeV)	$\mu = \mu_0^s/2$	$\mu = \mu_0^s$	$\mu = 2\mu_0^s$	$\mu = \mu_0^s/2$	$\mu = \mu_0^s$	$\mu = 2\mu_0^s$	$\sigma_s^{(mean)}$
170	4.5	4.7	4.8	4.2	4.4	4.5	4.55
171	4.4	4.6	4.7	4.1	4.3	4.4	4.45
172	4.3	4.5	4.6	4.0	4.2	4.3	4.35
173	4.2	4.4	4.5	3.9	4.1	4.2	4.25
174	4.1	4.3	4.4	3.85	4.0	4.1	4.15
175	4.0	4.2	4.3	3.8	3.9	4.0	4.05
176	3.9	4.1	4.2	3.7	3.8	3.9	3.95
177	3.8	4.0	4.1	3.6	3.7	3.8	3.85
178	3.75	3.9	4.0	3.5	3.65	3.75	3.78
179	3.7	3.8	3.9	3.45	3.6	3.7	3.7
180	3.6	3.7	3.85	3.4	3.5	3.6	3.6
181	3.5	3.65	3.8	3.3	3.4	3.5	3.53
182	3.45	3.6	3.7	3.25	3.35	3.4	3.48

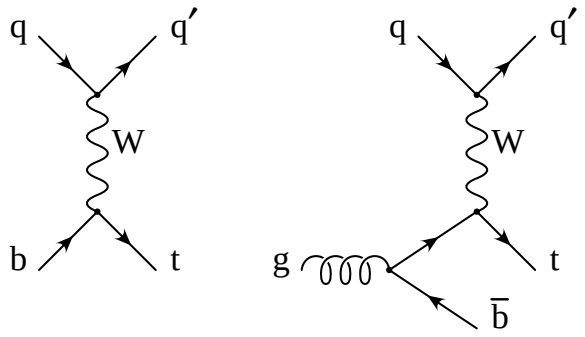

Figure 2.5: Feynman diagrams for the t-channel mode of single top production: $b\,q \to t\,q'$. A second process in which the incoming light quark is switched with a light $\bar{q}$ is also possible.

2.2.2 W-gluon Fusion

The W-gluon fusion production mode involves a t-channel W exchange, as shown in Figure 2.5. Thus, its final state consists of a top quark and a jet that tends to be forward. It relies on the possibility of finding bottom quarks inside the hadrons involved in a high energy collision in order to produce a single top quark. The name "W-gluon fusion" can be understood in that the physical picture is that the process actually involves a virtual gluon splitting into a $b\,\bar{b}$ pair, with one of the bottom quarks participating in the high energy scattering. One could thus compute the inclusive cross section starting from a quark-gluon initial state, but the result is not perturbatively reliable because the kinematic region in which the $b\,\bar{b}$ pair from the gluon splitting is approximately collinear with the initial gluon produces a contribution that is proportional to $\alpha_S \log m_t^2/m_b^2$, which for $m_t \sim 175$ GeV, $m_b \sim 4.5$ GeV, and $\alpha_S \sim 0.1$ is over-all of order 1. In fact, the nth order correction always contains a collinear piece which has the behavior $(\alpha_S \log m_t^2/m_b^2)^n$, which spoils the perturbative description of this process. A convergent perturbative expansion can be restored by resumming these large logarithms into a bottom quark parton distribution function [41]. This PDF is different from the light quark PDF's in that it is actually perturba-

tively derived from the gluon distribution function. In fact, this two particle to two particle ($2 \to 2$) description of the scattering represents the most important part of the W-gluon fusion kinematics, because the dominant kinematic configuration is one in which the incoming bottom is collinear with the gluon [42]. It should be kept in mind that the b PDF has effectively integrated out the $\bar{b}$ kinematics, so this formalism does not accurately describe the kinematic region in which the $\bar{b}$ has large transverse momentum (p_T). In this region, a description based on the two to three scattering is more appropriate (and since this is precisely the region in which the b is not collinear with the incoming gluon, it is well-defined in perturbation theory). The resulting NLO cross section is $\sigma_t = 2.53$ pb at the Tevatron and 241 pb at the LHC.

This strong dependence on the gluon PDF is a large source of uncertainty in the prediction for the W-gluon fusion cross section. The DIS experiments are much less sensitive to the gluon density than to the quark density, and thus the gluon density is much less well determined, particularly in the high momentum fraction region relevant for single top production. Though it is not a quantitative measure of the uncertainty from the PDF, this fact is reflected in the larger dependence of the W-gluon fusion rate on the choice of PDF in the computation.

The NLO QCD corrections to W-gluon fusion are slightly negative at both the Tevatron and LHC [43]. The NLO cross section varies by about $\pm 6\%$ at the Tevatron and $\pm 5\%$ at the LHC when the natural scale choice of $\mu_0^t = \sqrt{Q^2 + m_t^2}$ is varied by a factor of 2, where Q^2 is related to the W boson momentum by $Q^2 = -p_W^2$. This again indicates that the NLO inclusive rate is expected to be fairly insensitive to the uncomputed higher order QCD corrections. In Tables 2.4, 2.5, and 2.6, we show σ_t for various top masses, PDF choices, and scales at the Tevatron Run II and LHC. These rates are for the production process $b\,q \to t\,q'$, with $V_{tb} = 1$ and $V_{ts}, V_{td} = 0$.

Table 2.4: The NLO rates of $b\,q \to t\,q'$ (in pb) at the Tevatron Run II. At the Tevatron, the rate of $\bar{t}$ production is equal to the rate of t production.

	CTEQ4M			MRRS(R1)			
m_t (GeV)	$\mu = \mu_0^t/2$	$\mu = \mu_0^t$	$\mu = 2\mu_0^t$	$\mu = \mu_0^t/2$	$\mu = \mu_0^t$	$\mu = 2\mu_0^t$	$\sigma_t^{(mean)}$
170	1.255	1.31	1.365	1.18	1.22	1.26	1.265
171	1.235	1.285	1.355	1.16	1.195	1.235	1.24
172	1.215	1.26	1.34	1.14	1.175	1.215	1.22
173	1.195	1.24	1.32	1.12	1.155	1.195	1.20
174	1.175	1.225	1.30	1.105	1.135	1.175	1.18
175	1.155	1.205	1.275	1.085	1.12	1.155	1.165
176	1.135	1.19	1.25	1.07	1.105	1.135	1.15
177	1.115	1.17	1.225	1.05	1.085	1.12	1.13
178	1.095	1.115	1.20	1.035	1.07	1.10	1.115
179	1.075	1.14	1.175	1.02	1.055	1.08	1.10
180	1.06	1.12	1.155	1.00	1.035	1.065	1.08
181	1.045	1.10	1.14	0.985	1.015	1.045	1.06
182	1.03	1.08	1.125	0.97	0.995	1.03	1.04

Table 2.5: The NLO rates of $b\,q \to t\,q'$ (in pb) at the LHC.

	CTEQ4M			MRRS(R1)			
m_t (GeV)	$\mu = \mu_0^t/2$	$\mu = \mu_0^t$	$\mu = 2\mu_0^t$	$\mu = \mu_0^t/2$	$\mu = \mu_0^t$	$\mu = 2\mu_0^t$	$\sigma_t^{(mean)}$
170	156	161	165	154	157	164	159
171	154	160	164	153	155	162	157.5
172	152	159	163	152	153	161	156
173	150	157	162	150	152	160	154.5
174	149	156	160	149	151	158	153.5
175	147	155	159	148	150	157	152.5
176	146	154	158	147	149	155	151.5
177	144	153	157	146	148	154	150.5
178	142	152	155	145	147	152	149.5
179	141	151	154	143	146	151	148.5
180	140	150	153	142	145	149	147.5
181	139	148	152	141	144	148	146
182	138	147	151	140	143	147	145

Table 2.6: The NLO rates of $\bar{b}\,q \to \bar{t}\,q'$ (in pb) at the LHC.

	CTEQ4M			MRRS(R1)			
m_t (GeV)	$\mu = \mu_0^t/2$	$\mu = \mu_0^t$	$\mu = 2\mu_0^t$	$\mu = \mu_0^t/2$	$\mu = \mu_0^t$	$\mu = 2\mu_0^t$	$\sigma_t^{(mean)}$
170	90	93	96	90	98	95	95.5
171	89.5	91	95	89.5	96	95	93.5
172	89	89.5	94	89	94	93	91.8
173	88.5	89	93.5	88.5	92	92	90.5
174	88	88	93	88	90	91	89
175	87.5	87.5	92	87	89	90	88.3
176	87	87	91	86	88	89	87.5
177	86.5	86.5	90	84	87	88	86.8
178	86	86	89	83	86	87	86
179	85	85.5	88	82	85	86	85.3
180	84	85	86	81	84	85	84.5
181	83	84	85	80	83	84	83.5
182	82	83	84	78	82	82	82.5

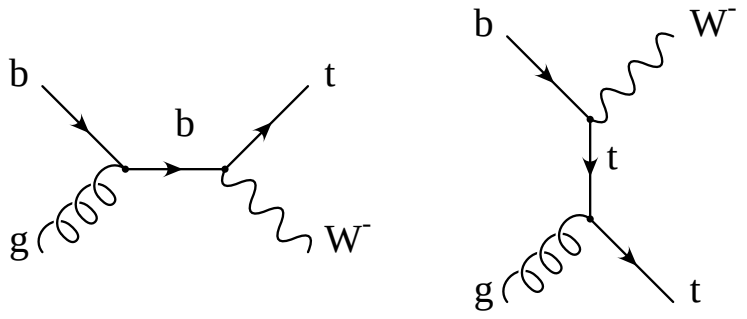

Figure 2.6: Feynman diagrams for the tW^- mode of single top production: $gb \to tW^-$.

2.2.3 tW^- Production

The tW^- mode of single top production proceeds from Feynman diagrams such as those presented in Figure 2.6. The final state consists of an on-shell W^- (which can decay either to quarks or leptons) and a top quark. It should be quite clear that the signature of this process is very distinct from the other two modes, because of the extra W^- decay products in the final state. This process also involves finding a bottom quark inside one of the colliding hadrons, and the same issues related to this fact that were present in the W-gluon fusion process discussed above are also important here, in particular a rather strong dependence on the gluon PDF used to obtain the prediction.

Though the complete NLO QCD corrections are not available, one can improve the LO estimates by including the $\mathcal{O}(1/\log m_t^2/m_b^2)$ corrections coming from Feynman diagrams such as those in Figure 2.7 There are two subtle points that must be carefully dealt with in carrying out this procedure. The first is that when the b PDF was defined, the collinear contributions from these diagrams was already resummed into what we called the LO contribution. Thus, in order to avoid double-counting this collinear region one must subtract out the piece already included in the LO

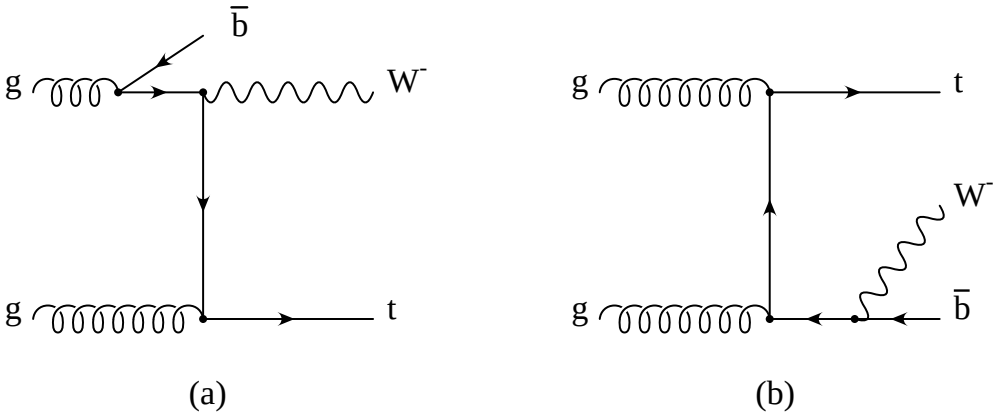

Figure 2.7: Representative Feynman diagrams for corrections to the $t\,W^-$ mode of single top production corresponding to (a) large log corrections associated with the b PDF and (b) LO $t\,\bar{t}$ production followed by the LO decay $\bar{t} \to W^-\,\bar{b}$.

contribution. The full cross section for $A\,B \to t\,W^-$ may thus be expressed as,

$$\sigma_{tW} = \sigma^0(A\,B \to t\,W^-) + \sigma^1(A\,B \to t\,W^-\,\bar{b}) - \sigma^S(A\,B \to t\,W^-\,\bar{b}), \tag{2.1}$$

with the individual terms given by,

$$\begin{aligned}
\sigma^0(A\,B \to t\,W^-) &= \int dx_1\,dx_2 \Big\{ f_{g/A}(x_1,\mu)\, f_{b/B}(x_2,\mu)\, \sigma(b\,g \to t\,W^-) \\
&\quad + f_{b/A}(x_1,\mu)\, f_{g/B}(x_2,\mu)\, \sigma(g\,b \to t\,W^-) \Big\} \\
\sigma^1(A\,B \to t\,W^-\,\bar{b}) &= \int dx_1\,dx_2\; f_{g/A}(x_1,\mu)\, f_{g/B}(x_2,\mu)\, \sigma(g\,g \to t\,W^-\,\bar{b}) \\
\sigma^S(A\,B \to t\,W^-\,\bar{b}) &= \int dx_1 dx_2 \Big\{ \tilde{f}_{b/A}(x_1,\mu)\, f_{g/B}(x_2,\mu)\, \sigma(b\,g \to t\,W^-) \\
&\quad + f_{g/A}(x_1,\mu)\, \tilde{f}_{b/B}(x_2,\mu)\, \sigma(g\,b \to t\,W^-) \Big\}.
\end{aligned} \tag{2.2}$$

The "modified b PDF", $\tilde{f}_{b/H}$, contains the collinear logarithm and splitting function $P_{b\leftarrow g}$ convoluted with the gluon PDF,

$$\tilde{f}_{b/H}(x,\mu) = \frac{\alpha_S(\mu)}{2\,\pi} \log\left(\frac{\mu^2}{m_b^2}\right) \int_x^1 \frac{dz}{z} \left[\frac{z^2 + (1-z)^2}{2}\right] f_{g/H}\left(\frac{x}{z},\mu\right). \tag{2.3}$$

Having included this subtraction piece, the problem of double-counting the collinear region is resolved.

The second subtle point in evaluating the large log contributions is that they contain contributions such as those found in Figure 2.7b that correspond to LO $g\,g \to t\,\bar{t}$ production followed by the LO decay $\bar{t} \to W^-\,\bar{b}$. This expresses the fact that as one considers higher orders in perturbation theory, the distinction between $t\,\bar{t}$ production and various types of single top production is blurred. However, when considering quantities that are properly defined, these corrections are small, and there is no problem distinguishing these processes. As a matter of book keeping, the corrections to $t\,W^-$ production involving an on-shell top are more intuitively considered a part of the LO $t\,\bar{t}$ rate, and thus it is important to subtract them out to avoid double counting in this kinematic region. This may be done by noting that in the region where the invariant mass of the $\bar{b}\,W^-$ system, M_{Wb}, is close to the top mass, the behavior of the partonic cross section $\sigma(gg \to t\,W^-\bar{b})$ may be expressed,

$$\begin{aligned}
\frac{d\sigma}{dM_{Wb}}(g\,g \to t\,W^-\,\bar{b}) &= \sigma^{LO}(g\,g \to t\bar{t})\,\frac{m_t\,\Gamma^{LO}(\bar{t} \to W^-\bar{b})}{\pi\,[(M_{Wb}^2 - m_t^2)^2 + m_t^2\,\Gamma_t^2]} \qquad (2.4)\\
&= \sigma^{LO}(g\,g \to t\bar{t})\,\frac{m_t\,\Gamma_t\,BR(\bar{t} \to W^-\bar{b})}{\pi\,[(M_{Wb}^2 - m_t^2)^2 + m_t^2\,\Gamma_t^2]}\\
&\to \sigma^{LO}(g\,g \to t\bar{t})\,BR(\bar{t} \to W^-\bar{b})\,\delta(M_{Wb}^2 - m_t^2)
\end{aligned}$$

where $\sigma^{LO}(g\,g \to t\bar{t})$ and $\Gamma^{LO}(\bar{t} \to W^-\bar{b})$ are the LO cross section and partial width, and Γ_t is the inclusive top decay width. The last distribution identity holds in the limit $\Gamma_t \ll m_t$. Having identified this LO on-shell piece, it may now be simply subtracted from $\sigma(g\,g \to t\,W^-\,\bar{b})$. The advantage to this formulation of the subtraction is that by taking the narrow width limit, one removes all of the on-shell $\bar{t}$ contribution. The interference terms between one of the on-shell $\bar{t}$ amplitudes and an amplitude without an on-shell $\bar{t}$ involve a Breit-Wigner propagator of the form, $(M_{Wb}^2 - m_t^2 + i\,m_t\Gamma_t)^{-1}$, which in the limit of small Γ_t, may be expressed as a principle valued integral in M_{Wb}. Following this prescription, and choosing a canonical scale choice of $\mu_0 = \sqrt{s}$, leads

to a large log correction to the $t\,W^-$ rate of -9.5% at the LHC, which is consistent with previous experience from the W-gluon fusion mode [34].

This problem of the on-shell top was dealt with another way in [37], where a cut was applied on M_{Wb}, to exclude the region of $|M_{Wb} - m_t| \leq 3\,\Gamma_t$. Following this prescription, one finds a much larger correction of about $+50\%$ to the $t\,W^-$ rate at the LHC. However, this is misleading because the large corrections are mostly coming from the region where the $\bar{t}$ is close to on-shell (though still at least 3 top widths away). In other words, the large positive correction comes from the tails of the Breit-Wigner distribution for on-shell $\bar{t}$ production. This can be simply understood by taking the prescription in [37] and varying the cut by increasing the interval about the on-shell $\bar{t}$ region that is excluded. One finds that the correction computed in this way varies quite strongly with the cut, and reproduces the subtraction method we have employed for the cut $|M_{Wb} - m_t| \leq 12\,\Gamma_t$. A further theoretical advantage of the subtraction method is that when one determines the $t\,\bar{t}$ and $t\,W^-$ rates, one would like to actually fit the data to the sum of the two rates, and thus the subtraction method allows one to simply separate this sum into the two contributions without introducing an arbitrary cut-off into the definition of the separation.

Even if one were to use a cut-off to effect the separation, there is a further problem in employing the cut $|M_{Wb} - m_t| \leq 3\,\Gamma_t$ to remove on-shell $t\,\bar{t}$ production. This is that from a purely practical point of view $3\,\Gamma_t \sim 4.5$ GeV, which is much smaller than the expected jet resolution at the Tevatron or LHC. Thus, it is not experimentally possible to impose this definition of the separation between $t\,W^-$ and $t\,\bar{t}$. A more realistic resolution is about 15 GeV [44], which corresponds to a subtraction of $|M_{Wb} - m_t| \leq 10\,\Gamma_t$. As we have seen above, this choice of the M_{Wb} cut agrees rather well with our subtraction method result.

The $t\,W^-$ process has been studied much less intensively than the other two modes, mostly owing to the fact that it has a small rate at the Tevatron Run II ($\sigma_{tW} = 0.094$ pb) that is probably unobservable. On the other hand, the rate is fairly considerable at the LHC ($\sigma_{tW} = 55.7$ pb) and it may be observable there. However, detailed simulations studying means by which the signal may be extracted from the large $t\bar{t}$ background are still underway. For completeness, we include in Tables 2.7 and 2.8 the LO rate (including the large log corrections described above) of $t\,W^-$ production at the Tevatron and LHC, for various choices of m_t, PDF, and scale, with the canonical scale choice set to $\mu_0 = \sqrt{s}$. As usual, the t and $\bar{t}$ rates have been summed, $V_{tb} = 1$, $V_{ts}, V_{td} = 0$ and no decay BR's are included. From these results, we see that varying the scale by a factor of two produces a variation in the resulting cross section of about $\pm 25\%$ at the Tevatron and $\pm 15\%$ at the LHC. This large scale dependence signals the utility in having a full NLO in α_S computation of this process in order to have a more theoretically reliable estimate for the cross section.

Table 2.7: The LO (with $\mathcal{O}(1/\log m_t^2/m_b^2)$ corrections) rates of $b\,g \to t\,W^-$ (in pb) at the Tevatron Run II. The rate of $\bar{t}$ production is equal to the rate of t production.

	CTEQ4L			MRRS(R1)			
m_t (GeV)	$\mu = \mu_0/2$	$\mu = \mu_0$	$\mu = 2\mu_0$	$\mu = \mu_0/2$	$\mu = \mu_0$	$\mu = 2\mu_0$	$\sigma_{tW}^{(mean)}$
170	0.0645	0.0505	0.0405	0.076	0.058	0.046	0.0545
171	0.063	0.049	0.0395	0.074	0.0565	0.0445	0.053
172	0.061	0.048	0.0385	0.072	0.055	0.0435	0.0515
173	0.0595	0.0465	0.0375	0.07	0.053	0.042	0.05
174	0.0575	0.045	0.0365	0.068	0.0515	0.041	0.0485
175	0.056	0.044	0.0355	0.066	0.05	0.0395	0.047
176	0.0545	0.0425	0.0345	0.064	0.049	0.0385	0.046
177	0.053	0.0415	0.0335	0.062	0.0475	0.0375	0.0445
178	0.0515	0.0405	0.0325	0.06	0.046	0.0365	0.0435
179	0.05	0.039	0.0315	0.0585	0.0445	0.0355	0.042
180	0.0485	0.038	0.0305	0.057	0.0435	0.0345	0.041
181	0.0475	0.037	0.03	0.0555	0.0425	0.0335	0.040
182	0.046	0.036	0.029	0.054	0.041	0.0325	0.0385

Table 2.8: The LO (with $\mathcal{O}(1/\log(m_t^2/m_b^2)$ corrections) rates for $b\,g \to t\,W^-$ (in pb) at the LHC. The rate of $\bar{t}$ production is equal to the rate of t production.

	CTEQ4L			MRRS(R1)			
m_t (GeV)	$\mu = \mu_0/2$	$\mu = \mu_0$	$\mu = 2\mu_0$	$\mu = \mu_0/2$	$\mu = \mu_0$	$\mu = 2\mu_0$	$\sigma_{tW}^{(mean)}$
170	33.0	28.2	24.5	39.0	33.0	28.4	30.6
171	32.2	27.5	24.0	38.3	32.5	27.9	30.0
172	31.6	27.1	23.6	37.6	31.8	27.4	29.4
173	31.1	26.6	23.1	38.0	31.3	26.9	28.9
174	30.5	26.1	22.7	36.2	30.7	26.4	28.4
175	29.9	25.6	22.2	35.4	30.1	26.0	27.9
176	29.4	25.2	21.8	34.8	29.6	25.5	27.4
177	28.9	24.7	21.5	34.2	28.9	25.0	26.8
178	23.3	24.2	21.1	33.6	28.4	24.6	26.3
179	27.8	23.7	20.7	33.0	27.9	24.1	25.8
180	27.2	23.3	20.3	32.4	27.4	23.7	25.4
181	26.8	22.9	20.0	31.8	26.9	23.2	24.9
182	26.3	22.5	19.6	31.2	26.4	22.9	24.5

2.3 New Physics in Single Top Production

As we have argued above, single top production is an important place to search for physics beyond the SM. This is reflected in the growing body of literature in which the effect of loops of new particles on the single top rate is examined [45]. In this section, we analyze several possible signals for new physics that could manifest themselves in single top production. These signals can be classified as to whether they involve the effects of a new particle (either fundamental or composite) that couple to the top quark, or the effect of a modification of the SM coupling between the top and other known particles. In fact these two classifications can be seen to overlap in the limit in which the additional particles are heavy and decouple from the low energy description. In this case the extra particles are best seen through their effects on the couplings of the known particles.

2.3.1 Additional Nonstandard Particles

Many theories of physics beyond the SM predict the existence of particles beyond those required by the SM itself. Examples include both the fundamental super-partners in a theory with SUSY, and the composite top-pions found in top-condensation and top-color models. In order for some kind of additional particle to contribute to single top production at a hadron collider, the new particle must somehow couple the top to one of the lighter SM particles. Thus, the new particle may be either a boson (such as a W' vector boson that couples to top and bottom) or a fermion (such as a b' quark that couples to the W boson and top).

Additional fermionic particles can couple the top and either one of the gauge bosons or the Higgs boson. In order to respect the color symmetry, this requires that the extra fermion occurs in a color triplet, and thus it is sensible to think of it as

some type of quark. In order to be invariant under the electromagnetic symmetry, this new "quark" should have either electric charge (Q) $+2/3$ or $-1/3$ in order for one to be able to construct couplings between the extra quark, the top quark, and the known bosons. Generally, we can refer to a $Q = +2/3$ extra quark as a t' and a $Q = -1/3$ extra quark as a b', though this does not necessarily imply that the extra quarks are in the same representation under $\mathrm{SU}(2)_L \times \mathrm{U}(1)_Y$ as the SM top and bottom. Additional fermions are not generally expected to be a large source of new contributions to single top production, because of strong constraints from other observables. On the other hand we will see that there are models with additional fermions to which single top production is a sensitive probe.

"Extra" bosons can contribute to single top production either by coupling top to the down-type quarks, in which case the boson must have electric charge $Q = \pm 1$ in order to maintain the electromagnetic symmetry, or by coupling top to the charm or up quarks, in which case the boson should be electrically neutral. One could also imagine a boson carrying an odd combination of color and electric charge that would allow it to couple to both top and a lepton field. Such bosons carrying both baryon- and lepton- number (leptoquarks) could arise, for example, from the generators of the part of the gauge group of a GUT that connects the electroweak and strong sectors of the GUT. In that case one would naturally suppose that these bosons have mass of the order of M_{GUT}, and thus may not play an important role in single top production at the weak scale. This GUT picture has the leptoquark as part of the gauge interactions, so the question as to whether or not top observables are an interesting means to study leptoquarks becomes a question as to whether or not the leptoquark has some reason to prefer to couple to the top quark. One could imagine that the grand unified interaction contains a sector corresponding to a family symmetry that could somehow cause this to be the case. Another interesting picture

of leptoquarks is one in which the SM quarks and leptons are bound states of some more fundamental set of particles (which we will refer to as preons). In that case the question as to whether or not the top quark is a good place to look for evidence of the preons depends on how the model arranges the various types of preons to build quarks and leptons. However, at a hadron collider the possible light parton initial states available are not suitable for production of a single leptoquark, and thus are not particularly interesting in the context of single top production[5]. For this reason, we will not focus on leptoquarks in the discussion below.

Extra Quarks

A simple extension of the SM is to allow for an extra set of quarks. Such objects exist in a wide variety of extensions to the SM. Examples of such theories include the top see-saw versions of the top-color [46] and top-flavor [47] models, which rely on additional fermions to participate in a see-saw mechanism to generate the top mass; SUSY theories with gauge mediated SUSY breaking that must be communicated from a hidden sector in which SUSY is broken to the visible sector through the interactions of a set of fields with SM gauge quantum numbers [48]; and even models with a fourth generation of fermions.

Direct search limits on extra quarks require that they be quite massive ($m_{q'} \geq 46 - 128$ GeV at the 95% C. L., depending on the decay mode [12]), and thus they cannot appear as partons in the incident hadrons at either Tevatron or LHC. This prevents them from significantly affecting the W-gluon fusion and tW^- rates. Thus, they are best observed either through their mixings with the third family (and thus their effect on the top couplings), or through direct production.

[5] It is interesting to note that a leptoquark with $Q = +2/3$ could play an important role in top decays through a process such as $t \to \nu L \to \nu b \ell^+$. This leads to a final state that is identical to a SM top decay, but with a very distinct kinematic structure

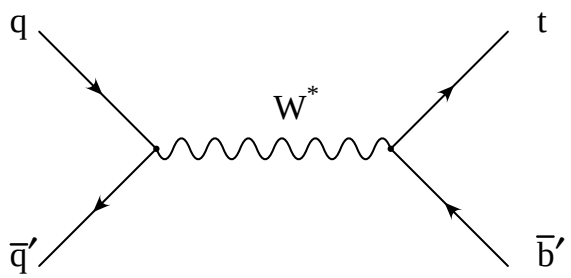

Figure 2.8: Feynman diagram for s-channel production of a single top and a b': $q\,\bar{q}' \to t\,\bar{b}'$.

As a particular example, a fourth generation of quarks could mix with the third generation through a generalized CKM matrix, and this could allow V_{tb} to deviate considerably from unity. In this case, all three modes of single top production would be expected to have considerably lower cross sections than the SM predicts. This already shows how the separate modes of single top production can be used to learn about physics beyond the SM. Other types of new physics could scale the three rates independently. Thus, if all three modes are measured to have cross sections that are the same fraction of the SM rates, it is an indication that the new physics modifies the top's coupling to the bottom and W (and not another pair of light particles), and further that the modification is the same regardless of the momentum flowing through the vertex (as is the case with the W-t-b interaction in the SM).

In addition to mixing effects, one could also hope to observe direct production of one of the fourth generation quarks, through reactions such as $q\,\bar{q}' \to t\,\bar{b}'$, shown in Figure 2.8. If the b' is somewhat heavier than the top, and $V_{tb'}$ is large, this process could be more important than QCD production of $b'\,\bar{b}'$ because of the greater phase space available to the lighter top. The production rates will depend on the magnitude of the W-t-b' coupling ($|V_{tb'}|^2$ in the model with a fourth family) and the mass of the b'. In Figure 2.9 we present the NLO rate for $t\bar{b}'$ production (as well as $\bar{t}b'$ production) without any decay BR's. Since the $|V_{tb'}|^2$ dependence may be factored out, these rates

assume $V_{tb'} = 1$. The collider signatures resulting from such a process depend on the decay modes available to the b'. If $m_{b'} > m_t + m_W$, it is likely to decay into a top quark and a W^-, and the events will have a $t\,\bar{t}$ pair with an additional $W^{\pm}$ boson. If this decay mode is not open, loop induced decays such as $b' \rightarrow b\,\gamma$ may become important, resulting in a signature $t\,\bar{b}$ plus a hard photon whose invariant mass with the b quark will reconstruct the mass of the b'.

Extra Gauge Bosons

Another simple extension of the SM is to postulate the existence of a larger gauge group which somehow reduces to the SM gauge group at low energies. Such theories naturally have additional gauge bosons, some of which may prefer to couple to the top (or even the entire third family). Examples of such theories include the top-color [21] and top-flavor [47, 49] models, which give special dynamics to the third family in order to explain the large top mass. As a specific example, we will consider the top-flavor model with an extra $\mathrm{SU}(2)_h$ gauge symmetry that generates a top mass through a see-saw effect [47].

This model has an over-all gauge symmetry of $\mathrm{SU}(2)_h \times \mathrm{SU}(2)_l \times \mathrm{U}(1)_Y$, and thus there are three additional weak bosons ($W'^{\pm}$ and Z'). The first and second generation fermions and third family leptons transform under $\mathrm{SU}(2)_l$, while the third generation quarks transform under $\mathrm{SU}(2)_h$. As was alluded to before, in order to cancel the anomaly and provide a see-saw mechanism to generate the top mass, an additional doublet of heavy quarks whose left-handed components transform under $\mathrm{SU}(2)_l$ and right-handed components transform under $\mathrm{SU}(2)_h$ is also present.

A set of scalar fields transforming under both $\mathrm{SU}(2)_l$ and $\mathrm{SU}(2)_h$ acquire a VEV, u, and break the symmetry to $\mathrm{SU}(2)_{l+h} \times \mathrm{U}(1)_Y$. From here the usual electro-weak symmetry breaking can be accomplished by introducing a scalar doublet which ac-

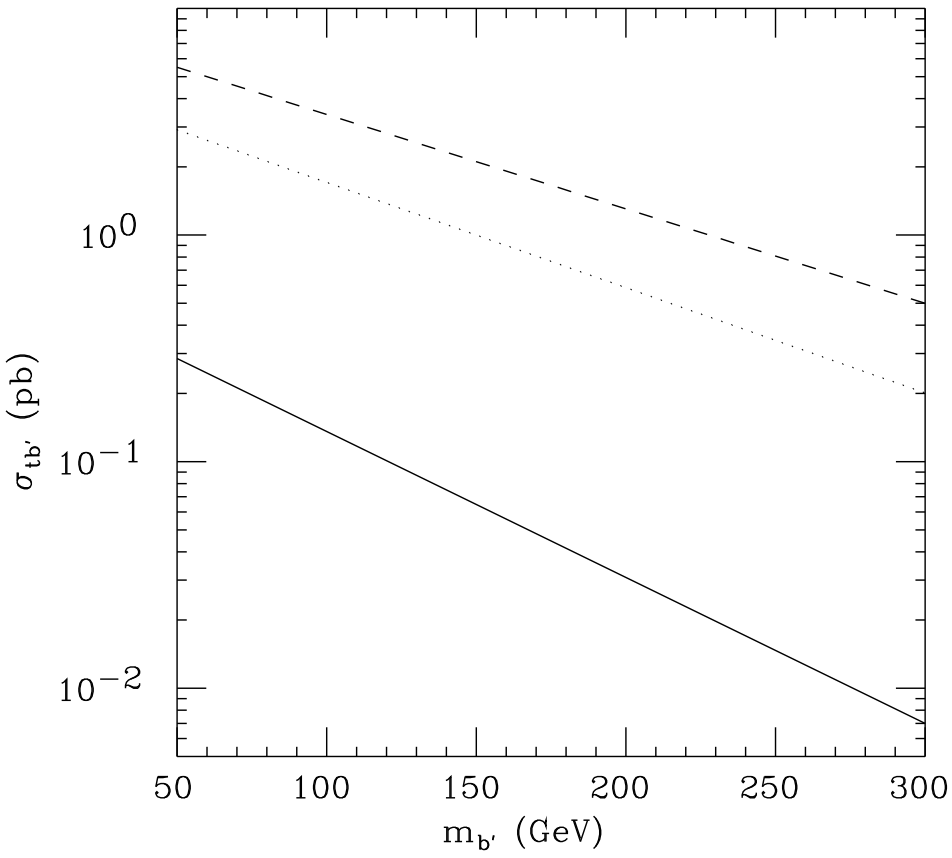

Figure 2.9: The NLO rates (in pb) for the process $q\,\bar{q}' \to W^* \to t\,\bar{b}'$ for various b' masses at the Tevatron (solid curve) and LHC (dashed curve), assuming $V_{tb'} = 1$. At the Tevatron, the rates of $q\,\bar{q}' \to W^* \to \bar{t}\,b'$ is equal to the $t\,\bar{b}'$ rate. The $\bar{t}\,b'$ rate at the LHC is shown as the dotted curve.

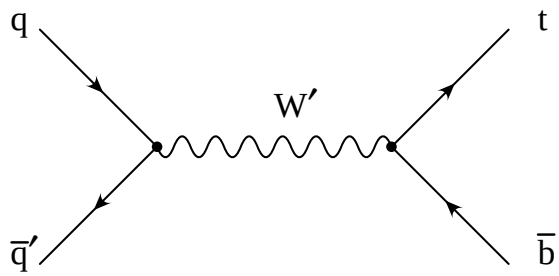

Figure 2.10: Feynman diagrams illustrating how a W' boson can contribute to single top production through $q\,\bar{q}' \to W' \to t\,\bar{b}$.

quires a VEV v, further breaking the gauge symmetry to $\mathrm{U}(1)_{EM}$. We write the covariant derivatives for the fermions as,

$$D^{\mu} \;=\; \partial^{\mu} + i g_l \, T_l^a \, W_l^{a\mu} + i g_h \, T_h^a \, W_h^{a\mu} + i g_1 \, \frac{Y}{2} \, B^{\mu}, \tag{2.5}$$

where $T^a_{l(h)}$ are the generators for $\mathrm{SU}(2)_{l(h)}$, Y is the hyper-charge generator, and $W^{a\mu}_{l(h)}$ and B^{μ} are the gauge bosons for the $\mathrm{SU}(2)_{l(h)}$ and $\mathrm{U}(1)_Y$ symmetries. The gauge couplings may be written,

$$g_l = \frac{e}{\sin\theta_W \cos\phi}\,, \qquad g_h = \frac{e}{\sin\theta_W \sin\phi}\,, \qquad g_1 = \frac{e}{\cos\theta_W}\,, \tag{2.6}$$

where ϕ is a new parameter in the theory. Thus this theory is determined by two additional quantities $x = u/v$, the ratio of the two VEV's, and $\sin^2\phi$, which characterizes the mixing between the heavy and light SU(2) gauge couplings.

At leading order, the heavy bosons are degenerate in mass,

$$M^2{}_{Z',W'} = {M_0}^2 \left(\frac{x}{\sin^2\phi\cos^2\phi} + \frac{\sin^2\phi}{\cos^2\phi} \right), \tag{2.7}$$

where ${M_0}^2 = \frac{e^2 v^2}{4\sin^2\theta_W \cos^2\theta_W}$. We can thus parameterize the model by the heavy boson mass, $M_{Z'}$, and the mixing parameter[6], $\sin^2\phi$. Low energy data requires that the mass of these heavy bosons, $M_{Z'}$, be greater than about 900 GeV [50].

[6] As shown in [49], for $\sin^2\phi \leq 0.04$, the third family fermion coupling to the heavy gauge bosons can become non-perturbative. Thus we restrict ourselves to considering $0.95 \geq \sin^2\phi \geq 0.05$.

The additional W' boson can contribute to the s-channel mode of single top production through virtual exchange of a W' as shown in Figure 2.10 [51]. In particular, if enough energy is available, the W' may be produced close to on-shell, and a resonant enhancement of the signal may result. Since the additional diagrams involve a virtual W', they will interfere with the SM W-exchange diagrams, and thus the net rate of single top production can be increased or decreased as a result, though the particular model under study always results in an increased s-channel single top rate. In Figure 2.11 the resulting NLO s-channel rate for $q\,\bar{q}' \to W, W' \to t\,\bar{b}$ at Tevatron and LHC is shown, as a function of the W' mass, for a few values of $\sin^2\phi$. The rate for $\bar{t}$ production through the same process is shown as well. While the final state particles for this case are the same as the SM s-channel mode, the distribution of the invariant mass of the $t\,\bar{b}$ system could show a Breit-Wigner resonance effect around $M_{W'}$, which serves to identify this type of new physics. However, if the mass of the W' is large compared to the collider energy, and its width broad, the resonance shape can be washed out even at the parton level. Jet energy smearing from detector resolution effects will further make such a resonance difficult to identify.

A t-channel exchange of the W' is also possible, but in that case a negligible effect is expected because the boson must have a space-like momentum, and thus the additional contributions are suppressed by $1/M_{W'}$, and are not likely to be visible. This argument applies quite generally to any heavy particle's effect on single top production. The s-channel rate is quite sensitive to a heavy particle because of the possibility of resonant production, whereas the t-channel rate is insensitive because the space-like exchange is suppressed by the heavy particle mass.

Clearly, the existence of a W' will not influence the rate of $t\,W^-$ production, but it could allow for exotic production modes such as $b\,g \to t\,W'$. If the W' has a strong coupling with the third family, then one would expect that its dominant decay

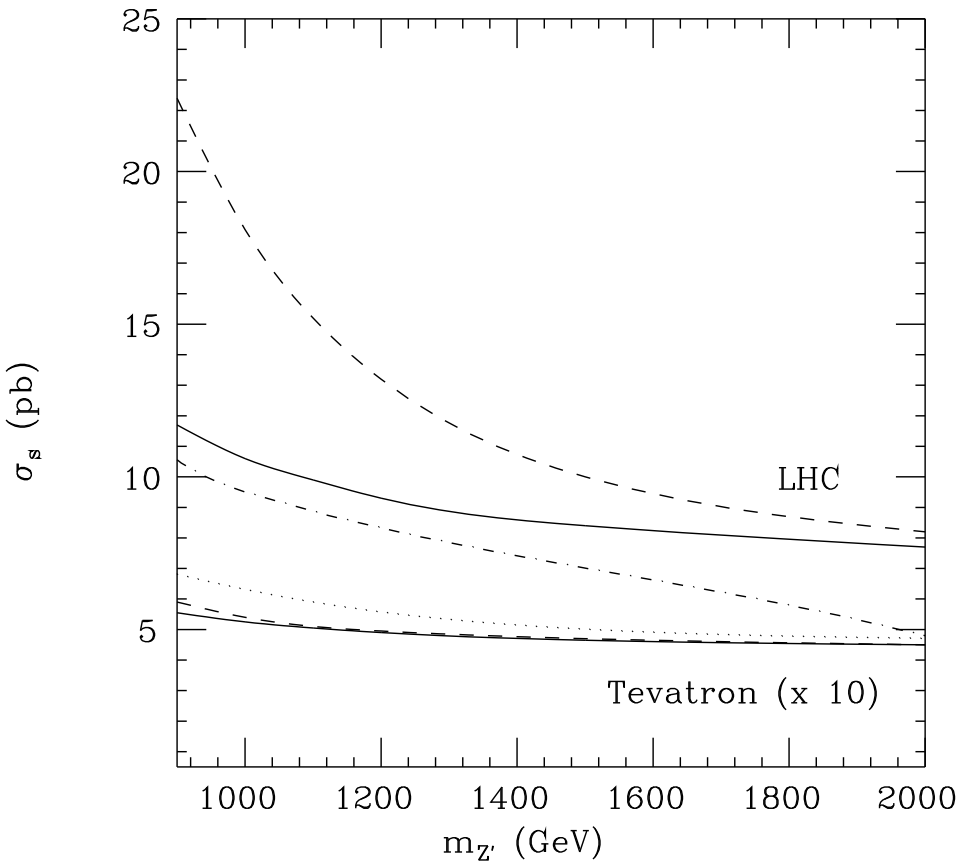

Figure 2.11: The NLO rate of $q\,\bar{q}' \to W, W' \to t\,\bar{b}$ (in pb) at the Tevatron (lower curves) and LHC (upper curves), for the top-flavor model with $\sin^2\phi = 0.05$ (solid curves) and $\sin^2\phi = 0.25$ (dashed curves), as a function of $M_{Z'} = M_{W'}$. The Tevatron cross sections are multiplied by a factor of 10. At the Tevatron, the $\bar{t}$ production rate is equal to the t rate. At the LHC the $\bar{t}$ rates are shown for $\sin^2\phi = 0.05$ (dotted curve) and $\sin^2\phi = 0.25$ (dot-dashed curve).

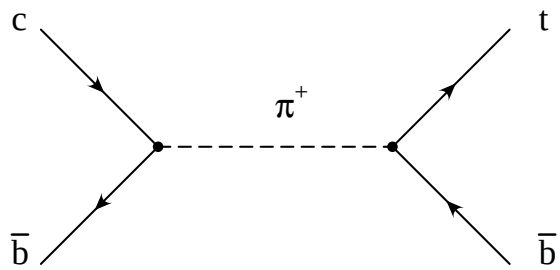

Figure 2.12: Feynman diagram illustrating how a charged top-pion can contribute to single top production through $c\,\bar{b} \to \pi^+ \to t\,\bar{b}$.

should be into $b\,\bar{t}$, and thus a final state of $t\,\bar{t}\,b$ would result with the $t\,\bar{b}$ invariant mass reconstructing the W' mass. Current limits on the W' mass in the top-flavor model make this mode nonviable at the Tevatron and unpromising at the LHC, with a cross section of 1.14 pb for $M_{W'} = 900$ GeV and $\sin^2\phi = 0.05$ including the large log contributions described in Section 2.2.3. However, an observation of this signal would be a clear indication of the nature of the new physics.

Extra Scalar Bosons

Scalar particles appear in many theories, usually associated with the spontaneous breaking of a symmetry. In the SM and the minimal supersymmetric extension, fundamental scalar fields of both neutral and charged character are present in the theory, and are expected to have a strong coupling with the top because of the role they play in generating fermion masses. In dynamical models such as the top-condensate and top-color assisted technicolor models, scalar particles exist as bound states of top and bottom quarks (as was seen in Chapter 1 this is how these models deal with the fine-tuning and naturalness problems of the SM). These composite scalars also have a strong coupling to the top because of their role in the generation of the top mass. This illustrates the fact that the large top mass naturally makes it a likely place to look for physics associated with the EWSB.

An illustrative example is provided by the charged composite top-pions ($\pi^{\pm}$) of the top-color model, which can be produced in the s-channel through $c\,\bar{b}$ fusion [52], $c\,\bar{b} \to \pi^{+} \to t\,\bar{b}$. The leading order Feynman diagram is shown in Figure 2.12. In this case the strong π^{+}-c-$\bar{b}$ coupling comes from mixing between the t and c quarks. In order to avoid constraints from the CKM matrix, this requires the mixing to occur between right-handed t and c quarks, and thus this interaction has a right-handed nature that will prove interesting when we study top polarization below.

Like the W', the $\pi^{\pm}$ contributes to the s-channel topology of single top production and can allow large resonant contributions. However, unlike the W', the π^{+} does not have a significant interference with the SM amplitudes, because the SM contribution is mostly from light quarks (u and $\bar{d}$). In Figure 2.13, we present the NLO single top rate from the top-pion process [53], for a variety of $\pi^{\pm}$ masses with the t_R-c_R mixing set equal to 20%. The two other modes of single top production are once again relatively insensitive to the $\pi^{\pm}$. The t-channel process has additional contributions suppressed by $1/M^2_{\pi^{\pm}}$ and the fact that the $\pi^{\pm}$ does not couple to light quarks. The $t\,W^{-}$ mode is insensitive because presumably the $\pi^{\pm}$ is generally distinguishable from a $W^{\pm}$ boson, and so $g\,b \to \pi^{-}\,t \to \bar{t}\,b\,t$ will not be mistaken for $t\,W^{-}$ production.

Different types of scalar particles that couple top and bottom can be analyzed in a similar fashion. The s-channel mode allows for resonant production, which can show a large effect, where-as the t-channel mode is suppressed by the space-like momentum (and large mass) of the exchanged massive particle. The $t\,W^{-}$ mode is insensitive because in that case the W is actually observed in the final state. The technipions in a technicolor model can contribute to single top production in this way [54]. Another example is provided by SUSY models with broken R-parity, in which the scalar partners of the leptons (sleptons) can couple with the top and bottom quarks, and will contribute to single top production [55].

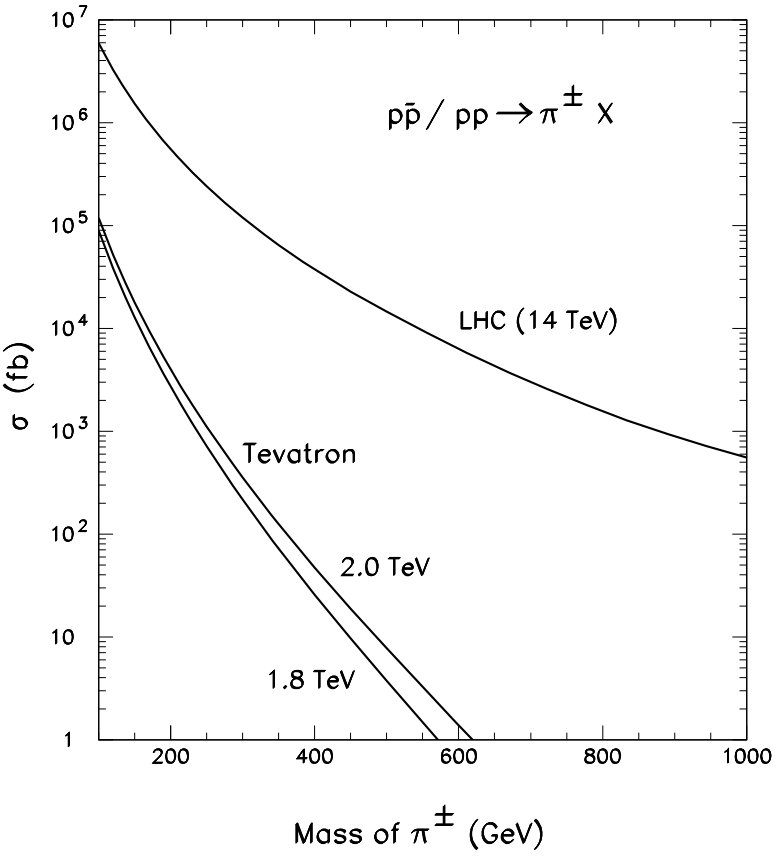

Figure 2.13: The LO rate of single top production through the reaction $c\,\bar{b} \to \pi^+ \to t\,\bar{b}$ as a function of $M_{\pi^\pm}$, assuming a t_R-c_R mixing of 20%. These rates include t and $\bar{t}$ production, which are equal for both Tevatron and LHC.

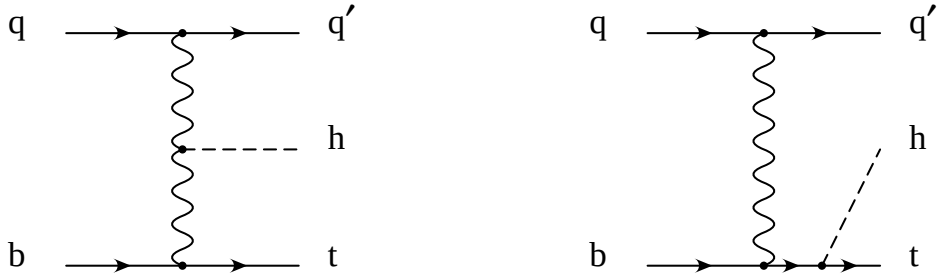

Figure 2.14: Feynman diagrams for associated production of a neutral scalar and single top quark: $q\,b \to q'\,t\,h$.

As a final note, there is the interesting process in which a neutral scalar (like the Higgs of the SM) is produced in association with a single top quark [56]. Feynman diagrams are shown in Figure 2.14. This process is of interest because while the magnitude of the h-W-W and h-t-t couplings can be measured independently by studying $q\,\bar{q}' \to W^* \to W\,h$ and $q\,\bar{q}\;(g\,g) \to h\,t\,\bar{t}$, the relative phase between the couplings can be found from the process $q\,b \to q'\,t\,h$, as that phase information is contained in the interference between the two diagrams shown in Figure 2.14. This process is extremely small compared to the other two mentioned (with a SM cross section of 6×10^{-5} pb at the Tevatron and 0.1 pb at the LHC for $m_h = 100$ GeV and including both t and $\bar{t}$ production), and thus it is not promising a discovery mode. The small SM rate results from the fact that the interference term provides a strong cancellation of the rate, reducing it by a factor of about 5. This indicates that this process is very strongly sensitive to any physics that modifies the relative phase between the h-t-t and h-W-W couplings from the SM relation. Thus, it contains important information not available in the other two processes.

2.3.2 Modified Top Quark Interactions

Another interesting set of properties of the top that can be studied in single top production are the top couplings to light particles. As was shown in Section 1.3.4,

the electroweak chiral Lagrangian provides a powerful way to study such effects model-independently. Following the EWCL approach, we write an effective Lagrangian to describe low energy physics as,

$$\mathcal{L}_{eff} \;=\; \mathcal{L}_{SM} + \mathcal{L}_4 + \mathcal{L}_5, \tag{2.8}$$

where $\mathcal{L}_{SM}$ refers to the usual SM Lagrangian described in Chapter 1, and $\mathcal{L}_4$ and $\mathcal{L}_5$ are the Lagrangians containing deviations from the SM in terms of operators of mass dimension 4 and 5, respectively.

Terms which have the potential to modify single top production include mass dimension 4 operators [57],

$$\begin{aligned}\mathcal{L}_4 \;=\; & \frac{e}{\sqrt{2}\,\sin\,\theta_W} W^+{}_\mu \left(\kappa^L_{Wtb}\, e^{i\,\phi^L_{Wtb}}\, \bar{b}\,\gamma^\mu\, P_L\, t + \kappa^R_{Wtb}\, e^{i\,\phi^R_{Wtb}}\, \bar{b}\,\gamma^\mu\, P_R\, t\right) \\ & + \frac{e\,\kappa_{Ztc}}{2\,\sin\theta_W\,\cos\theta_W} Z_\mu \Big(\, e^{i\,\phi^L_{Ztc}}\,\sin\theta_{Ztc}\,\bar{c}\,\gamma^\mu\, P_L\, t + \\ & e^{i\,\phi^R_{Ztc}}\,\cos\theta_{Ztc}\,\bar{c}\,\gamma^\mu\, P_R\, t\,\Big) + H.c.,\end{aligned} \tag{2.9}$$

which can be classified as two operators which modify the SM top weak interactions, as well as two flavor-changing neutral current operators involving the Z boson, t, and c quarks. Additional dimension 4 FCNC operators with the c quark replaced by the u quark are also possible. We have included the CP violating phases $\phi^{L(R)}_{Wtb(Ztc)}$ in the interactions for generality, though they are not always considered in the literature. In addition there are dimension 5 operators that involve interactions between new sets of particles and the top[7] and can contribute to single top production. These include the FCNC operators,

[7]There are also dimension five operators involving the sets of particles that already appear in Equation 2.9 [58]. Since naive dimensional analysis [59] suggests that at low energies these operators are less significant than their dimension four counterparts, we limit $\mathcal{L}_5$ to the dimension 5 operators which involve only new sets of fields.

$$\mathcal{L}_5 = \frac{g_S\sqrt{2}\,G^a_{\mu\nu}}{\Lambda_{gtc}}\Big(\, e^{i\,\phi^L_{gtc}}\ \sin\theta^L_{gtc}\,\bar{c}\,T^a\,\sigma^{\mu\nu}\,P_L\,t \tag{2.10}$$

$$+\, e^{i\,\phi^R_{gtc}}\ \sin\theta^R_{gtc}\,\bar{c}\,T^a\,\sigma^{\mu\nu}\,P_R\,t\Big)$$

$$+\frac{2\sqrt{2}\,e\,F_{\mu\nu}}{3\,\Lambda_{\gamma tc}}\Big(\, e^{i\,\phi^L_{\gamma tc}}\ \sin\theta^L_{\gamma tc}\,\bar{c}\,\sigma^{\mu\nu}\,P_L\,t + e^{i\,\phi^R_{\gamma tc}}\ \cos\theta^R_{\gamma tc}\,\bar{c}\,\sigma^{\mu\nu}\,P_R\,t\Big) + H.c.,$$

which couple the charm quark to the top and gluon or photon fields. Once again, we have included CP violating phases $\phi^{L(R)}_{gtc(\gamma tc)}$ which are not generally considered in the literature. Additional operators with the charm replaced by the up quark are also possible. As dimension 5 operators, these terms have couplings with dimension of inverse mass that have been written in the form of $1/\Lambda_{gtc}$ and $1/\Lambda_{\gamma tc}$. If the underlying theory is strongly coupled, these mass scales may be thought of as the energy scale in which the SM breaks down and must be replaced with the underlying theory. However, it should be kept in mind that if the underlying theory is weakly coupled, this interpretation is somewhat obscured by the fact that the energy scales Λ will also include small factors of the fundamental interaction strength and loop suppression factors. Even in this case, an experimental constraint on Λ is very useful because it will provide constraints on the parameters of an underlying model that makes a prediction for it.

The dimension 4 terms which modify the W-t-b vertex will clearly have a large impact on single top production [34]. However, κ^R_{Wtb} is already very strongly constrained by low energy $b \to s\,\gamma$ data [60], which requires [61],

$$-.0035 \geq (\ \kappa^R_{Wtb}\cos\phi^R_{Wtb} + 20\,{\kappa^R_{Wtb}}^2\ ) \leq 0.0039, \tag{2.11}$$

provided that κ^L_{Wtb} is somewhat smaller than 1. Given this strong constraint, it is unlikely that further information about κ^R_{Wtb} can be gleaned from single top production, so we will assume $\kappa^R_{Wtb} = 0$ in the discussion below. On the other hand, all three

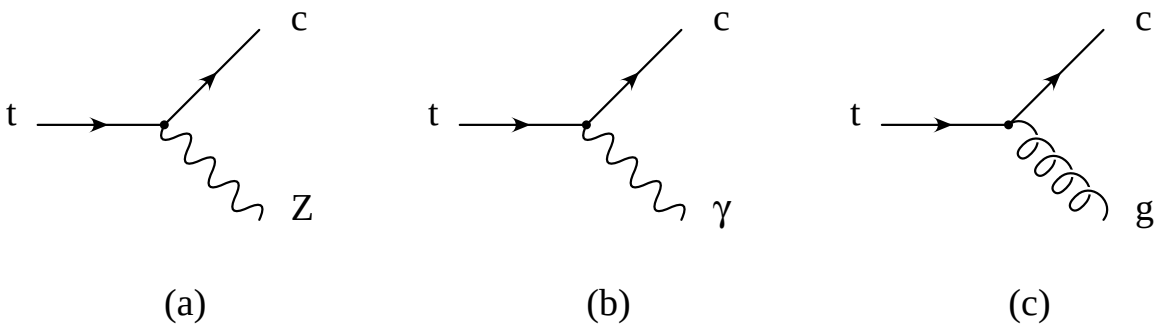

Figure 2.15: Feynman diagrams showing FCNC top decays through (a) $t \to Z\,c$, (b) $t \to \gamma\,c$, and (c) $t \to g\,c$.

modes are sensitive to κ^L_{Wtb}, and will be proportional to $(1 + {\kappa^L_{Wtb}}^2 + 2\,\kappa^L_{Wtb}\,\cos\phi^L_{Wtb})$ much the same way that they will all be sensitive to V_{tb} in the SM[8].

The flavor-changing neutral current terms in $\mathcal{L}_4$ and $\mathcal{L}_5$ will also contribute to single top production, and since they involve particles lighter than the top mass, will also contribute to top decays through Feynman diagrams such as those shown in Figure 2.15, which illustrate FCNC t decays to c. The FCNC interactions between t and u will allow for exotic decays of the same type, but with the c quark exchanged with a u quark. One could hope to learn about these anomalous FCNC couplings both by studying single top production and top decays. However, this brings us back to the problem with using top decays to determine the magnitude of a coupling - the decay can provide information about the relative branching fraction of the exotic decay compared to the SM top decay $t \to W^+\,b$, but since it does not allow one to measure the top decay width, it cannot provide a limit on the size of the exotic operator without first making an assumption concerning the nature of the W-t-b interaction. In fact, one might think that single top would suffer from the same difficulty in distinguishing the magnitude of new physics in the W-t-b interaction

[8]This is because the dimension 4 term that is proportional to κ^L_{Wtb} in $\mathcal{L}_4$ does not depend on the momenta of the interacting particles, as is the case for the SM W-t-b interaction. For higher dimension W-t-b operators, which may depend on the momenta, each single top mode will respond differently to the new interaction, and thus could be used to distinguish one operator from another.

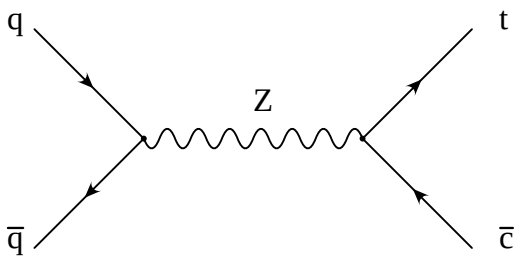

Figure 2.16: Feynman diagram showing how a FCNC Z-t-c interaction contributes to the s-channel mode of single top production through $q\,\bar{q} \rightarrow Z^* \rightarrow t\,\bar{c}$.

from new physics in a FCNC interaction. However, as we shall see, one can use the three modes of single top production separately to disentangle the FCNC new physics from the possibility of W-t-b new physics.

The three FCNC operators have a similar structure of a light c (or u) quark interacting with a top and a neutral vector boson. Thus, we can discuss their impact on the three single top processes rather generally by considering the specific example of the Z-t-c operator. In examining the FCNC operators in Equations 2.9 and 2.10, we note that they can have left-handed and right-handed interactions with different interaction coefficients (and even different phases). For now we will restrict our discussion to the case where all of the phases are zero, and discuss only the magnitude of the interactions, set by Λ_{gtc}, $\Lambda_{\gamma tc}$, and κ_{Ztc}. We will return to the subject of exploring their chiral structure when we consider top polarization in Section 2.4.

The Z-t-c operator will allow for additional contribution to the s-channel mode of single top production through reactions such as $q\,\bar{q} \rightarrow Z^* \rightarrow t\,\bar{c}$, shown in Figure 2.16. This reaction has different initial and final state from the SM s-channel mode, and thus there is no opportunity for interference between SM and new physics contributions. The fact that the new physics process has a $\bar{c}$ instead of a $\bar{b}$ in the final state has a drastic practical consequence that the new physics production mechanism probably cannot be experimentally extracted at all, because in order to separate the

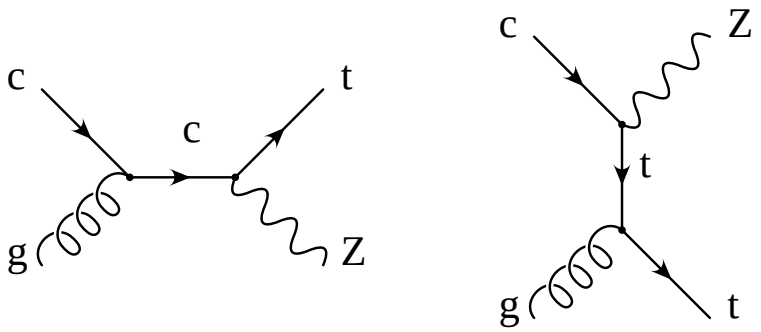

Figure 2.17: Feynman diagrams showing how a FCNC Z-t-c interaction contributes to the exotic mode of single top production $g\,c \to t\,Z$.

s-channel mode from the large $t\,\bar{t}$ and W-gluon fusion backgrounds, it is necessary to tag the $\bar{b}$ produced in association with the top in the s-channel mode, in addition to the b from the top decay. Thus, while a FCNC operator could contribute to s-channel production of a single top, it will not be counted as such[9].

The $t\,W^-$ mode cannot receive a contribution from a FCNC, though a FCNC will generally allow for new exotic production mechanisms such as $g\,c \to t\,Z$ shown in Figure 2.17. From this consideration, along with the analysis of the $t\,W^-$ mode in Section 2.3.1, we see that the $t\,W^-$ mode has a special quality because both the top and the W are in the final state (and thus identifiable). Thus, it is sensitive to new physics which modifies the W-t-b interaction[10], but it is not sensitive to nonstandard physics involving new particles or FCNC's. Thus, the $t\,W^-$ mode represents a chance to study the W-t-b vertex without contamination from other types of new physics.

The W-gluon fusion mode of single top production is quite sensitive to a FCNC involving the top and one of the light partons, through processes such as $c\,q \to t\,q$, from Feynman diagrams such as those shown in Figure 2.18. The FCNC operators

[9]It could be possible to search for s-channel production via a FCNC with a specialized strategy differing from the usual one employed to extract the W^* process, but such a search will suffer from large backgrounds from $t\,\bar{t}$ and W-gluon fusion single top processes.

[10] Of course it is also sensitive to the W-t-s and W-t-d interactions, but these have been measured to be small [12].

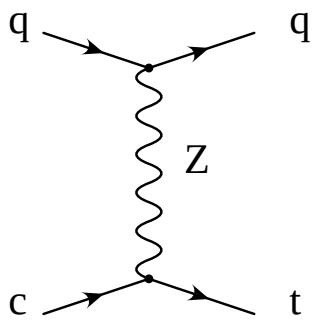

Figure 2.18: Feynman diagram showing how a FCNC Z-t-c interaction contributes to the t-channel mode of single top production through $c\,q \to t\,q$.

involve a different set of spectator quarks in the reaction, and thus they do not interfere with the SM t-channel process. In fact, because the W-gluon fusion mode requires finding a b inside a hadron, which has less probability than finding a lighter parton, the FCNC's involving u or c quarks already receive an enhancement relative to the SM t-channel rate purely from the parton densities. This can somewhat compensate for a (presumably) smaller FCNC coupling. This shows the sense in which the t-channel single top mode is sensitive to the top quark's decay properties. The same type of new physics which opens up new top decay modes (and thus modifies the top's total width) will also modify the t-channel rate of single top production, because the same light partons into which the top may decay are also responsible for producing single tops in the t-channel process. Thus, one can think of the t-channel process as a kind of measure of the inclusive top width.

Because of the strong motivation to use single top production to study FCNC operators involving the top quark, detailed simulations of the effect of the g-t-c operator on single top production were performed [24], and found that this operator could be constrained by the process $q\,\bar{q} \to t\,\bar{c}$ to $\Lambda_{gtc} \geq 4.5$ TeV at Run II of the Tevatron if no new physics signal were to be found. Further refinements on this idea [62] showed that it could be improved by including other reactions such as $g\,c \to t$, $g\,c \to g\,t$,

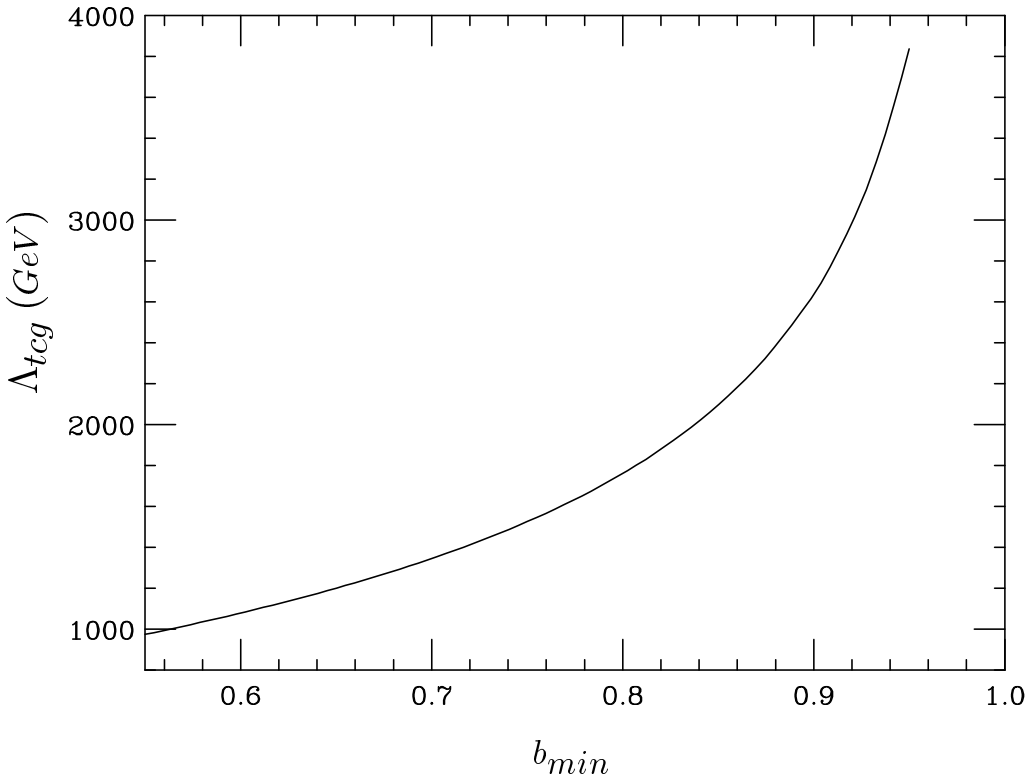

Figure 2.19: The correlation between the maximum cross section of $q\,\bar{q} \to t\,\bar{c}$, σ_{tc}, and the minimum BR($t \to W\,b$) assuming the t-c-g operator is the only source of nonstandard physics in top decays, b_{min}.

$q\,c \to t\,q$, and $g\,g \to t\,\bar{c}$ to $\Lambda_{gtc} \geq 10.9$ TeV at the Tevatron Run II. In [63] it was pointed out that since the same g-t-c operator contributes to both single top production and the top decay $t \to c\,g$, one can look for the correlation in the BR($t \to c\,g$) and the anomalous rate of single top production to verify that this particular operator is responsible for a given observation of a new physics effect. In Figure 2.19 we present the correlation between the BR for the FCNC decay (assuming no other new physics is present) and the process $q\,\bar{q} \to t\,\bar{c}$ expected from the g-t-c operator. Observation of this correlation (or one relating a different single top production process with the $t \to g\,c$ decay) could be the smoking gun in identifying the g-t-c operator as being responsible for a deviation in single top production.

Detailed simulations of the Z-t-c and γ-t-c operators have so far been confined to studies of top decays [64, 65]. The quantity $|\kappa_{Ztc} \sin\theta_{Ztc}|$ is constrained by low energy data on flavor-mixing processes to be less than the order of magnitude of 0.05 [64]. These studies indicate that from Run II at the Tevatron top decays should provide constraints of $\Lambda_{gtc} \geq 7.9$ TeV, $\kappa_{Ztc} \leq 0.29$, and will not improve the bounds on $\Lambda_{\gamma tc}$ from the current $b \to s\,\gamma$ limit of about 5 TeV. Of course, as we have argued before, it was necessary to assume a SM W-t-b interaction in order to use decays to say anything at all about these operators. The effect of the Z-t-c operator to the inclusive t-channel production rate is to contribute an additional 0.13 pb at the Tevatron Run II and 12.6 pb at the LHC, assuming $\kappa_{Ztc} = 0.29$, and including the NLO QCD corrections for both t and $\bar{t}$ production. Low energy constraints indicate that $\kappa_{Ztc} = 0.29$ requires $|\sin\theta_{Ztc}| \leq 0.17$, and the inclusive cross sections are insensitive when θ_{Ztc} is varied in this range. The γ-t-c operator can be studied at a hadron collider through the reaction $\gamma\,c \to t$ (where the photon is treated as a parton inside the proton) [66], though this exotic production mechanism suffers from potentially large SM backgrounds.

2.4 Top Polarization

The polarization of top quarks represents another way to probe the properties of top interactions. In the SM, the W-t-b vertex is entirely left-handed, which means that the top polarization information is passed on to the W boson and b quark into which the top decays. Since the W interaction with the light fermions into which it decays is also left-handed, the W polarization information is thus also reflected in the kinematics of its decay products. The same weak interaction is also responsible for single top production, which has the consequence that single tops also show a large degree of polarization. The discussion below is based on the SM amplitudes for top production and decay presented in [34].

2.4.1 The W^+ Polarization: The W-t-b Interaction

In order to probe the chiral structure of the W-t-b interaction, it is enough to consider the W polarization of top decays. As was shown in [34], the left-handed nature of the SM interaction demands that the produced W bosons be either left-handed or longitudinally polarized, and predicts the specific ratio of

$$\frac{N_0}{N_-} = \frac{m_t^2}{2\,M_W^2 + m_t^2} \simeq 70\%. \tag{2.12}$$

The degree of W polarization from top decays can be reconstructed by studying the angle between the W momentum and the charged lepton momentum, in the W rest frame.

It is desirable to employ top decays in order to probe the W-t-b interaction, because in the case of a top decay, the W and b are observed, and thus one can be sure that it is this interaction that is responsible for the effect one is seeing, which may not be the case if there is new physics in single top production. Further, once one has probed the chiral structure of the W-t-b interaction, one can then employ

this information to unfold the top decay and reconstruct the polarization of the top itself, as will be explained below.

2.4.2 The Top Polarization

Once the chiral structure of the W-t-b interaction has been probed through top decays, and the SM left-handed structure verified, the top decay products can be used in order to study the polarization of the produced top quarks themselves. As we will see, this can be very useful in determining what sort of new physics is responsible for an observed deviation in single top production. Currently, there are two important bases for describing the top polarization. The usual helicity basis measures the component of top spin along its axis of motion (in the center of mass frame - because the top mass is large its helicity is not a Lorentz invariant quantity). The so-called "optimized basis" [67] relies on the SM dynamics responsible for single top production in order to find a direction (either along the direction of one of the incoming hadrons or produced jets) which results in a larger degree of polarization for the top quark. In the discussion below, we will describe the modes of single top production in both bases, and analyze the particular strengths and weaknesses of each.

Before looking at a particular process or basis, it is worth describing how one can determine the top polarization from its decay products [34]. A simple heuristic argument based on the left-handed nature of the W interactions and the conservation of angular momentum can be made, and is displayed diagrammatically in Figure 2.20. The analysis is carried out in the rest frame of the top quark, and is slightly different for a left-handed or a longitudinally polarized W boson participating in the decay. In the left-handed W case, the fact that the b quark must be left-handed forces it to move along the direction of the top polarization. The W thus moves against this direction. When the W decays, the charged lepton (ℓ^+) must be right-handed, so it prefers to

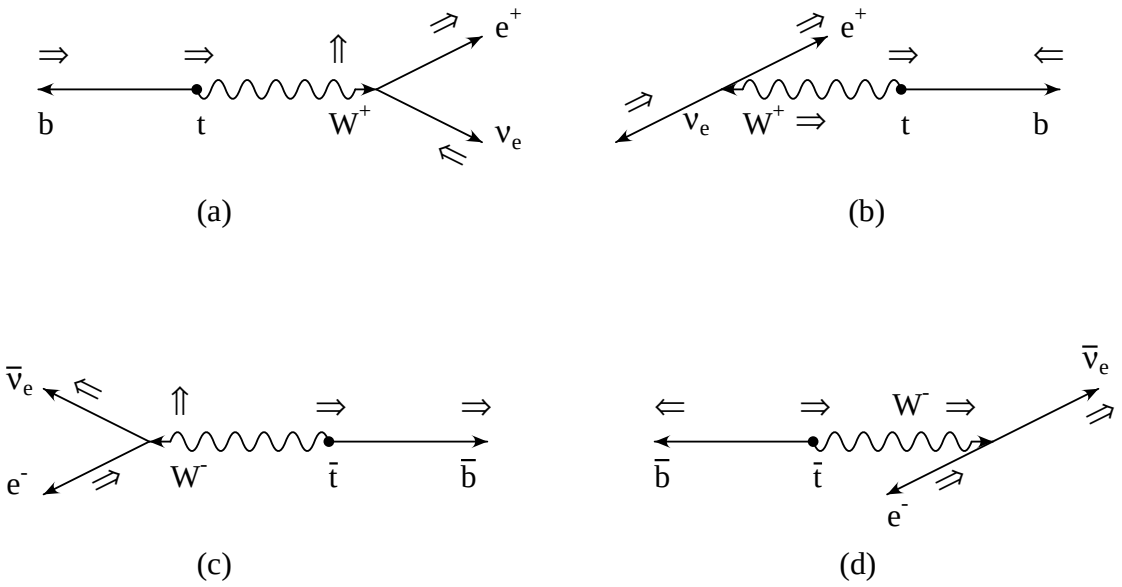

Figure 2.20: A diagram indicating schematically the correlation between the charged lepton ($e^{\pm}$) from a top decay, and the top spin, in the top rest frame. The arrows on the lines indicate the preferred direction of the momentum in the top rest frame, while the large arrows alongside the lines indicate the preferred direction of polarization. As shown, the e^+ (e^-) from a t ($\bar{t}$) decay prefers to travel along (against) the direction of the t ($\bar{t}$) polarization.

move against the W direction, in the same direction as the top polarization. When the W boson is longitudinally polarized, it prefers to move in the same direction as the top spin. Its decay products prefer to align along the W polarization, and since the W is boosted in the direction of the top polarization, the charged lepton again prefers to move along the top spin axis. As shown in Figure 2.20, a similar argument can be made for the $\bar{t}$ spin, but in this case the charged lepton prefers to move against the $\bar{t}$ spin axis. From this point onward, we restrict our discussion to top quarks, but it should be clear how they apply to $\bar{t}$ as well. The simple angular momentum argument is reflected in a more detailed computation of the distribution,

$$\frac{1}{\Gamma}\frac{d\Gamma}{d\cos\theta}(t \to W^+ b \to \ell^+ \nu_\ell b) \;=\; \frac{1}{2}(1+\cos\theta)\,, \tag{2.13}$$

where θ is the angle between the top polarization and the direction of the charged lepton, in the top rest frame, and Γ is the partial width for a semi-leptonic top decay

in the SM. In principle, one has only to decide on a scheme for relating the top polarization to some axis, and one can fit the distribution,

$$F(\cos\theta) \;=\; \frac{A}{2}\,(1+\cos\theta) + \frac{1-A}{2}\,(1-\cos\theta)\,, \tag{2.14}$$

to determine the degree of polarization (A) along this axis. In practice, there are complications arising from the fact that the endpoints of the distribution tend to be distorted by the cuts required to isolate the signal from the background, and the fact that in reconstructing the top rest frame, the component of the unobserved neutrino momentum along the beam axis (p_ν^z) is unknown. One may determine this quantity up to a two-fold ambiguity by requiring the top decay products to have an invariant mass that is close to m_t. However, the ambiguity in this procedure will also have some effect on the distribution, and so careful study is required. One can also use the asymmetry between events with $\cos\theta > 0$ and $\cos\theta < 0$ to characterize the degree of polarization of the top, which may be helpful if the data set is limited by poor statistics.

W^* Production

The degree of top polarization in the W^* process is straight-forward to compute in the helicity basis [34]. Using the CTEQ4M PDF's, we find that about 75% of the top quarks produced through the s-channel process at the Tevatron are left-handed, and 76% of them are left-handed at the LHC.

The optimized basis improves the helicity basis result at the Tevatron by noting that in the SM, the W^* process produces top quarks whose polarization is always along the direction of the initial anti-quark involved in the scattering. At the Tevatron, the vast majority ($\sim 97\%$) of these anti-quarks come from the $\bar{p}$ (which has valence anti-quarks). Thus, one expects that by choosing to measure the top polarization along

the $\bar{p}$ direction in the top rest frame, one can raise the degree of polarization from 75% to 97%. This represents a large improvement for Tevatron polarization studies of the W^* process. However, at the LHC there are no valence anti-quarks, and thus no optimized basis to analyze the W^* top polarization (though as we have seen, at the LHC the helicity basis results in a fair degree of left-handed top production anyway).

W-gluon Fusion

The discussion of polarization in the W-gluon fusion process is somewhat tricky, mostly owing to the fact that as we have seen above, the detailed kinematics of this process are sensitive to higher orders of perturbation theory. It is clear that the kinematic region described by the process $q\,b \to q'\,t$ is the dominant one, but a precise calculation of the interplay between the $2 \to 2$ scattering contribution and the $2 \to 3$ scattering contribution is still lacking. Thus, one must be careful in claiming what degree of polarization results from a particular basis.

In the helicity basis, the $2 \to 2$ description has the top quarks 100% left-handed when produced from the $u\,b \to d\,t$ sub-process. In fact, at both Tevatron and LHC the $\bar{d}\,b \to \bar{u}\,t$ sub-process is quite small, and thus the over-all degree of polarization is about 97%. On the other hand, the $2 \to 3$ description shows a degree of polarization that is much lower, and depends on the choice of the bottom mass used in the computation. This is an indication that this method of computation is not perturbatively stable. Thus, it is fair to say that the degree of polarization in the helicity basis is high, but at the moment no reliable determination is available.

The optimized basis once again makes use of the fact that the top polarization is 100% along the direction of the spectator anti-quark in the reaction. At both Tevatron and LHC, this is dominantly the spectator jet in the final state. This basis thus results in a top which is about 96% polarized along the direction of the spectator

jet. In [67], it was shown that this basis is also not sensitive to the value of the bottom mass, and thus is perturbatively reliable.

2.4.3 New Physics and Top Polarization

As we have seen, new physics may alter the structure of single top production. It may be that the new physics effects will reveal themselves, and tell us something about their nature by causing a large deviation in one or more of the single top production cross sections. In that case one can study the distribution of the top polarization in order to learn something further about the nature of the nonstandard production mechanism.

In Section 2.3.1, it was demonstrated that either a charged scalar top-pion or W' gauge boson can have a substantial effect on single top production in the s-channel mode. Assuming for the moment that such a deviation has been observed, one can then use the top polarization in order to narrow down the class of models responsible for such an effect. The W' boson couples to the left-handed top and bottom quarks, and thus an analysis of the resulting top polarization will be the same as the SM prediction. Namely, the helicity basis will show 75% of the tops to be left-handed (76% at the LHC) and the optimized basis will show 97% at the Tevatron. However, the $\pi^{\pm}$ has a right-handed interaction, completely at odds to the SM. In fact, there is another difference between the W' and the $\pi^{\pm}$ that is also very important. Like the SM W boson, the W' is a vector particle, and thus carries angular momentum information between the initial state and final state in the s-channel process. However, the $\pi^{\pm}$, as a scalar particle, does not carry such information. Thus, the optimized basis, which relies on the correlation between top spin and the initial $\bar{d}$ momentum fails to apply to a scalar production mechanism, and if one were to use it to analyze the polarization of the top coming from this type of new physics effect, one would

come to the wrong conclusion that the produced tops were unpolarized. On the other hand, in the helicity basis the top quarks produced from the $\pi^{\pm}$ show very close to 100% right-handed polarization. This demonstrates the utility of using *both* bases. If there is new physics in single top production, not only is it unclear at the outset which basis will show a larger degree of polarization, but we can use them together to distinguish a vector from a scalar exchange, thus learning about the nature of the new particle without directly observing it.

Study of polarization can also be useful in disentangling the operators in the effective Lagrangian in Equations 2.9 and 2.10. As we saw, those operators have left-handed and right-handed versions, and thus the distribution of top polarizations will depend on the relative strength of the two. Thus, by studying top polarization, one could begin to disentangle the chiral structure of the operator responsible for a deviation in single top production, giving further insight into the nature of the full theory that accurately describes higher energies.

2.5 Top Quark Properties

Having gone over in detail the physics one can probe with single top production, it is worth summarizing what we have learned and examining how one can use the different top quark observables to extract information about the top that maximizes the available information. In the preceeding sections we have seen that single top production allows one to measure the magnitude of the top's weak interactions (unlike top decays). The three modes of single top production are sensitive to different types of new physics. All three modes are sensitive to modification of the W-t-b interaction, with the $t\,W^-$ mode distinguished by the fact that it is rather insensitive to any other types of new physics. The s-channel mode is sensitive to certain types of additional

particles. And the t-channel mode is sensitive to physics which modifies the top decay properties, in particular to FCNC interactions. In this light, it is rather unfortunate that the tW^- mode is so small at the Tevatron that it is not likely to be useful there, as it can allow one to measure the strength of the W-t-b vertex, which would be a good first step in disentangling the information from the s- and t-channel modes.

Without the tW^- mode, one will most likely have to study the correlation of the s- and t- channel rates in the plane of $\sigma_s - \sigma_t$ in order to attempt to understand if a new physics effect is present, and how one should interpret it if it is observed. In Figure 2.21 we show this plane, including the SM point (with the contour of $3\,\sigma$ deviation around it) and the points from the the top-flavor model (with $M_{Z'} = 900$ GeV and $\sin^2\phi = 0.05$), the top-color model with a charged top-pion (with mass $m_\pi^\pm = 250$ GeV and t_R-c_R mixing of 20%) and a FCNC Z-t-C operator (with $\kappa_{Ztc} = 0.29$, $\sin\theta_{Ztc} = 0.2$, and $\phi^R_{Ztc} = \phi^L_{Ztc} = 0$). This illustrates how to use the knowledge we have about the sensitivity of the W^* and W-gluon fusion modes to find a likely explanation for a new physics effect. A deviation in σ_s that is not also reflected in σ_t is most likely due to the effect of nonstandard particles. A deviation in σ_t that is not also seen in σ_s is likely from a FCNC. A deviation that is comparable in both rates is most likely from a modification of the W-t-b interaction. In the very least, if the SM is a sufficient description of single top production, the fact that the two rates are consistent will allow one to use them to extract V_{tb} with confidence that new physics is not distorting the measurement.

Additional information is provided by polarization information. By studying the W polarization from top decays, one learns about the nature of the W-t-b interaction. By studying the top polarization, in both the helicity and optimized bases, one can learn more about the chiral structure of nonstandard top interactions, either by probing the chiral structure of the interactions, or even the scalar/vector nature of a

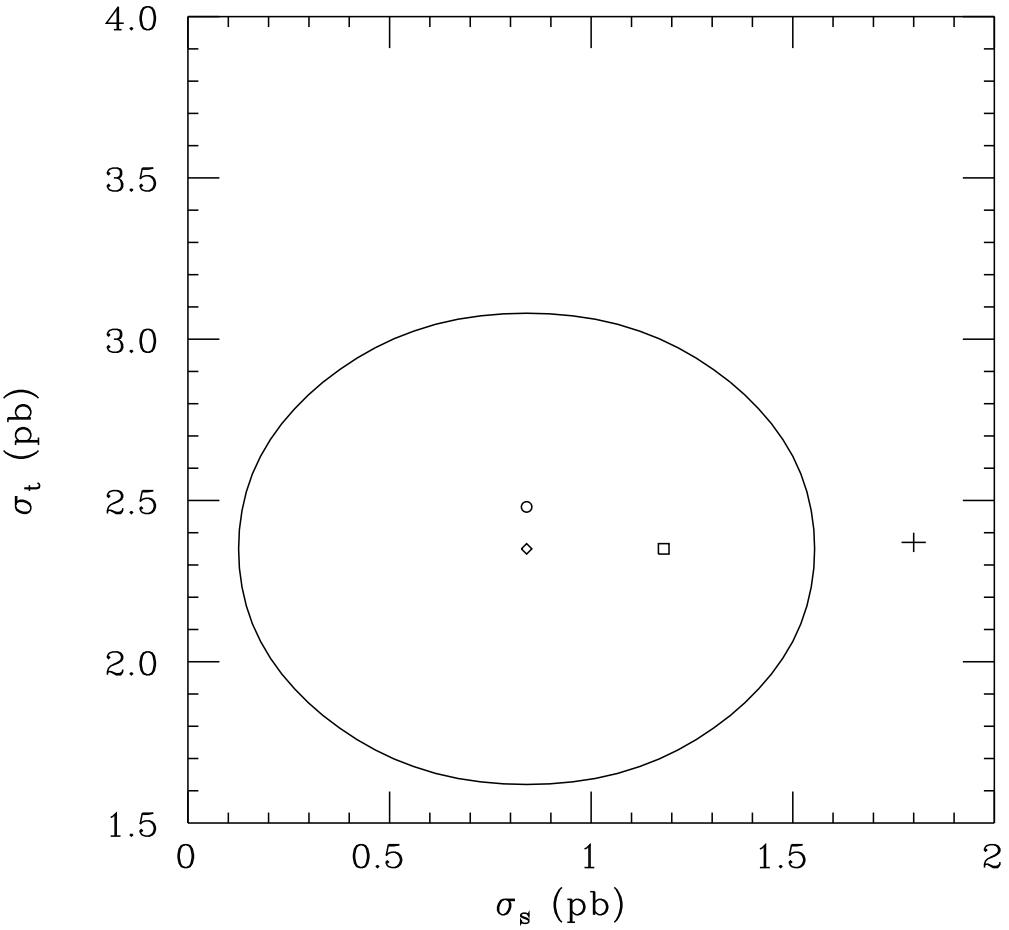

Figure 2.21: The location of the Tevatron SM point (the diamond) in the σ_s-σ_t plane, and the 3σ deviation curve. Also shown are the points for the top-flavor model (with $M'_Z = 900$ GeV and $\sin^2\phi = 0.05$) as the square, the FCNC Z-t-c vertex ($\kappa^Z_{tc} = 0.29$) as the circle, and a model with a charged top-pion ($m_{\pi^\pm} = 250$ GeV and t_R-c_R mixing of $\sim 20\%$) as the cross. All cross sections sum the t and $\bar{t}$ rates.

virtual particle participating in single top production.

Chapter 3

Higgs with Enhanced Yukawa Coupling to Bottom

3.1 Introduction

As we have seen, the mystery of the EWSB is one of the primary challenges for modern particle physics. The large top mass, of the same order as the EWSB scale, suggests that top may play a special role in the generation of mass. This occurs in models with dynamical top-condensate or top-color scenarios [20, 21] as well as in SUSY theories [18]. Since the bottom quark is the iso-spin partner of the top quark, its Yukawa coupling with a Higgs boson can be closely related to that of the top quark. In [68], we demonstrated that because of the small mass of bottom ($m_b \sim 4.5$ GeV) relative to top ($m_t \sim 175\,\text{GeV}$), studying the b Yukawa coupling can effectively probe new physics beyond the SM.

In this Chapter, we study the detection of a Higgs boson (ϕ) at hadron colliders in the context of models where the bottom has an enhanced Yukawa coupling (y_b) to the scalar Higgs. We begin with a model-independent analysis for Higgs production associated with $b\bar{b}$ jets, through the reactions $p\,\bar{p} \to \phi\,b\,\bar{b} \to b\bar{b}b\bar{b}$, and $p\,p \to \phi\,b\,\bar{b} \to b\bar{b}b\bar{b}$ at the Tevatron Run II and LHC, to determine their ability to probe models of dynamical EWSB and SUSY theories through this process.

3.2 Signal and Background

We are interested in studying production of $\phi b\bar{b} \to b\bar{b}b\bar{b}$ at the Run II of the Tevatron and the LHC. The signal events result from QCD production of a primary $b\bar{b}$ pair, with a Higgs boson (ϕ) radiated from one of the bottom quark lines as shown in Figure 3.1. The Higgs boson then decays into a secondary $b\bar{b}$ pair to form a $b\bar{b}b\bar{b}$ final state. Because our detection strategy relies upon observing the primary b quarks in the final state (and thus demands that they have large transverse momentum), our calculation of the $\phi b\bar{b}$ signal rate from diagrams such as those shown in Figure 3.1 is expected to be reliable. This is in contrast to the *inclusive* rate of ϕ production at a hadron collider, in which one does not require a final state topology with four distinct jets. In this case a calculation based upon Feynman diagrams such as those shown in Figure 3.1 may not be reliable. It would be better to consider the Higgs boson production via bottom quark fusion, such as $b\bar{b} \to \phi$ and $gb \to \phi b$, with cares to avoid double counting its production rate [69]. (This calculation would resum some large logarithms which are included in the definition of the bottom parton distribution function within the proton, much as was true for single top production in Chapter 2.) We have chosen to search in the four jet final topology because the QCD background for 3 jets is much larger than that for 4 jets, and thus it would be more difficult to extract a 3 jet signal. Since the signal consists of four b (including $\bar{b}$) jets, the dominant backgrounds at a hadron collider come from production of $Zb\bar{b} \to b\bar{b}b\bar{b}$, seen in Figure 3.2, purely QCD production of $b\bar{b}b\bar{b}$, seen in Figure 3.3, and $b\bar{b}jj$, where j indicates a light quark or a gluon, shown in Figure 3.4 which can occasionally fake a b-jet signature in the detector.

In order to derive model-independent bounds on the couplings of the scalar particles with the bottom quark, we consider K, the square-root of the enhancement

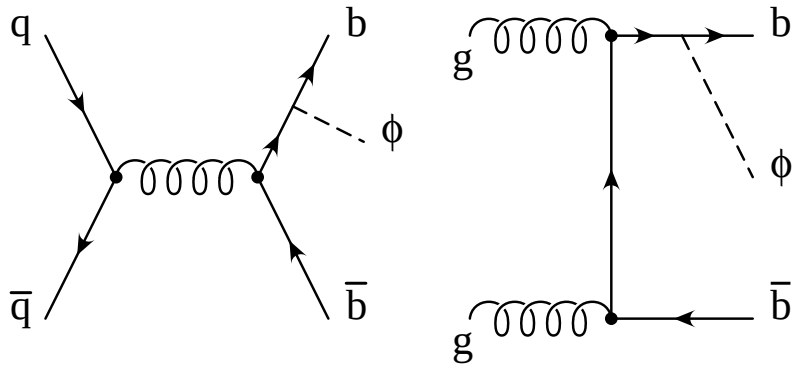

Figure 3.1: Representative leading order Feynman diagrams for $\phi b\bar{b}$ production at a hadron collider. The decay $\phi \to b\bar{b}$ is not shown.

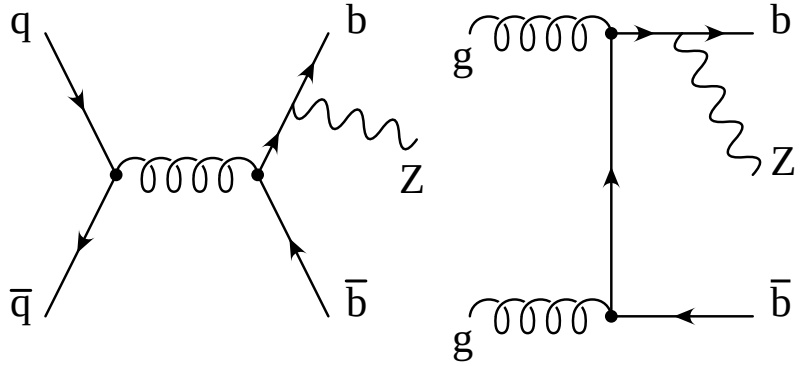

Figure 3.2: Representative Feynman diagrams for leading order $Zb\bar{b}$ production at a hadron collider. The decay $Z \to b\bar{b}$ is not shown.

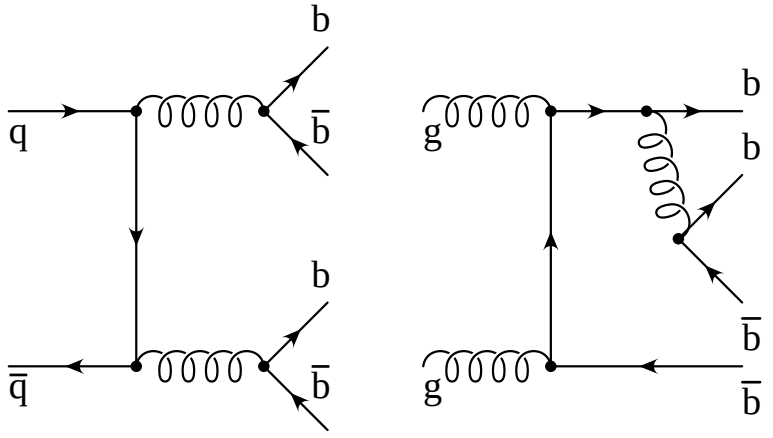

Figure 3.3: Representative leading order Feynman diagrams for QCD $b\bar{b}b\bar{b}$ production at a hadron collider.

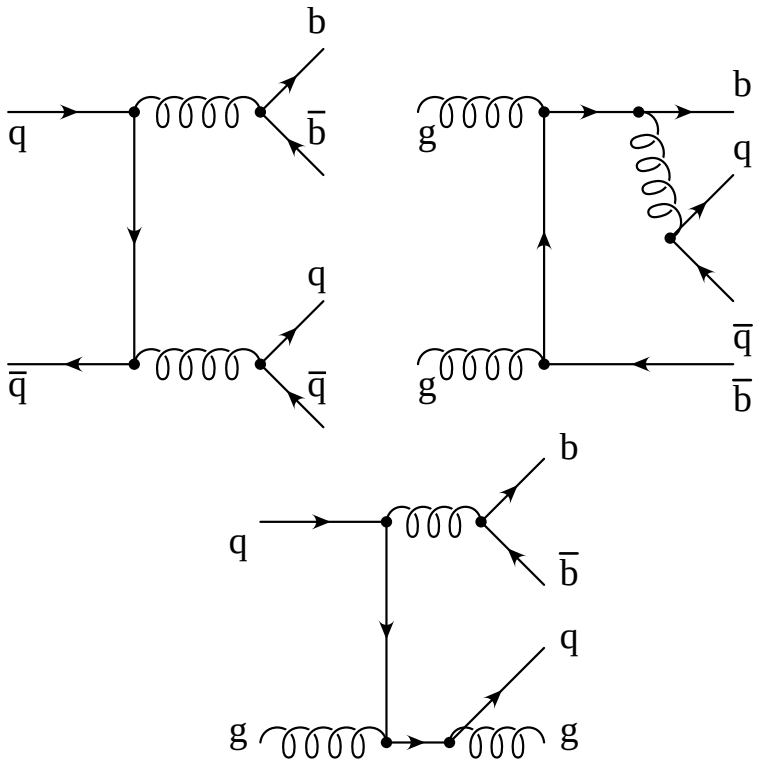

Figure 3.4: Representative leading order Feynman diagrams for QCD $b\bar{b}jj$ production at a hadron collider.

factor for the production of $\phi b\bar{b} \to b\bar{b}b\bar{b}$ over the SM prediction. By definition,

$$K = \frac{y_b}{(y_b)_{\rm SM}}, \tag{3.1}$$

in which $(y_b)_{\rm SM} = \sqrt{2}\, m_b/v$ is the SM bottom Yukawa coupling and y_b is the bottom Yukawa coupling in the new physics model under the consideration. The decay branching ratio of ϕ to $b\bar{b}$ is model-dependent, and is not included in the calculations of this section. (Namely, $BR(\phi \to b\bar{b})$ is set to one). When analyzing the specific models in the following sections, we include the appropriate BR for that model.

We compute the signal and the backgrounds at the parton level, using leading order (LO) results from the MADGRAPH package [70] for the signal and the backgrounds, including the sub-processes initiated by $q\bar{q}$ and gg (and in the case of $b\bar{b}jj$, qg and $\bar{q}g$). While the complete next-to-leading order (NLO) calculations are not currently available for the signal or background cross sections, we draw upon existing results for high p_T $b\bar{b}$ production at hadron colliders [71] and thus estimate the NLO effects by including a k-factor of 2 for all of the signal and background rates. We will estimate the theoretical uncertainty in the signal and background cross sections below. We use the CTEQ4L [39] parton distribution functions (PDF's) and set the factorization scale, μ_0, to the average of the transverse masses of the primary b quarks, and the boson (ϕ or Z) transverse mass[1] for the $\phi b\bar{b}$ and $Zb\bar{b}$ processes, and use a factorization scale of $\mu_0 = \sqrt{\hat{s}}$, where $\hat{s}$ is the square of the partonic center of mass energy, for the $b\bar{b}b\bar{b}$ and $b\bar{b}jj$ background processes. It is expected that a large part of the total QCD $b\bar{b}b\bar{b}$ and $b\bar{b}jj$ rates at the Tevatron or LHC energies will come from fragmentation effects, which we have neglected in our LO matrix element calculation. However as we shall see below, due to the strong p_T and isolation cuts which are necessary to improve the signal-to-background ratio, we expect that these effects will

[1] The transverse mass of particle i is given by $m_T^{(i)} \equiv \sqrt{m_i^2 + {p_T^{(i)}}^2}$.

be suppressed, and thus will only have a small effect on our results. Similarly, we expect that after imposing the necessary kinematic cuts, the signal and the background rates are less sensitive to the choice of the factorization scale. In this section, unless otherwise noted, we will restrict our discussion of numerical results to a signal rate corresponding to a scalar mass of $m_\phi = 100$ GeV, and an enhancement factor of $K = m_t/m_b \approx 40$. We will consider the experimental limits which may be placed on K as a function m_ϕ below.

In order to simulate the detector acceptance, we require the p_T of all four of the final state jets to be $p_T \geq 15$ GeV, and that they lie in the central region of the detector, with rapidity $|\eta| \leq 2$. We also demand that the jets are resolvable as separate objects, requiring a cone separation of $\Delta R \geq 0.4$, where $\Delta R \equiv \sqrt{\Delta\varphi^2 + \Delta\eta^2}$. ($\Delta\varphi$ is the separation in the azimuthal angles.) In the second column of Table 3.1 we present the number of events in the signal and background processes at the Tevatron Run II which satisfy these acceptance cuts, assuming 2 fb^{-1}of integrated luminosity. As can be seen, the large background makes it difficult to observe a signal in the absence of a carefully tuned search strategy to enhance the signal-to-background ratio. In presenting these numbers, we have assumed that it will be possible to trigger on events containing high p_T jets (and thus retain all of the signal and background events). This capability is essential for our analysis.

The typical topology of the bottom quarks in the signal events is a "lop-sided" structure in which one of the bottom quarks from the Higgs decay has a rather high p_T of about $m_\phi/2$, whereas the other three are typically much softer. Thus, the signal events typically have one bottom quark which is much more energetic than the other three. On the other hand, the QCD $b\bar{b}b\bar{b}$ (or $b\bar{b}jj$) background is typically much more symmetrical, with pairs of bottom quarks (or fake b's) with comparable p_T. In order

Table 3.1: The signal and background events for 2 $\text{fb}^{-1}$of Tevatron data, assuming $m_\phi = 100\,\text{GeV}$, $2\Delta m_\phi = 26\,\text{GeV}$, and $K = 40$ after imposing the acceptance cuts, p_T cuts, and reconstructed m_ϕ cuts described in the text. (A k-factor of 2 is included in both the signal and the background rates.)

Process	Acceptance Cuts	p_T Cuts	ΔR Cut	ΔM Cut
$\phi b\bar{b}$	4923	1936	1389	1389
$Zb\bar{b}$	1432	580	357	357
$b\bar{b}b\bar{b}$	5.1×10^4	3760	1368	1284
$b\bar{b}jj$	1.2×10^7	1.5×10^6	6.3×10^5	5.9×10^5

to exploit this, we order the b quarks by their transverse momentum,

$$p_T^{(1)} \geq p_T^{(2)} \geq p_T^{(3)} \geq p_T^{(4)}, \tag{3.2}$$

and require that the bottom quark with highest transverse momentum have $p_T^{(1)} \geq 50$ GeV, and that $p_T^{(2)} \geq 30$ GeV and $p_T^{(3,4)} \geq 20$ GeV. In the third column of Table 3.1 we show the effect of these cuts on the signal and backgrounds. As can be seen, these cuts reduce the signal by about 60%, while drastically reducing the QCD $b\bar{b}b\bar{b}$ background by about 90%.

Since the p_T spectrum of the leading jets is determined by the mass of the scalar boson produced, the leading p_T cuts can be optimized to search for a particular m_ϕ. From the discussion above, the optimal cut on $p_T^{(1)}$ can be seen to be close to $m_\phi/2$ whereas the optimal cut on $p_T^{(2)}$ is somewhat lower (generally closer to $m_\phi/3$). We adopt these optimized p_T cuts for each mass considered, when estimating the search reach of the Tevatron or LHC.

Another effective method for reducing the QCD background is to tighten the isolation cut on the bottom quarks. In the QCD $b\bar{b}b\bar{b}$ background, one of the $b\,\bar{b}$ pairs is preferentially produced from gluon splitting. Because of the collinear enhancement,

the invariant mass of this $b\bar{b}$ pair tends to be small, and the ΔR separation of these two b's prefers to be as small as possible. On the contrary, in the signal events, the invariant mass of the $b\bar{b}$ pair from the ϕ-decay is on the order of m_ϕ, and the ΔR separation is large because the angular distribution of b in the rest frame of the scalar ϕ is flat. Thus, by increasing the cut on ΔR to $\Delta R \geq 0.9$ we can improve the significance of the signal. As shown in column four of Table 3.1, this cut further decreases the signal by about 30%, and the QCD $b\bar{b}b\bar{b}$ background by about 65%. In the end, their event rates are about the same.

One can further improve the significance of the signal by attempting to reconstruct the mass of the scalar resonance. This can be difficult in principle, because one does not know *a priori* what this mass is, or which bottom quarks resulted from the ϕ decay in a given event. It may be possible to locate the peak in the invariant mass distribution of the secondary b quarks resulting from the ϕ decay, though with limited statistics and a poor mass resolution this may prove impractical. However, one can also scan through a set of masses, and provide 95% C.L. limits on the presence of a Higgs boson (with a given enhancement to the cross section, K) in the $b\bar{b}b\bar{b}$ data sample for each value of m_ϕ in the set. In order to do this, we assume a Higgs mass, and find the pair of b quarks with invariant mass which best reconstructs this assumed mass. We reject the event if this "best reconstructed" mass is more than $2\Delta m_\phi$ away from our assumed mass, where $2\Delta m_\phi$ is the maximum of either twice the natural width of the scalar under study (Γ_ϕ) or the twice experimental mass resolution. We estimate the experimental mass resolution for an object of mass m_ϕ to be,

$$\Delta m_\phi \;=\; 0.13\, m_\phi \sqrt{100\,\mathrm{GeV}/\, m_\phi}. \tag{3.3}$$

Under this assumption, the natural width of the bosons in the specific models of new physics considered below are usually smaller than this experimental mass resolution.

As shown in the fifth column of Table 3.1, this cut has virtually no effect on the signal or $Zb\bar{b}$ background (for a 100 GeV Higgs) while removing about another 10% of the $b\bar{b}b\bar{b}$ background.

As will be discussed below, the natural width of the Higgs bosons in both the MSSM and the models of strong EWSB that we wish to probe in this paper are generally much smaller than our estimated experimental mass resolution, and thus one might think that an improved experimental mass resolution could considerably improve the limits one may place on a scalar particle with a strong b interaction. However, the models in which we are interested generally have one or more nearly mass-degenerate bosons with similarly enhanced bottom Yukawa couplings. If the extra scalars are much closer in mass than the experimental mass resolution (and the natural width of the bosons), the signal can thus include separate signals from more than one of them. Thus there is potentially a trade-off in the ΔM cut between reduction of the background and acceptance of the signal from more than one scalar resonance. In order to estimate the potential improvement for discovering a single Higgs boson, we have examined the effect on the significance one obtains if the cut on the invariant mass which best reconstructs m_ϕ is reduced to Δm_ϕ as opposed to $2\Delta m_\phi$ as was considered above. We find that this improved mass resolution further reduces the QCD $b\bar{b}b\bar{b}$ background by about another 40%. Assuming four b tags (as discussed below), this improved mass resolution increases the significance of the signal from about 12.2 to 14.6, which will improve the model-independent lower bound on K by about 10%. Thus, an improved mass resolution would most likely be helpful in this analysis.

Another method to further suppress background rate is to observe that in the background events, the b quarks whose invariant mass best reconstructs m_ϕ come from the same gluon. This is because, after imposing all the kinematical cuts discussed

above, the matrix elements are dominated by Feynman diagrams in which one very far off-shell gluon decays into a $b\bar{b}$ pair, as opposed to interference of many production diagrams, which dominates the lower invariant mass region. Thus, for m_ϕ greater than about 100 GeV, the background event produces b quarks with the characteristic angular distribution of a vector decaying into fermions, $1 + \cos^2\theta$, in the rest frame of the $b\bar{b}$ system. This is distinct from the signal distribution, which comes from a scalar decay, and is flat in $\cos\theta$. Thus, for masses above 100 GeV, we further require $|\cos\theta| \leq 0.7$ after boosting back to the rest frame of the $b\bar{b}$ pair which we have identified as coming from the scalar boson ϕ.

In order to deal with the large QCD $b\bar{b}jj$ background, it is important to be able to distinguish jets initiated by b quarks from those resulting from light quarks or gluons. We estimate the probability to successfully identify a b quark passing the acceptance cuts outlined above to be 60%, with a probability of 0.5% to misidentify a jet coming from a light quark or gluon as a b jet [72]. In Table 3.2 we show the resulting number of signal and background events passing our optimized cuts at the Tevatron, assuming 2 fb^{-1}of integrated luminosity, after demanding that two or more, three or more, or four b-tags be present in the events, and the resulting significance of the signal (computed as the number of signal events divided by the square root of the number of background events). We find that requiring 3 or more b-tags results in about the same significance of 12.2σ as requiring 4 b-tags. However, we see that for the chosen parameters ($m_\phi = 100$ GeV and $K = m_t/m_b \approx 40$), even with only 2 or more b-tags, one arrives at a significance of about 3σ, and thus has some ability to probe a limited region of parameters. From the large significance, we see that the Tevatron may be used to place strong constraints on Higgs particles with enhanced bottom quark Yukawa couplings, and that the ability to tag 3 or more of the bottom quarks present in the signal can probe a larger class of models (or parameter space of

Table 3.2: The signal and background events for 2 $\text{fb}^{-1}$of Tevatron data, assuming $m_\phi = 100\,\text{GeV}$, $2\Delta m_\phi = 26\,\text{GeV}$, and $K = 40$ for two or more, three or more, or four b-tags, and the resulting significance of the signal.

Process	2 or more b-tags	3 or more b-tags	4 b-tags
$\phi b\bar{b}$	1139	660	180
$Zb\bar{b}$	293	170	46
$b\bar{b}b\bar{b}$	1054	610	166
$b\bar{b}jj$	1.2×10^5	2141	4
Significance	3.3	12.21	12.25

the models) as compared to what is possible if only 2 or more of the bottom quarks are tagged. In the analysis below, to allow for the possibility that the $b\bar{b}jj$ background may be somewhat larger than our estimates, we require 4 b-tags, though as we have demonstrated above, we do not expect a large change in the results if 3 or 4 b-tags were required instead.

This analysis can be repeated for any value of m_ϕ, using the corresponding p_T for that particular mass described above. It is interesting to note that the signal composition in terms of the gg or $q\bar{q}$ initial state depends on the collider type and the mass of the produced boson, which controls the type of PDF and the typical region of $x \sim m_\phi^2/S$ at which it is evaluated. At the Tevatron, for $m_\phi = 100$ GeV, the signal is 99% gg initial state before cuts, and 87% after cuts, while for $m_\phi = 200$ GeV, it is 99% gg initial state before cuts, and 85% after cuts. Thus, at the Tevatron, one ignores about 15% of the signal if one relies on a calculation employing only the gg initial state. At the LHC, for $m_\phi = 100$, the signal is very close to 100% gg initial state before cuts and 99% after cuts, and for $m_\phi = 500$ GeV, it is 99% gg initial state

Table 3.3: Event numbers of signal (N_S), for one Higgs boson, and background (N_B) for a 2 fb^{-1}of Tevatron data and a 100 fb^{-1}of LHC data, for various values of m_ϕ, after applying the cuts described in the text, and requiring 4 b-tags. An enhancement of $K = 40$ is assumed for the signal, though the numbers may be simply scaled for any $K_{\rm new}$ by multiplying by $(K_{\rm new}/40)^2$.

	Tevatron		LHC	
m_ϕ (GeV)	N_S	N_B	N_S	N_B
75	583	640	3.4×10^6	4.8×10^6
100	180	216	2.0×10^6	3.0×10^6
150	58	92	9.2×10^5	1.2×10^6
200	17	31	4.2×10^5	5.6×10^5
250	4.8	8.8	1.9×10^5	2.0×10^5
300	1.3	2.1	83000	70000
500			12000	5700
800			1500	406
1000			407	70

before cuts, and 99% after cuts. This indicates that at the LHC, very accurate results are possible from a calculation considering only the gg initial state. The resulting numbers of signal and (total) background events after cuts for various boson masses are shown in Table 3.3.

From these results, one may derive the minimum value of K, $K_{\rm min}$, for a scalar boson with mass m_ϕ to be discovered at the Tevatron or the LHC via the production mode $b\bar{b}\phi(\to b\bar{b})$. Similarly, if signal is not found, one can exclude models which predict the enhancement factor K to be larger than $K_{\rm min}$. To give a model-independent result, we assume that the width of the ϕ is much less than the estimated experimental mass resolution defined above, which is the case for the models studied in this paper. We determine $K_{\rm min}$ by noting that in the presence of a Higgs boson with enhanced bottom Yukawa couplings, the number of expected signal events passing

our selection criterion is given by $N_S = K^2\, N_S^{(SM)}$, where $N_S^{(SM)}$ is the number of signal events expected for a scalar of mass m_ϕ with SM coupling to the b quark (assuming $\mathrm{Br}(\phi \to b\bar{b}) = 1$), whereas the number of background events expected to pass our cuts, N_B, is independent of K. Thus, requiring that no 95% C.L. deviation is observed in the $b\bar{b}b\bar{b}$ data sample (and assuming Gaussian statistics) determines

$$K_{\min} = \sqrt{\frac{1.96\,\sqrt{N_B}}{N_S^{(SM)}}}, \tag{3.4}$$

where 1.96σ is the 95% C.L. in Gaussian statistics. In Figure 3.5, we show the resulting 95% C.L. limits one may impose on $K_{\min}$ as a function of m_ϕ from the Tevatron with 2, 10, and 30 fb^{-1}and from the LHC with 100 fb^{-1}, as well as the discovery reach of the LHC at the 5σ level. Our conclusions concerning the LHC's ability to probe a Higgs boson with an enhanced b Yukawa coupling are very similar to those drawn in [73], but are considerably more optimistic than those in [74], where the conclusion was that the $b\bar{b}jj$ background is considerably larger than our estimate (though there are elements of the search strategy which differ between those of [74] and ours as well, and their simulation of the ATLAS detector is certainly more sophisticated). In [74] the backgrounds were simulated using PYTHIA [75] to generate two to two hard scatterings and then generating the additional jets from a parton showering algorithm. As noted above, in the light of the strong (ordering of) p_T and isolation cuts applied to select the signal events, we feel that a genuine four body matrix element calculation such as was used in our analysis provides a more reliable estimate of this background.

We have examined the scale and PDF dependence of our calculation for the signal and background rates at the Tevatron, and find that in varying the scale between one half and twice its default choice (defined above), $\mu = \mu_0/2$ and $\mu = 2\mu_0$, the $\phi b\bar{b}$ signal and $Zb\bar{b}$ background rates both vary from the result at $\mu = \mu_0$ by about 30%, while

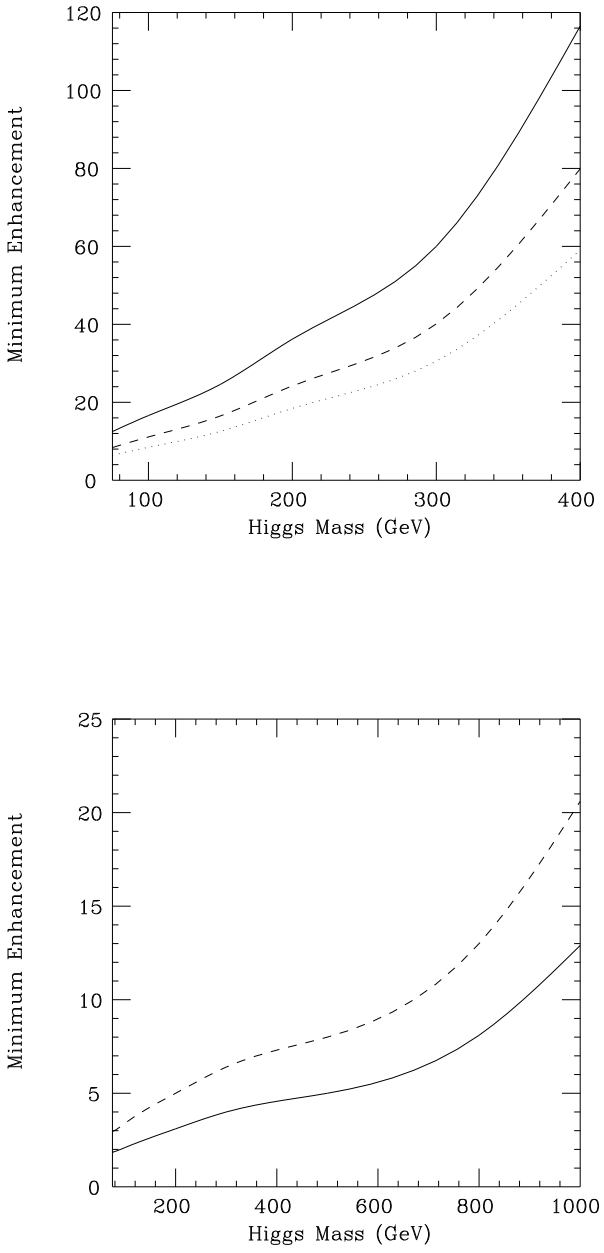

Figure 3.5: In the upper figure is the model-independent minimum enhancement factor, $K_{\min}$, excluded at 95% C.L. as a function of scalar mass (m_ϕ) for the Tevatron Run II with 2 fb^{-1}(solid curve), 10 fb^{-1}(dashed curve) and 30 fb^{-1}(dotted curve). The lower figure shows the same factor, $K_{\min}$, excluded at 95% C.L. (solid curve) and discovered at 5σ (dashed curve) as a function of m_ϕ for the LHC with 100 fb^{-1}.

the $b\bar{b}b\bar{b}$ and $b\bar{b}jj$ backgrounds vary by about 45%. This strong scale dependence is indicative of the possibility of large higher order corrections to the leading order rate. Thus, in order to better understand the true signal and background rates, it would be useful to pursue these calculations to NLO. We have also compared the difference in the results from the MRRS(R1) PDF [40] and the CTEQ4L PDF, and find a variation of about 10% in the resulting signal and background rates. Since these separate sources of uncertainty (from PDF and scale dependence) are non-Gaussianly distributed, there is no way to rigorously combine them. Thus, we conservatively choose to add them linearly, finding a total uncertainty of about 40% in the signal rate ($N_S^{(SM)}$), and 50% in the background rate (N_B). From the derivation of $K_{\min}$ above, we see that these uncertainties in signal and background rate (which we assume to be uncorrelated) combine to give a fractional uncertainty in $K_{\min}$,

$$\frac{\delta K_{\min}}{K_{\min}} = \sqrt{\left(\frac{\delta N_S^{(SM)}}{2\,N_S^{(SM)}}\right)^2 + \left(\frac{\delta N_B}{4\,N_B}\right)^2}, \tag{3.5}$$

where $\delta N_S^{(SM)}$ and δN_B are the absolute uncertainties in $N_S^{(SM)}$ and N_B, respectively. From this result, we see that in terms of a more precise theoretical determination of $K_{\min}$, one gains much more from a better understanding of the signal rate than a better determination of the backgrounds. Applying our estimate of the uncertainty from PDF and scale dependence to Eq. (3.5), we find an over-all theoretical uncertainty in $K_{\min}$ of about 25%.

3.3 Implications for Models of Dynamical EWSB

Examples of the strongly interacting EWSB sector with composite Higgs bosons are top-condensate and top-color models [20, 21], in which new strong dynamics associated with the top quark play a crucial role for top and W, Z mass generation. A

generic feature of these models is a naturally large Yukawa coupling of the bottom quark, of the same order as that of top ($y_t \sim 1$), due to the infrared quasi-fixed-point structure [76] and particular boundary conditions for (y_b, y_t) at the compositeness scale.

3.3.1 The Two Higgs Doublet Extension of the BHL Model

The effective theory of the top-condensate model is the SM without its elementary Higgs boson, but with 4-Fermi interaction terms induced from (unspecified) strong dynamics at a high scale Λ instead. The minimal Bardeen-Hill-Lindner (BHL) top-condensate model with three families [20], contains only one type of 4-Fermi vertex for $< \bar{t}t >$ condensation which generates the masses for the top, and the W, and Z bosons. However, the top mass required to obtain the correct boson masses is too large to reconcile with experiment. Thus, we consider the two Higgs doublet extension (2HDE) [78] as an example (which, with some improvements [20, 46], is expected to produce an acceptable m_t), and examine its prediction for the $\phi b\bar{b}$ rate. The 4-Fermi interactions of the 2HDE model produce condensates in both the $t\bar{t}$ and $b\bar{b}$ channels, which generate the EWSB and induce two composite Higgs doublets Φ_t and Φ_b. The Yukawa interactions take the form,

$$y_t \left(\bar{\Psi}_L \, \Phi_t \, t_R + H.c. \right) + y_b \left(\bar{\Psi}_L \, \Phi_b \, b_R + H.c. \right). \tag{3.6}$$

In the above equation, $\bar{\Psi}_L$ is the left-handed third family quark doublet and t_R is the right-handed top, and so forth. This model predicts $y_t(\Lambda) = y_b(\Lambda) \gg 1$ at the scale Λ [20, 78]. In fact, one finds that $y_t(\mu) \approx y_b(\mu)$ for any $\mu < \Lambda$, because the renormalization group equations governing the running of y_t and y_b are identical except for the small difference in the the t and b hypercharges [20, 76]. Due to the dynamical $< \bar{t}t >$ and $< \bar{b}b >$ condensation, the two composite Higgs doublets develop

VEV's,

$$\begin{aligned} < \Phi_t > &= (v_t, 0)^T / \sqrt{2} \\ < \Phi_b > &= (0, v_b)^T / \sqrt{2}. \end{aligned} \tag{3.7}$$

The bottom mass is given by $m_b = y_b\, v_b/\sqrt{2}$, and must match the experimental value at scale $\mu = m_b \sim 4.5$ GeV. Assuming the Yukawa couplings $y_t \sim y_b \sim 1$, this requires the two VEV's to have ratio,

$$\frac{v_t}{v_b} \simeq 39 = \tan\beta. \tag{3.8}$$

We thus see that in this model, the bottom quark has a Yukawa coupling of the same order as the top quark, which implies that $\tan\beta = v_t/v_b$ is naturally large.

The 2HDE has three neutral scalars, the lightest with enhanced bottom coupling being the pseudoscalar,

$$P = \sqrt{2}(\sin\beta\ \mathrm{Im}\,\Phi_b^0 + \cos\beta\ \mathrm{Im}\,\Phi_t^0), \tag{3.9}$$

whose mass (M_P) is less than about 233 GeV for $\Lambda = 10^{15}$ GeV [78]. Given y_b and M_P, one can calculate the production rate of $P\,b\,\bar{b}(\to b\,\bar{b}\,b\,\bar{b})$ at hadron colliders, and thus for a given M_P one can determine the minimal y_b value needed for the Tevatron and LHC to observe the signal. As shown in Figure 3.6a, the Tevatron Run II data with $2\,\mathrm{fb}^{-1}$ will exclude such a model with $M_P \sim 200$ GeV at 95%C.L.

3.3.2 Top-color Assisted Technicolor

The top-color-assisted technicolor models (TCATC) [21] postulate the gauge structure $\mathcal{G} = \mathrm{SU}(3)_1 \times \mathrm{SU}(3)_2 \times \mathrm{U}(1)_1 \times \mathrm{U}(1)_2 \times \mathrm{SU}(2)_L$ at the scale above Λ to explain the dynamic origin of the 4-Fermi couplings described above. At $\Lambda \sim 1$ TeV, $\mathcal{G}$ spontaneously breaks down to $\mathrm{SU}(3)_C \times \mathrm{U}(1)_Y \times \mathrm{SU}(2)_L$, and additional massive

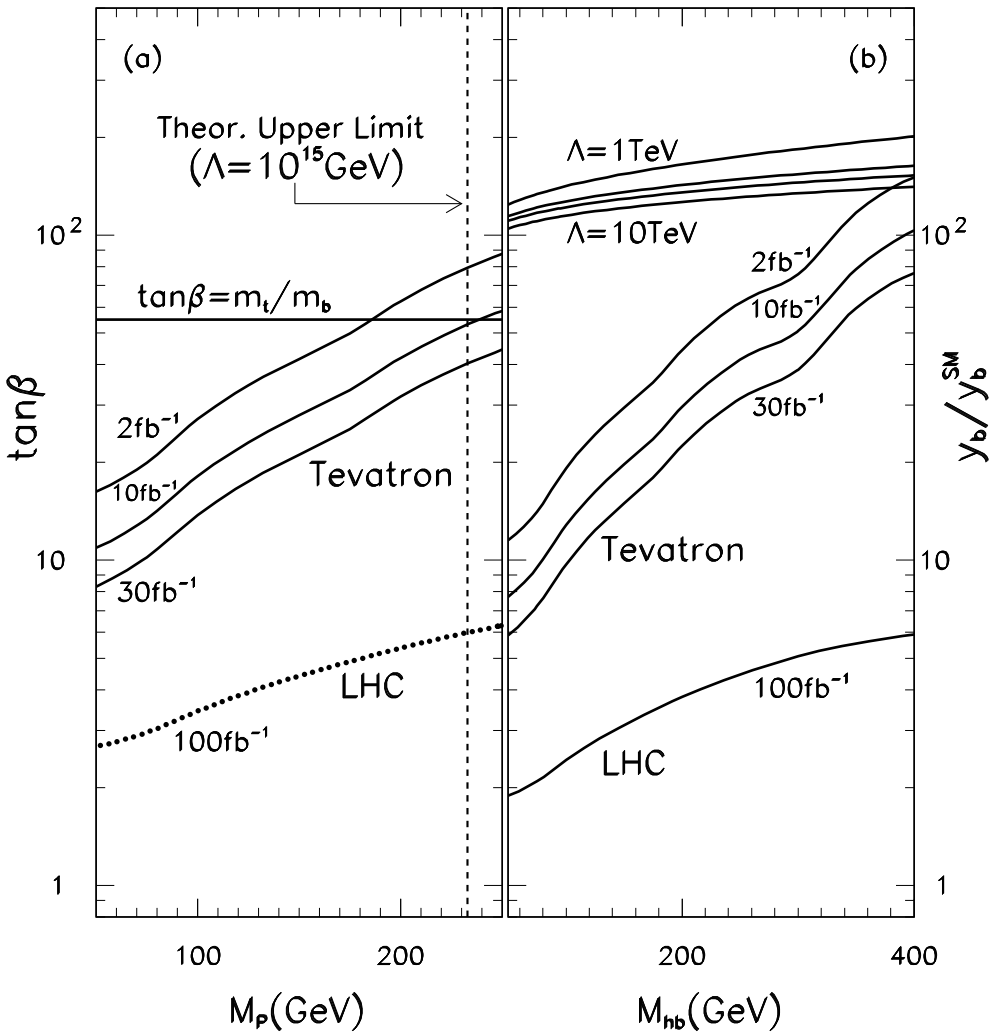

Figure 3.6: The reach of the Tevatron and LHC for the models of (a) 2HDE and (b) TCATC. Regions below the curves can be excluded at 95%C.L. In (b), the straight lines indicate $y_t(\mu = m_t)$ for typical values of the top-color breaking scale, Λ. y_b is predicted to be very close to y_t.

gauge bosons are produced in color octet (B^a) and singlet (Z') states. Below the scale Λ, the effective 4-Fermi interactions are generated in the form,

$$\mathcal{L}_{4F} = \frac{4\,\pi}{\Lambda^2}\left[\left(\kappa + \frac{2\kappa_1}{9\,N_c}\right)\bar{\Psi}_L\,t_R\,\bar{t}_R\,\Psi_L + \left(\kappa - \frac{\kappa_1}{9\,N_c}\right)\bar{\Psi}_L\,b_R\,\bar{b}_R\,\Psi_L\right], \tag{3.10}$$

where κ and κ_1 originate from the strong $SU(3)_1$ and $U(1)_1$ dynamics, respectively. In the low energy effective theory at the EWSB scale, two composite Higgs doublets are induced with the Yukawa couplings

$$y_t = \sqrt{4\pi\left(\kappa + 2\frac{\kappa_1}{9N_c}\right)} \tag{3.11}$$

$$y_b = \sqrt{4\pi\left(\kappa - \frac{\kappa_1}{9N_c}\right)},$$

It is clear that, unless κ_1 is unnaturally larger than κ, y_b is expected to be only slightly below y_t. The $U(1)_1$ force is attractive in the $<\bar{t}t>$ channel but repulsive in the $<\bar{b}b$ channel, thus t, but not b, acquires a dynamical mass, provided $y_b(\Lambda) < y_{\rm crit} = \sqrt{8\pi^2/3} < y_t(\Lambda)$. (In this model, b acquires a mass mainly from a top-color instanton effect [21].) Furthermore, the composite Higgs doublet Φ_t, but not Φ_b, develops a VEV, i.e., $v_t \neq 0$ and $v_b = 0$.

In TCATC, the top-color interaction generates m_t, but is not responsible for the entire EWSB. Thus, Λ can be as low as $O(1-10)\,$TeV (which avoids the severe fine-tuning needed in the minimal models [20, 78]), and correspondingly, $v_t = 64-88\,$GeV for $\Lambda = 1-5$ TeV by the Pagels-Stokar formula. The smaller value of v_t predicted in the TCATC model, compared to $v = 246\,$GeV makes the top coupling to Φ_t stronger, i.e., $y_t = 2.8-3.9$ at $\mu = m_t$, than in the SM ($y_t \sim 1$). As explained above, this results in a large bottom Yukawa interaction, y_b, as well. Thus, the neutral scalars h_b and A_b in the doublet Φ_b, which are about degenerate in mass, have an enhanced coupling to the b-quark.

In Figure 3.6b, we show the minimal value of $y_b/(y_b)_{SM}$ needed to observe the TCATC model signal as a function of M_{h_b}. As shown, if M_{h_b} is less than about 400 GeV, the Tevatron Run II data can effectively probe the scale of the top-color breaking dynamics, assuming the TCATC model signal is observed. If the signal is not found, the LHC can further explore this model up to large M_{h_b}. For example, for $M_{h_b} = 800\,\text{GeV}$, the required minimal value of $y_b/(y_b)_{SM}$ is about 9.0 at 95%C.L. Similar conclusions can be drawn for a recent left-right symmetric extension [79] of the top-condensate scenario, which also predicts a large b-quark Yukawa coupling.

3.4 Implications for Supersymmetric Models

The EWSB sector of the MSSM model includes two Higgs doublets with a mass spectrum including two neutral CP-even scalars h^0 and H^0, one CP-odd pseudoscalar A^0 and a charged pair $H^\pm$. The Higgs sector is completely determined at tree level by fixing two parameters, conventionally chosen to be the ratio of the VEV's, $\tan\beta$, and the pseudoscalar mass, m_A [80]. At loop level, large radiative corrections to the Higgs boson mass spectrum are dominated by the contributions of top quarks and squarks in loops [81]. In this study we employ the full one loop results [82] to generate the Higgs mass spectrum assuming the sfermion masses, μ, scalar tri-linear parameters, and $\text{SU}(2)_L$ gaugino masses at the electro-weak scale are those chosen in the LEP Scan A2 set. There is some sensitivity to this choice of parameters, coming from the Higgs mass spectrum and coupling to bottom quarks [68, 83].

The parameter $\tan\beta$ is free in the MSSM, and the Higgs mass is constrained by $m_h, m_A > 75\,\text{GeV}$ for $\tan\beta > 1$ [13]. Since the couplings of h^0-b-$\bar{b}$, H^0-b-$\bar{b}$ and A^0-b-$\bar{b}$ are proportional to $\sin\alpha/\cos\beta$, $\cos\alpha/\cos\beta$ and $\tan\beta$, respectively, they can receive large enhancing factor when $\tan\beta$ is large. This can lead to detectable $b\bar{b}b\bar{b}$ signal

events at the LHC, as was previously studied in [73]. We calculate the enhancement factor K predicted by the MSSM for given values of $\tan\beta$ and m_A. In Figure 3.7 we present the discovery reach of the Tevatron and the LHC, assuming the LEP Scan A2 soft-breaking parameters, and that all the superparticles are so heavy that Higgs bosons will not decay into them at tree level. For comparison, the region that will be covered by LEP II is also shown.

The BR for $\phi \to b\bar{b}$ is close to one for most of the parameter space above the discovery curves. Moreover, for $\tan\beta \gg 1$, the h^0 is nearly mass-degenerate with the A^0 (if m_A is less than $\sim$120 GeV) and otherwise with H^0. We thus include both scalars in the signal rate provided their masses differ by less than Δm_h. The MSSM can also produce additional $b\bar{b}b\bar{b}$ events through production of $h^0 Z \to b\bar{b}b\bar{b}$ and $h^0 A^0 \to b\bar{b}b\bar{b}$, however these rates are expected to be relatively small when the Higgs-bottom coupling is enhanced, and the resulting kinematics are different from the $\phi b\bar{b}$ signal. Thus we conservatively do not include these processes in our signal rate.

From Figure 3.7 we deduce that if a signal is not found, the MSSM with $\tan\beta >$ 45 (30, 20) can be excluded for m_A up to 200 GeV at the 95% C.L. by Tevatron data with a luminosity of 2 (10, 30) fb^{-1}; while the LHC can exclude a much larger m_A (for $m_A = 800$ GeV, the minimal value of $\tan\beta$ is about 5). These Tevatron bounds thus improve a recent result obtained by studying the $b\bar{b}\tau\tau$ channel [84]. We note that studying the $\phi b\bar{b}$ mode can probe an important region of the $\tan\beta$-m_A plane which is not easily covered by other production modes at hadron colliders, such as $pp \to t\bar{t} + \phi(\to \gamma\gamma) + X$ and $pp \to \phi(\to ZZ^*) + X$ [85]. Also, in this region of parameter space the SUSY Higgs boson h^0 is clearly distinguishable from a SM one.

The above results provide a general test for many SUSY models, for which the

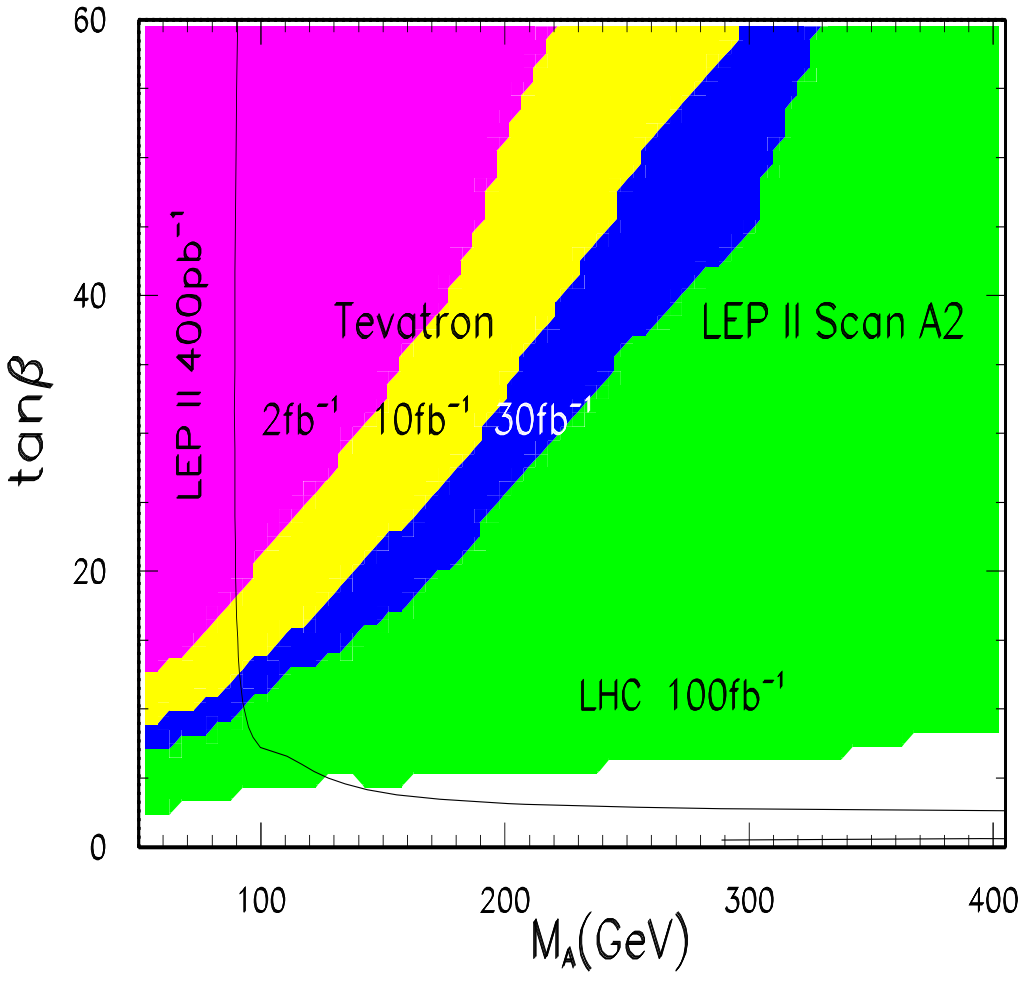

Figure 3.7: The regions above the curves in the $\tan\beta$-m_A plane can be probed at the Tevatron and LHC with a 95% C.L.. The soft breaking parameters correspond to the LEP Scan A2 set. The region below the solid line will be covered by LEP II.

MSSM is the low energy effective theory. In the MSSM, the effect of SUSY breaking is parametrized by a large set of soft-breaking (SB) terms ($\sim O(100)$), which in principle should be derived from an underlying model. We discuss, as examples, the Supergravity and Gauge-mediated (GM) models with large $\tan\beta$. In the supergravity-inspired model [86] the SUSY breaking occurs in a hidden sector at a very large scale, of $O(10^{10-11})$ GeV, and is communicated to the MSSM through gravitational interactions. In the simplest model of this kind, all the SB parameters are expressed in terms of 5 universal inputs. The case of large $\tan\beta$, of $O(10)$, has been examined within this context [87], and it was found that in such a case $m_A \sim 100$ GeV. Hence, these models can be cleanly confirmed or excluded by measuring the $b\bar{b}b\bar{b}$ mode at the Tevatron and LHC.

The GM models assume that the SUSY-breaking scale is much lower, of $O(10^{4-5})$ GeV, and the SUSY breaking is communicated to the MSSM superpartners by ordinary gauge interaction [48]. This scenario can predict large $\tan\beta$ (~ 30). However, some models favor $m_A \gtrsim 400\,\text{GeV}$ [88], which would be difficult to test at the Tevatron, though quite easy at the LHC. Nevertheless, in some other models, a lighter pseudoscalar is possible (for instance, $\tan\beta = 45$ and $m_A = 100$) [89], and the $b\bar{b}b\bar{b}$ mode at hadron colliders can easily explore such a SUSY model.

3.5 Conclusions

In conclusion, the large QCD production rate at a hadron collider warrants the detection of a light scalar with large ϕ-b-$\bar{b}$ coupling. This process can provide useful information concerning dynamical models of EWSB and on the MSSM, either through discovery or by limiting the viable region of parameters in the model.

At LEP-II and future e^+e^- linear colliders, because of the large phase space sup-

pression factor for producing a direct 3-body final state as compared to first producing a 2-body resonant state, the $b\bar{b}A^0$ and $b\bar{b}h^0$ rates predicted by the MSSM are dominated by the production of $A^0\,h^0$ and $h^0\,Z$ pairs via electroweak interactions. Hence, the e^+e^- collider is less able to directly probe the ϕ-b-$\bar{b}$ coupling. This has the effect that our process is complimentary to the the LEP studies, in that it is sensitive to a different region of SUSY parameter space.

Chapter 4

Associated Production of Gauginos with Gluinos at NLO

As we saw in Chapter 1, one of the attractive solutions to the problems with the Higgs sector of the SM is to introduce weak scale supersymmetry, which removes the instability of the Higgs mass under quantum corrections, and deals with the triviality problem. Thus, the discovery of SUSY would constitute a major development in understanding the EWSB. In this chapter we demonstrate how the NLO SUSY-QCD corrections to the production of a gaugino($\tilde{\chi}$) in association with a gluino ($\tilde{g}$) are moderately sizable, and significantly improve the theoretical stability of the cross section [90], which is important in interpreting experimental data in terms of a SUSY discovery or exclusion.

Supersymmetry predicts the existence of supersymmetric partners for each of the particles of the standard model. The search for these sparticles is a principal motivation of the forthcoming Run II of the Fermilab Tevatron collider and of the CERN Large Hadron Collider (LHC) program. A potentially important, but heretofore largely overlooked, discovery channel is the associated production of a spin-1/2 gaugino with a spin-1/2 gluino or with a spin-0 squark ($\tilde{q}$). Color-neutral gauginos couple with electroweak strength, whereas the colored squarks and gluinos couple strongly.

Associated production is therefore a semi-weak process in that it involves one somewhat smaller coupling constant than the pair production of colored sparticles. However, in popular models of SUSY breaking [48, 86], the mass spectrum favors much lighter masses for the low-lying neutralinos and charginos than for the squarks and gluinos. This mass hierarchy means that the phase space for production of neutralinos and charginos, the corresponding partonic luminosities, and the production cross sections will be greater than those for gluinos and squarks. These advantages are potentially decisive at a collider with limited energy, such as the Tevatron. Furthermore, associated production has a clean experimental signature. For example, the lowest lying neutralino is the (stable) lightest supersymmetric particle (LSP) in supergravity (SUGRA) models [86], manifest as missing energy in the events, and it is the second lightest in gauge-mediated models [48]. In models with a very light gluino [91], there could be large rates for $\tilde{g}\tilde{\chi}$ production, with simple signatures, whereas $\tilde{g}\tilde{g}$ production suffers from large hadronic jet backgrounds.

Experimental investigations are facilitated by firm theoretical understanding of the expected sizes of the cross sections for production of the superparticles. In the case of hadron-hadron colliders, the large strong coupling strength (α_S) results in potentially large contributions to cross sections from terms beyond leading order (LO) in a perturbative quantum chromodynamics (QCD) evaluation of the cross section. For accurate theoretical estimates, it is necessary to extend the calculations to next-to-leading order (NLO) or beyond. NLO contributions generally reduce and stabilize dependence on undetermined parameters such as the renormalization and factorization scales. To date, associated production has been calculated only in LO [92], but NLO results exist for hadroproduction of gluinos and "light" squarks[1] [93], top

[1]By light squarks, we refer to the squarks which are the superpartners of light quarks (u, d, s, c, and b). In most models of SUSY breaking these scalars have masses on the order of a few hundred GeV.

squarks [94], sleptons [95, 96], and gauginos [96]. Studies have begun to incorporate these NLO results into Monte Carlo simulations [97, 98].

In this Chapter we present the first NLO (in SUSY-QCD) calculation of hadroproduction of a $\tilde{g}$ in association with a $\tilde{\chi}$, including contributions from virtual loops of colored sparticles and particles and three-particle final states involving the emission of light real particles. We extract the ultraviolet, infrared, and collinear divergences by use of dimensional regularization and employ standard $\overline{\rm MS}$ renormalization and mass factorization procedures. In the course of computing the virtual contributions, we encountered new divergent four-point functions. The contributions from real emission of light particles are treated with a phase space slicing method. We provide predictions for inclusive cross sections at Tevatron and LHC energies. We focus on the $\tilde{g}\tilde{\chi}$ final state, rather than on the associated production of $\tilde{q}\tilde{\chi}$, because at the energy of the Tevatron the LO cross sections for $\tilde{g}\tilde{\chi}$ are 3 to 6 times greater than those for $\tilde{q}\tilde{\chi}$ when $m_{\tilde{g}} = m_{\tilde{q}} = 300$ GeV, and 6 to 15 times greater when $m_{\tilde{g}} = m_{\tilde{q}} = 600$ GeV. In obtaining the $\tilde{q}\tilde{\chi}$ cross sections, we sum over five flavors of squarks and anti-squarks.

4.1 Leading Order Cross Sections

In LO of SUSY-QCD, the associated production of a gluino and a gaugino proceeds through the subprocess $q\bar{q} \to \tilde{g}\tilde{\chi}$ with a t-channel or a u-channel squark exchange. We assume that there is no mixing between squarks of different generations and that the squark mass eigenstates are aligned with the squark chirality states, equivalent to the assumption that the two squarks of a given flavor are degenerate in mass. We ignore the $n_f = 5$ light quark masses in all of the kinematics and couplings. Under these assumptions, the massless incoming quarks and antiquarks have a particular helicity, and thus the Feynman diagrams in which a right-handed squark is exchanged cannot

interfere with those mediated by a left-handed squark. In evaluating the Feynman diagrams involving Majorana and explicitly charge-conjugated fermions, we follow the approach of [99]. In the case of charged gauginos, only the left-handed squarks participate, whereas neutral gauginos receive contributions from both left- and right-handed squarks.

The LO matrix element summed (averaged) over the colors and helicities of the outgoing (incoming) particles has the analytic form [92]

$$\overline{|\mathcal{M}^B|}^2 = \frac{8\pi\,\hat{\alpha}_S}{9} \quad \left[\quad \frac{\hat{X}_t\, t_{\tilde{g}}\, t_{\tilde{\chi}}}{(t-m^2_{\tilde{q}_t})^2} - \frac{2\,\hat{X}_{tu}\, s\, m_{\tilde{g}}\, m_{\tilde{\chi}}}{(t-m^2_{\tilde{q}_t})(u-m^2_{\tilde{q}_u})} + \frac{\hat{X}_u\, u_{\tilde{g}}\, u_{\tilde{\chi}}}{(u-m^2_{\tilde{q}_u})^2} \right]. \qquad (4.1)$$

Here, $m_{\tilde{q}_{t,u}}$ is the mass of the squark exchanged in the t- and u-channels, and $\hat{\alpha}_S = \hat{g}_S^2/4\pi$ is the coupling between quarks, squarks, and gluinos (at leading order it is equal to the gauge coupling constant α_S). $\hat{X}_{t,tu,u}$ stand for the weak couplings of quarks, squarks, and gauginos which will be explained below, and the quantities s, t, and u are the usual Mandelstam invariants at the partonic level with $t_{\tilde{g},\tilde{\chi}} = t - m^2_{\tilde{g},\tilde{\chi}}$ and $u_{\tilde{g},\tilde{\chi}} = u - m^2_{\tilde{g},\tilde{\chi}}$.

For production of a neutralino of type $\tilde{\chi}^0_j$, the $\hat{X}$ are given by [100]

$$\hat{X}_t = \hat{X}_u = \hat{X}_{tu} = 2\left| e\, e_q\, N'_{j\,1} + \frac{e}{\sin\theta_W\, \cos\theta_W} \left(T_q - e_q\, \sin^2\theta_W \right) N'_{j\,2} \right|^2. \qquad (4.2)$$

In the expressions above, e is the electric charge, θ_W the weak mixing angle, T_q the third component of the weak isospin for the squark, and e_q is the charge of the quark in units of e. For up-type quarks $e_q = 2/3$ and for down-type quarks $e_q = -1/3$. The matrix N' is the transformation from the interaction to mass eigenbasis defined in [100]. The expressions for production of positive chargino of type $\tilde{\chi}^+_j$ are

$$\hat{X}_t = \frac{e^2}{\sin^2\theta_W} |V_{j\,1}|^2, \qquad (4.3)$$

$$\hat{X}_{tu} = \frac{e^2}{\sin^2\theta_W} \mathrm{Re}\,(\, V_{j\,1}\, U^*_{j\,1}),$$

$$\hat{X}_u = \frac{e^2}{\sin^2\theta_W}|U_{j\,1}|^2,$$

and for the negative chargino $\tilde{\chi}_j^-$ they have the form,

$$\hat{X}_t = \frac{e^2}{\sin^2\theta_W}|U_{j\,1}|^2, \tag{4.4}$$

$$\hat{X}_{tu} = \frac{e^2}{\sin^2\theta_W}\,\mathrm{Re}\,(\,V_{j\,1}^*\,U_{j\,1}),$$

$$\hat{X}_u = \frac{e^2}{\sin^2\theta_W}|V_{j\,1}|^2,$$

where U and V are the chargino transformation matrices from interaction to mass eigenstates defined in [100]. As was mentioned above, in the case of chargino production, the exchanged squark is always left-handed.

4.2 Next-to-Leading Order Corrections

At NLO in SUSY-QCD the cross section receives contributions from virtual loop diagrams and from real parton emission diagrams. The virtual contributions arise from the interference of the Born amplitudes with the related one-loop amplitudes containing self-energy corrections, vertex corrections, and box diagrams. We include the full supersymmetric spectrum of strongly interacting particles in the virtual loops, i.e. squarks and gluinos as well as quarks and gluons.

4.2.1 Virtual Loop Corrections

Since the virtual loop contributions are ultraviolet and infrared divergent, we regularize the cross section by computing the phase space and matrix elements in $n = 4 - 2\epsilon$ dimensions. We calculate the traces of Dirac matrices using the "naive" γ_5 scheme in which γ_5 anticommutes with all other γ_μ matrices. This choice is justified for anomaly-free one-loop amplitudes. The γ_5 matrix enters the calculation through

both the quark-squark-gluino and quark-squark-gaugino couplings. We simplify the integration over the internal loop momenta by reducing all tensorial integration kernels to expressions that are only scalar in the loop momentum [101]. The resulting one-, two-, three-, and some of the four-point functions were computed in the context of other physical processes [93]. However, we compute two previously unknown divergent four-point functions; these new functions arise because the final state gluino and gaugino generally have different masses. We evaluate the scalar four-point functions by calculating the absorptive parts with Cutkosky cutting rules and the real parts with dispersion techniques.

The ultraviolet (UV) divergences are manifest in the one- and two-point functions as poles in $1/\epsilon$. We remove them by renormalizing the coupling constants in the $\overline{\rm MS}$ scheme at the renormalization scale Q and the masses of the heavy particles (squarks and gluinos) in the on-shell scheme. The self-energies for external particles are multiplied by a factor of $1/2$ for proper wave function renormalization. A difficulty arises from the fact that spin-1 gluons have $n-2$ possible polarizations, whereas spin-$1/2$ gluinos have 2, leading to broken supersymmetry in the $\overline{\rm MS}$ scheme. The simplest procedure to restore supersymmetry is with finite shifts in the quark-squark-gluino and quark-squark-gaugino couplings [102].

In addition to the ultraviolet singularities, the virtual corrections have collinear and infrared singularities that show up as $1/\epsilon$ or $1/\epsilon^2$ poles in the derivatives of the two-point function and in the three- and four-point functions. These infrared singularities appear as factors times parts of the Born matrix elements. They can be separated into C_F and N_C color classes, depending on the color flow and the Abelian or non-Abelian nature of the correction vertices. They are cancelled eventually by corresponding soft and collinear singularities from the real three particle final state corrections.

4.2.2 Real Emission Corrections

The real corrections to the production of gluinos and gauginos arise from three particle final-state subprocesses in which additional gluons and massless quarks and antiquarks are emitted: $q\bar{q} \to \tilde{g}\tilde{\chi}g$, $qg \to \tilde{g}\tilde{\chi}q$, and $\bar{q}g \to \tilde{g}\tilde{\chi}\bar{q}$.

The n-dimensional phase space for $2 \to 3$ scattering may be factored into the phase space for $2 \to 2$ scattering and the phase space for the subsequent decay of one of the two final state particles with squared invariant mass $s_4 = (p_1 + p_3)^2 - m_1^2$ into two particles with momenta p_1 and p_3, parametrized in the rest frame of particles 1 and 3 [103]. We follow the procedure of [103] and reduce all of the angular integrals. to the form

$$\begin{aligned} I_n^{(k,l)} &= \int_0^\pi \sin^{1-2\epsilon}(\theta_1)\, d\theta_1 \int_0^\pi \sin^{-2\epsilon}(\theta_2)\, d\theta_2 \\ &\times \quad (a + b\cos\theta_1)^{-k}(A + B\cos\theta_1 + C\sin\theta_1\cos\theta_2)^{-l}. \end{aligned} \tag{4.5}$$

Analytic expressions for the integrals $I_n^{(k,l)}$ for different k, l may be found in [103]. The angular integrations involving negative powers of $t' = (p_b - p_3)^2$ and $u' = (p_a - p_3)^2$, where p_a and p_b are the four-momenta of the incoming partons, produce poles in $1/\epsilon$ which correspond to the collinear singularities in which particle 3 is collinear with particle a or b. Because these singularities have a universal structure, they may be removed from the cross section and absorbed into the parton distribution functions according to the usual mass factorization procedure [104].

In addition to the collinear singularities described above, the corrections involving real gluon emission also have infrared (IR) singularities arising when the energy of the emitted gluon approaches zero. These singularities appear as poles in s_4 in the cross section and must also be extracted so that they can be combined with corresponding terms in the virtual corrections and shown to cancel. In order to make this cancellation

conveniently, we slice the gluon emission phase space into hard and soft pieces,

$$\frac{d^2\hat{\sigma}_{ij}^R}{dt_{\tilde{\chi}}du_{\tilde{\chi}}} = \int_0^{\Delta} ds_4 \, \frac{d^3\sigma^S}{dt_{\tilde{\chi}}\, du_{\tilde{\chi}}\, ds_4} + \int_{\Delta}^{s_4{}^{max}} ds_4 \, \frac{d^3\sigma^H}{dt_{\tilde{\chi}}\, du_{\tilde{\chi}}\, ds_4}, \tag{4.6}$$

where Δ is an arbitrary cut-off between soft and hard gluon radiation. When the cut-off is much smaller than the other invariants, the s_4 integration for the soft term becomes simple and can be evaluated analytically, leading to explicit logarithms of the form $\log \Delta/m_{\tilde{g}}^2, \log^2 \Delta/m_{\tilde{g}}^2$. The hard term is free from infrared and, after mass factorization, also collinear singularities and can be evaluated numerically in four dimensions. This procedure leads to an implicit logarithmic dependence of the hard term on the cut-off Δ which cancels the explicit logarithmic dependence in the soft term.

4.3 NLO Inclusive Cross Sections

To obtain numerical results for the cross sections, we work within a particular SUGRA scheme, though the cross sections depend principally on the masses of the $\tilde{\chi}$ and $\tilde{g}$ and are otherwise fairly independent of the details of the SUSY breaking. The physical gluino and gaugino masses as well as the gaugino mixing matrices are calculated from the minimal SUGRA scenario. We choose the common scalar and gaugino masses at the GUT scale to be $m_0 = 100$ GeV, $m_{1/2} = 150$ GeV, trilinear coupling $A_0 = 300$ GeV, and the ratio of the Higgs vacuum expectation values $\tan\beta = 4$. The absolute value of the Higgs mass parameter μ is fixed by electroweak symmetry breaking, and we choose $\mu > 0$. For this set of parameters, we find the neutralino masses $m_{\tilde{\chi}_{1-4}^0}$ to be 55, 104, 283, and 309 GeV with $m_{\tilde{\chi}_3^0} < 0$ inside a polarization sum. The chargino masses $m_{\tilde{\chi}_{1,2}^{\pm}}$ are 102 and 308 GeV and therefore almost degenerate with the masses of the $m_{\tilde{\chi}_2^0}$ and $m_{\tilde{\chi}_4^0}$, respectively. This is a fairly general feature of the mSUGRA spectrum.

The total hadronic cross section is obtained from the partonic cross section through the convolution

$$\sigma^{h_1 h_2}(S, Q^2) = \sum_{i,j=g,q,\overline{q}} \int_\tau^1 \mathrm{d}x_1 \int_{\tau/x_1}^1 \mathrm{d}x_2 \; f_i^{h_1}(x_1, Q^2) f_j^{h_2}(x_2, Q^2) \hat{\sigma}_{ij}(x_1 x_2 S, Q^2), \tag{4.7}$$

where $\tau = \frac{4m^2}{S}$, with $m = (m_{\tilde{g}} + m_{\tilde{\chi}})/2$, and S is the square of the hadronic center-of-mass energy For the NLO predictions, we employ the CTEQ4M parametrization [39] for the parton densities $f(x, Q^2)$ in the proton or antiproton and a two-loop approximation for the strong coupling constant α_S with $\Lambda^{(5)} = 202$ MeV. To compute LO quantities we use the CTEQ4L LO PDF's and the one-loop approximation for α_S with $\Lambda^{(5)} = 181$ MeV.

In Figures 4.1 and 4.2 we present predictions for total hadronic cross sections at the Tevatron and the LHC, as a function of the physical gluino mass. To obtain these results, we use the average produced mass as the hard scale Q in Equation 4.8, $Q = m/2$. We vary the SUGRA parameter $m_{1/2}$ between 100 and 400 GeV and keep the other SUGRA parameters fixed at the values listed above. As the gluino mass increases over the range shown in the figure, the corresponding gaugino mass ranges are 31 to 163 GeV for $\tilde{\chi}_1^0$, 62 to 317 GeV for $\tilde{\chi}_2^0$ and $\tilde{\chi}_1^\pm$, 211 to 666 GeV for $\tilde{\chi}_3^0$, and 240 to 679 GeV for $\tilde{\chi}_4^0$ and $\tilde{\chi}_2^\pm$. The chargino cross sections are summed over production of positive and negative charges.

We observe that the cross sections for $\tilde{\chi}_2^0$ and $\tilde{\chi}_1^\pm$ and those for $\tilde{\chi}_4^0$ and $\tilde{\chi}_2^\pm$ are very similar in magnitude at the Tevatron, as are their respective masses. One might expect the largest cross section for the lightest gaugino $\tilde{\chi}_1^0$. However, its coupling is dominantly Bino-like and smaller than the W_3ino-like coupling[2] of $\tilde{\chi}_2^0$ which therefore has a larger cross section at small $m_{\tilde{g}}$ despite its larger mass. The heavier gauginos

[2]The Bino and W_3ino are the superpartners of the B and W_3 gauge bosons discussed in Chapter 1.

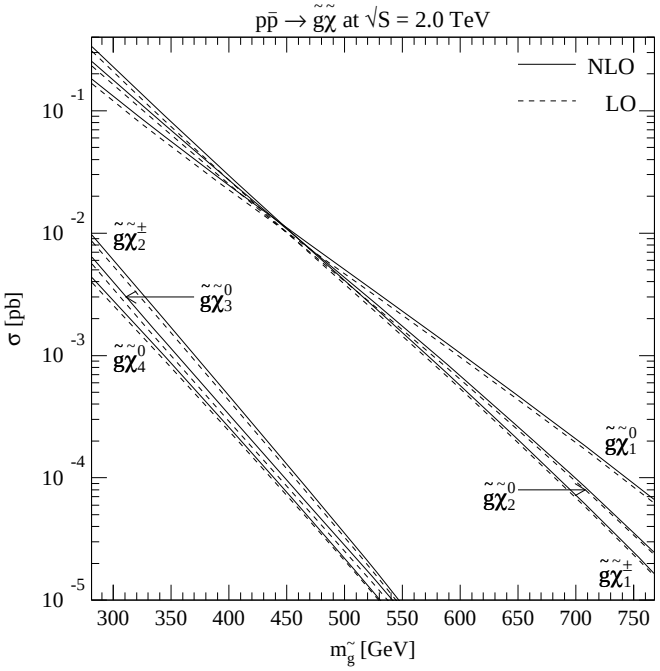

Figure 4.1: Total hadronic cross sections for the associated production of gluinos and gauginos at Run II of the Tevatron. NLO results are shown as solid curves, and LO results as dashed curves. We vary the SUGRA scenario as a function of $m_{1/2} \in [100; 400]$ GeV and provide the cross sections as a function of the physical gluino mass $m_{\tilde{g}}$. The chargino cross sections are summed over positive and negative chargino rates.

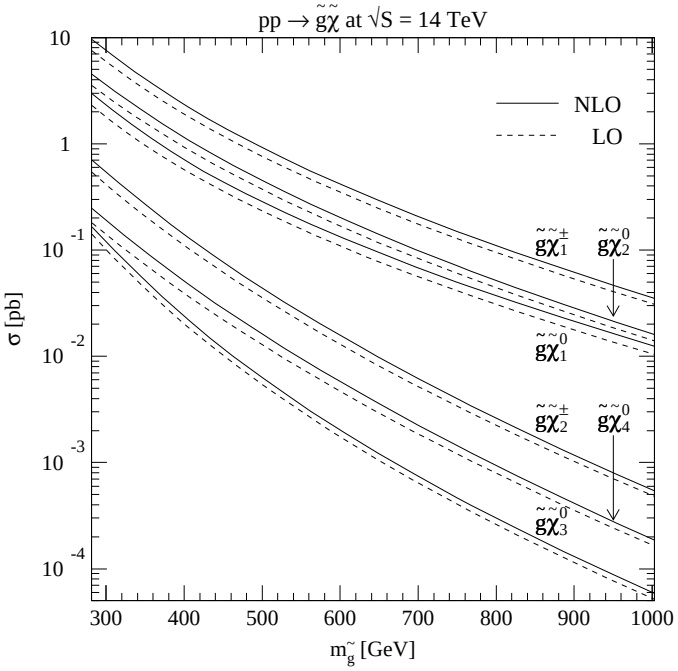

Figure 4.2: Total hadronic cross sections for the associated production of gluinos and gauginos at the LHC. NLO results are shown as solid curves, and LO results as dashed curves. We vary the SUGRA scenario as a function of $m_{1/2} \in [100; 400]$ GeV and provide the cross sections as a function of the physical gluino mass $m_{\tilde{g}}$. The chargino cross sections are summed over positive and negative chargino rates.

$\tilde{\chi}^0_{3,4}$ and $\tilde{\chi}^\pm_2$ are dominantly higgsino-like and their cross sections are suppressed by more than an order of magnitude with respect to those of the lighter gauginos.

At the Tevatron, the NLO contributions increase the cross sections by 5 to 15% at the hard scattering scale $Q = (m_{\tilde{g}} + m_{\tilde{\chi}})/2$, depending on the channel considered and the values of the masses. At the LHC, the increases are in the range of 15 to 35%. The purely NLO qg incident channel contributes significantly at the LHC, in addition to the $q\bar{q}$ channel, particularly for the lighter gauginos, whereas the qg channel plays an insignificant role at the Tevatron. In the event sparticles are not observed, the predicted increases translate into more restrictive experimental mass limits.

The enhancements of the cross sections are modest and, as such, underscore the validity of perturbative predictions for the processes considered. A further important benefit of the NLO computation is the considerable reduction in theoretical uncertainty associated with variation of the renormalization and factorization scale Q. For the processes studied here, this dependence is typically $\pm 10\%$ at the Tevatron when Q is varied over the interval Q/m from 0.5 to 2, compared to $\pm 25\%$ in leading order. At the LHC, the dependences are $\pm 9\%$ at NLO and $\pm 12\%$ at LO.

We limit ourselves to total cross sections. Differential distributions in the transverse momentum p_T and the rapidity η of the produced sparticles will be published elsewhere [105], along with figures of scaling functions, renormalization/factorization scale dependence, K-factors, and several appendices containing a detailed exposition of the calculation.

4.4 Summary

In summary, we provide NLO predictions of the cross sections for the associated production of gauginos and gluinos at hadron colliders. If supersymmetry exists at

the electroweak scale, the cross section for this process is expected to be large and observable at the Fermilab Tevatron and/or the CERN LHC. It is enhanced by the large color charge of the gluino and the (in many SUSY models) small mass of the light gauginos. The cross sections for $\tilde{g}\tilde{\chi}_2^0$ and $\tilde{g}\tilde{\chi}_1^\pm$ production are comparable, and the largest, because of their Wino-like couplings. As we have seen, the NLO predictions are modestly larger than the LO values but considerably more stable.

Chapter 5

Conclusions

In this work, we have seen that the Standard Model of particle physics, while fabulously successful at describing high energy physics experiments, suffers from a number of puzzles that indicate that it is not a fundamental theory, but should be replaced by something else to describe the physics at very short distances. The primary puzzle confronting particle physicists today is the understanding of the electroweak symmetry breaking, responsible for the large masses of the weak bosons and the top quark. The fact that the top is so much heavier than the other fermions seems to indicate that it may play some special role. Its large mass further indicates that it is a natural laboratory to test hypotheses concerning the nature of the symmetry breaking.

If the top does play a special role in nature, one must discover this fact through careful study of its properties. In particular, the electroweak interactions are likely to feel the effect of the true mechanism for the weak symmetry breaking, and are perhaps the most interesting properties to examine. Single top production is a vital means to study these weak interactions at a hadron collider, and thus we have spent considerable time describing the physics of single top production, to see how one can hope to use it as a tool to study the top's electroweak interactions. We have seen that the three modes of single top production, along with studies of top decays and

top polarization, represent a wealth of information about the top quark.

We have further studied the bottom quark, whose special partnership with the top may allow it to inherit some of the top's nonstandard properties. In particular, we have seen that this can result in an enhancement of the bottom coupling to scalar particles. It has been demonstrated that processes involving associated production of Higgs bosons with bottom quarks can provide interesting information about a wide class of models of the weak symmetry breaking, from supersymmetric theories to theories with dynamical EWSB.

We have also seen that the superpartners of the electroweak gauge bosons, the charginos and neutralinos can be produced in association with the gluino, superpartner to the gluon. This process provides an interesting means to search for evidence of supersymmetry at hadron colliders such as the Tevatron and LHC. In order to obtain a reliable theoretical prediction for the cross section, one must include higher orders in SUSY QCD. We have shown that the NLO corrections to this process are fairly large, and dramatically increase the stability of the theoretical prediction, indicating the necessity to include them.

With the advent of the Tevatron Run II, to be followed in a few years time by the LHC, we stand on the threshold of a wealth of information concerning the mechanism of the EWSB. The processes described above represent vital means to interpret this information. Regardless of whether one favors one particular description or another, it is an exciting time, as our conceptions of the symmetry breaking are confronted with reality.

Bibliography

[1] S. Weinberg, Phys. Rev. Lett. **19**, 1264 (1967); Phys. Rev. **D5**, 1412 (1972);
A. Salam, in *Nobel Symposium No. 8*, ed. N. Svartholm, Almqvist and Wiksell, Stockholm, 1968;
S. Glashow, Nucl. Phys. **22** 579 (1961);
D.J. Gross and F. Wilczek, Phys. Rev. **D8**, 3633 (1973); Phys. Rev. **D9**, 908 (1974);
H.D. Politzer, Phys. Rep. **14C**, 129 (1974).

[2] For a pedagogical overview of the SM, see, J. Hewett, "The Standard Model and Why it Works", TASI-97 lectures (1997).

[3] C.N. Yang and R.N. Mills, Phys. Rev. 96, 191 (1954).

[4] For a pedagogical introduction, see chapter three of, M. Peskin and D. Schroeder, *An Introduction to Quantum Field Theory*, Addison-Wesley, 1995.

[5] L. Faddeev and V. Popov, Phys. Lett. **25B**, 29 (1967).

[6] E. Noether, Nachr. kgl. Ges. Wiss. Gottingen, 235 (1918).

[7] J.C. Taylor, Nucl. Phys. **B33**, 436 (1971);
A. Slavnov, Theor. Math. Phys. **10**, 99 (1972);
C. Becchi, A. Rouet, and R. Stora, Comm. Math. Phys. **42**, 127 (1975).

[8] G. t'Hooft, Nucl. Phys. **B33**, 173 (1971).

[9] G. t'Hooft, Nucl. Phys. **B35**, 167 (1971);
G. t'Hooft and M. Veltman, Nucl. Phys. **B50**, 318 (1972);
B.W. Lee and J. Zinn-Justin, Phys. Rev. **D5**, 3121 (1972).

[10] P.W. Higgs, Phys. Lett. **12**, 132 (1964); Phys. Rev. **145**, 1156 (1966);
F. Englert and R. Brout, Phys. Rev. Lett. **13**, 321 (1964);
G.S. Guralnik, C.R. Hagen, and T.W.B. Kibble, Phys. Rev. Lett. **13**, 585 (1964).

[11] N. Cabibbo, Phys. Rev. Lett. **10**, 531 (1963);
M. Kobayashi and K. Maskawa, Prog. Theor. Phys. **49**, 652 (1973).

[12] Review of Particle Properties, Phys. Rev. **D54**, 1 (1996).

[13] Thomas Greening, "Search for the Standard Model Higgs Boson at LEP", DPF 99 Conference Proceedings (1999); hep-ex/9903013.

[14] W.–M. Yao, "Standard Model Higgs and Top Mass Measurements at the Tevatron", DPF 99 Conference Proceedings (1999); hep-ex/9903068.

[15] For a detailed exposition of SM Higgs physics issues and original references, see, J.F. Gunion, H.E. Haber, G. Kane, and S. Dawson, *The Higgs Hunter's Guide*, Addison-Wesley, 1990.

[16] B.W. Lee, C. Quigg, and G.B. Thacker, Phys. Rev. Lett. **38**, 883 (1977); Phys. Rev. **D16**, 1519 (1977).

[17] J. Wess and B. Zumino, Nucl. Phys. **B70**, 39 (1974).

[18] H. P. Nilles, Phys. Rep. **110**, 1 (1984);
H. Haber and G. L. Kane, Phys. Rep. **117**, 75 (1985);
For a recent review, S. Dawson, "The MSSM and Why it Works", TASI-97 lectures, hep-ph/9712464 (1997).

[19] For a review, S.F. King, Nucl. Phys. Proc. Suppl. **16**, 635 (1990).

[20] W.A. Bardeen, C.T. Hill, and M. Linder, Phys. Rev. **D41**, 1647 (1990);
For a recent review, G. Cvetic, hep-ph/9702381 (1997).

[21] C.T. Hill, Phys. Lett. **B345**, 483 (1995).

[22] R. Peccei and X. Zhang, Nucl. Phys. **B337**, 269 (1990);
E. Malkawi and C.-P. Yuan, Phys. Rev. **D50**, 4462 (1994).

[23] An interesting introduction to the EWCL is in, D. Kaplan, "Effective Lagrangians", TASI-97 lectures (1997).

[24] E. Malkawi and T. Tait, Phys. Rev. **D54**, 5758 (1996).

[25] P. Nason, S. Dawson, and R. K. Ellis, Nucl. Phys. **B303**, 607 (1988);
G. Altarelli, M. Diemoz, G. Martinelli, and P. Nason, Nucl. Phys. **B308**, 724 (1988).

[26] J.D. Bjorken and E.A. Paschos, Phys. Rev. **185**, 1975 (1969);
R.P. Feynman, Phys. Rev. Lett. **23**, 1415 (1969).

[27] D. Amati, R. Petronzio and G. Veneziano, Nucl. Phys. **B140**, 54; **B146**, 29 (1978);
R.K. Ellis, H. Georgi, M. Machacek, H.D. Politzer and G.G. Ross, Nucl. Phys. **B152**, 285 (1979);
S.B. Libby and G. Sterman, Phys. Rev. **D18**, 3252 (1978).

[28] P. Nason, S. Dawson, and R. K. Ellis, Nucl. Phys. **B303**, 607 (1988); Nucl. Phys. **B327**, 49 (1989); Nucl. Phys. **B335**, 260 (1990);
G. Altarelli, M. Diemoz, G. Martinelli, and P. Nason, Nucl. Phys. **B308**, 724 (1988);
W. Beenakker, H. Kuijf, W.L. van Neerven, and J. Smith, Phys. Rev. **D40**, 54 (1989);
R. Meng, G.A. Schuler, J. Smith, and W.L. van Neerven, Nucl. Phys. **B339**, 325 (1990);

W. Beenakker, W.L. van Neerven, R. Meng, G.A. Schuler, and J. Smith, Nucl. Phys. **B351**, 507 (1991);
R.K. Ellis, Phys. Lett. **B259**, 492 (1992);
E. Laenen, J. Smith, and W.L. van Neerven, Nucl. Phys. **B369**, 543 (1992); Phys. Lett. **B321**, 254 (1994);
N. Kidonakis and J. Smith, Phys. Rev. **D51**, 6092 (1995);
S. Catani, M. Mangano, P. Nason, and L. Trentadue, Phys. Lett. **B378**, 329 (1996); Nucl. Phys. **B478**, 273 (1996);
E. Berger and H. Contopanagos, Phys. Lett. **B361**, 115 (1995); Phys. Rev. **D54**, 3085 (1996); hep-ph/9706206;
N. Kidonakis and G. Sterman, Nucl. Phys. **B505**, 321 (1997);
N. Kidonakis, J. Smith, and R. Vogt, Phys. Rev. **D56**, 1553 (1997).

[29] M. Klein, H. Pietschmann, and H. Rupertsberger, Phys. Lett. **B153**, 341 (1985).

[30] I. Bigi, Y. Dokshitzer, V. A. Khoze, J. Kühn, and P. Zerwas, Phys. Lett. **181B**, 157 (1986);
M. Jezabek and J. Kühn, Phys. Lett. **B329**, 317 (1994).

[31] S. Cortese and R. Petronzio, Phys. Lett. **253B**, 494 (1991);
T. Stelzer and S. Willenbrock, Phys. Lett. **B357**, 125 (1995).

[32] S. Dawson, Nucl. Phys. **B249**, 42 (1985);
C.–P. Yuan, Phys. Rev. **D41**, 42 (1990); CCAST Symposium 1993, 259 (1993); Valencia Elem. Part. Phys. 1995, 148 (1995); *5th Mexican Workshop of Particles and Fields*, Puebla, Mexico (1995);
R. K. Ellis, and S. Parke Phys. Rev. **D46**, 3785 (1992).;
T. Stelzer, Z. Sullivan, and S. Willenbrock, Phys. Rev. **D58**, 094021 (1998).

[33] G. Ladinsky, and C.–P. Yuan, Phys. Rev. **D43**, 789 (1991);
S. Moretti, Phys. Rev. **D56**, 7427 (1997).

[34] For detailed study of the single top kinematics, including discussion of the related physics, see, D. O. Carlson, Ph.D. Thesis, Michigan State University (1995).

[35] D. O. Carlson, and C.–P. Yuan, Particle Phys. & Phen. 1995, 172 (1995);
T. Tait and C.–P. Yuan, hep-ph/9710372.

[36] A. P. Heinson, A. S. Belyaev, and E.E. Boos, Phys. Rev. **D56**, 3114 (1997).

[37] A.S. Belyaev, E.E. Boos, and L.V. Dudko, Phys. Rev. **D59**, 075001 (1999).

[38] M. C. Smith and S. Willenbrock, Phys. Rev. **D54**, 6696 (1996);
S. Mrenna and C.–P. Yuan, Phys. Lett. **B416**, 200 (1998).

[39] H. Lai, J. Huston, S. Kuhlmann, F. Olness, J. Owens, D. Soper, W.-K. Tung, and H. Weerts, Phys. Rev. **D55**, 1280 (1997).

[40] A. Martin, R. Roberts, M. G. Ryskin, and W. J. Stirling, Eur. Phys. J. **C2**, 287 (1998).

[41] J.C. Collins and W.–K. Tung, Nucl. Phys. **B278**, 934 (1986);
F. Olness and W.–K. Tung, Nucl. Phys. **B308**, 813 (1988);
M. Aivazis, F. Olness, and W.–K. Tung, Phys. Rev. Lett. **65**, 2339 (1990); Phys. Rev. **D50**, 3085 (1994);
M. Aivazis, J.C. Collins, F. Olness, and W.–K. Tung, Phys. Rev. **D50**, 3102 (1994).

[42] S. Willenbrock and D. Dicus, Phys. Rev. **D34**, 155 (1986).

[43] G. Bordes, and B. van Eijk, Z. Phys. **C 57**, 81 (1993); Nucl. Phys. **B435**, 23 (1995);
T. Stelzer, Z. Sullivan, and S. Willenbrock, Phys. Rev. **D56**, 5919 (1997).

[44] ATLAS Letter of Intent, CERN/LHCC/92-4, October 1992;
CMS Letter of Intent, CERN/LHCC/92-3, October 1992.

[45] C.–S. Li, R. Oakes, and J.–M. Yang, Phys. Rev. **D55**, 1672 (1997); Phys. Rev. **D55**, 5780 (1997);
C.–S. Li, R. Oakes, J.–M. Yang, H.–Y. Zhou, Phys. Rev. **D57**, 2009 (1998);
S. Bar-Shalom, D. Atwood, A. Soni, Phys. Rev. **D57**, 1495 (1998).

[46] B. Dobrescu and C. Hill, Phys. Rev. Lett. **81**, 2634 (1998);
R.S. Chivukula, B. Dobrescu, H. Georgi, and C. Hill, Phys. Rev. **D59**, 075003 (1999).

[47] H.–J. He, T. Tait, and C.–P. Yuan, in preparation.

[48] For a recent review, C. Kolda, Nucl. Phys. Proc. Suppl. **62**, 266 (1998).

[49] X. Li and E. Ma, Phys. Rev. Lett. **47**, 1788 (1988); *ibid.* **60**, 495 (1988);
X. Li and E. Ma, Phys. Rev. **D 46**, 1905 (1992);
X. Li and E. Ma, J. Phys. **G19**, 1265 (1993);
E. Malkawi, T. Tait, and C.–P. Yuan, Phys. Lett. **B385**, 304 (1996);
D. J. Muller and S. Nandi, Phys. Lett. **B383**, 345 (1996).

[50] E. Malkawi and C.–P. Yuan, hep-ph/9810353.

[51] E. Simmons, Phys. Rev. **D55**, 5494 (1997).

[52] H.–J. He and C.–P. Yuan, hep-ph/9810367.

[53] C. Balazs, H.–J. He and C.–P. Yuan, hep-ph/9812263.

[54] P. Baringer, P. Jain, D.W. McKay, and L. Smith, Phys. Rev. **D56**, 2914 (1997).

[55] R. Oakes, K. Whisnant, J.–M. Yang, B.–L. Young, X. Zhang, Phys. Rev. **D57**, 534 (1998).

[56] J.L. Diaz-Cruz, M.A. Perez, and J.J. Toscano, Phys. Lett. **B398**, 347 (1997).

[57] D. Carlson, E. Malkawi, and C.–P. Yuan, Phys. Lett. **B337**, 145 (1994);
E. Malkawi, and C.–P. Yuan, Phys. Rev. **D50**, 4462 (1994);
E. Malkawi, and C.–P. Yuan, Phys. Rev. **D52**, 472 (1995).

[58] F. Larios and C.–P. Yuan, Phys. Rev. **D55**, 7218 (1997);
F. Larios, T. Tait, and C.–P. Yuan, Phys. Rev. **D57**, 3106 (1998).

[59] A. Manohar and H. Georgi, Nucl. Phys. **B234**, 189 (1984).

[60] T. Skwarnicki, talk at ICHEP98, Vancouver, Canada (1998);
M. Alam et al, CLEO collaboration, Phys. Rev. Lett. **74**, 2885 (1998).

[61] K. Chetyrkin, M. Misiak, and M. Munz, Phys. Lett. **B400**, 206 (1997);
F. Larios, M. A. Pérez, and C.–P. Yuan, hep-ph/9903394.

[62] M. Hosch, K. Whisnant, and B.–L. Young, Phys. Rev. **D56**, 5725 (1997);
T. Han, M. Hosch, K. Whisnant, B.–L. Young, and X. Zhang, Phys. Rev. **D58**, 073008 (1998).

[63] T. Tait and C.–P. Yuan, Phys. Rev. **D55**, 7300 (1997).

[64] T. Han, R.D. Peccei, and X. Zhang, Nucl. Phys. **B454**, 527 (1995).

[65] T. Han, K. Whisnant, B.L. Young, X. Zhang, Phys. Lett. **B385**, 311 (1996);
T. Han, K. Whisnant, B.L. Young, and X. Zhang, Phys. Rev. **D55**, 7241 (1997).

[66] C.–P. Yuan, private communication.

[67] G. Mahlon and S. Parke, Phys. Rev. **D55**, 7249 (1997).

[68] J.L. Diaz-Cruz, H.-J. He, T. Tait, and C.-P. Yuan, Phys. Rev. Lett. **80**, 4641 (1998);
C. Balazs, J.L. Diaz-Cruz, H.-J. He, T. Tait, and C.-P. Yuan, Phys. Rev. **D59**, 055016 (1999).

[69] D. Dicus and S. Willenbrock, Phys. Rev. **D39**, 751 (1989);
D. Dicus, T. Stelzer, Z. Sullivan, and S. Willenbrock Phys. Rev. **D59**, 094016 (1999).

[70] W. F. Long and T. Stelzer, Comput. Phys. Commun. **81**, 357 (1994).

[71] M. Mangano, P. Nason, and G. Ridolfi, Nucl. Phys. **B373**, 295 (1992);
S. Dawson and L. Reina, Phys. Rev. **D57**, 5851 (1998).

[72] Dan Amidei and R. Brock, "Report of the TeV 2000 Study Group on Future EW Physics at Tevatron", 1995.

[73] J. Dai, J. Gunion, and R. Vega, Phys. Lett. **B345**, 29 (1995); **B387**, 801 (1996).

[74] E. Richter-Was and D. Froidevaux, Z. Phys. **C76**, 665 (1997).

[75] T. Sjostrand, Comput. Phys. Commun. **82**, 74 (1994);
S. Mrenna, Comput. Phys. Commun. **101**, 232 (1997).

[76] C.T. Hill *et al.*, Nucl. Phys. **B262**, 517 (1985).

[77] W.A. Bardeen, C.T. Hill, and M. Linder, Phys. Rev. **D41**, 1647 (1990).

[78] M.A. Luty, Phys. Rev. **D41**, 2893 (1990);
M. Suzuki, Phys. Rev. **D41**, 3457 (1990).

[79] M. Lindner and E. Schnapka, hep-ph/9712489.

[80] J. Gunion and H. Haber, Nucl. Phys. **B272**, 1 (1986).

[81] For a review, H. Haber, hep-ph/9707213.

[82] M. Carena, M. Quiros, and C. Wagner, Nucl. Phys. **B461**, 407 (1996).

[83] M. Carena, S. Mrenna, and C. Wagner, hep-ph/9808312.

[84] M. Drees, M. Guchait, and P. Roy, Phys. Rev. Lett. **80**, 2047 (1998); **81**, 2394 (1998).

[85] J. Gunion and L. Orr, Phys. Rev. **D46** (92) 2052;
J.L. Diaz-Cruz, O. Sampayo, J. Mod. Phys. **A8** (93) 4339.

[86] R. Arnowitt and P. Nath, hep-ph/9708254.

[87] M. Drees and M. Nojiri, Nucl. Phys. **B369**, 54 (1992).

[88] R. Rattazzi and U. Sarid, hep-ph/9612464.

[89] J. Bagger et al., Phys. Rev. **D55**, 3188 (1997);
H. Baer et al., Phys. Rev. **D55**, 4463 (1997).

[90] E. Berger, M. Klasen, and T. Tait, hep-ph/9902350.

[91] G. Farrar, Nucl. Phys. Proc. Suppl. **62**, 485 (1996); S. Raby and K. Tobe, Nucl. Phys. **B539**, 3 (1999).

[92] S. Dawson, E. Eichten, and C. Quigg, Phys. Rev. **D31**, 1581 (1985);
H. Baer, D.D. Karatas, and X. Tata, Phys. Rev. **D42**, 2259 (1990).

[93] W. Beenakker, R. Höpker, M. Spira, and P.M. Zerwas, Nucl. Phys. **B492**, 51 (1997).

[94] W. Beenakker, M. Krämer, T. Plehn, M. Spira, and P.M. Zerwas, Nucl. Phys. **B515**, 3 (1998).

[95] H. Baer, B.W. Harris, and M. Hall Reno, Phys. Rev. **D57**, 5871 (1998).

[96] W. Beenakker, M. Klasen, M. Krämer, T. Plehn, M. Spira, and P.M. Zerwas, in preparation.

[97] E.L. Berger, M. Klasen, and T. Tait, Phys. Rev. **D59**, 074024 (1999).

[98] S. Mrenna, hep-ph/9902471 (1999).

[99] A. Denner, H. Eck, O. Hahn, and J. Küblbeck, Nucl. Phys. **B387**, 467 (1992).

[100] J. F. Gunion and H. Haber, Nucl. Phys. **B272**, 1 (1986).

[101] G. Passarino and M. Veltman, Nucl Phys. **B160**, 151 (1979).

[102] S.P. Martin and M.T. Vaughn, Phys. Lett. **B318**, 331 (1993).

[103] W. Beenakker, H. Kuijf, and W.L. van Neerven, Phys. Rev. **D40**, 54 (1989).

[104] G. Altarelli, R.K. Ellis, and G. Martinelli, Nucl. Phys. **B157**, 461 (1979).

[105] E.L. Berger, M. Klasen, and T. Tait, in preparation.